National Library of Canada

Acquisitions and Bibliographic Services Branch

395 Wellington Street
Ottawa, Ontario
K1A 0N4

Bibliothèque nationale du Canada

Direction des acquisitions et des services bibliographiques

395, rue Wellington
Ottawa (Ontario)
K1A 0N4

Your file   Votre référence

Our file   Notre référence

NOTICE

The quality of this microform is heavily dependent upon the quality of the original thesis submitted for microfilming. Every effort has been made to ensure the highest quality of reproduction possible.

If pages are missing, contact the university which granted the degree.

Some pages may have indistinct print especially if the original pages were typed with a poor typewriter ribbon or if the university sent us an inferior photocopy.

Reproduction in full or in part of this microform is governed by the Canadian Copyright Act, R.S.C. 1970, c. C-30, and subsequent amendments.

AVIS

La qualité de cette microforme dépend grandement de la qualité de la thèse soumise au microfilmage. Nous avons tout fait pour assurer une qualité supérieure de reproduction.

S'il manque des pages, veuillez communiquer avec l'université qui a conféré le grade.

La qualité d'impression de certaines pages peut laisser à désirer, surtout si les pages originales ont été dactylographiées à l'aide d'un ruban usé ou si l'université nous a fait parvenir une photocopie de qualité inférieure.

La reproduction, même partielle, de cette microforme est soumise à la Loi canadienne sur le droit d'auteur, SRC 1970, c. C-30, et ses amendements subséquents.

Canada

A Silicon Micromachined Subminiature Condenser Microphone: Analysis, Design, Fabrication and Testing

Jagdish Patel

A
Thesis
in
the Department of Mechanical Engineering

Presented in Partial Fulfillment of the Requirements
for the Degree of Master of Applied Science
at
Concordia University
Montreal, Quebec, Canada

February, 1995
©Jagdish Patel

National Library of Canada
Bibliothèque nationale du Canada

Acquisitions and Bibliographic Services Branch
Direction des acquisitions et des services bibliographiques

395 Wellington Street
Ottawa, Ontario
K1A 0N4

395, rue Wellington
Ottawa (Ontario)
K1A 0N4

Your file Votre référence

Our file Notre référence

THE AUTHOR HAS GRANTED AN IRREVOCABLE NON-EXCLUSIVE LICENCE ALLOWING THE NATIONAL LIBRARY OF CANADA TO REPRODUCE, LOAN, DISTRIBUTE OR SELL COPIES OF HIS/HER THESIS BY ANY MEANS AND IN ANY FORM OR FORMAT, MAKING THIS THESIS AVAILABLE TO INTERESTED PERSONS.

L'AUTEUR A ACCORDE UNE LICENCE IRREVOCABLE ET NON EXCLUSIVE PERMETTANT A LA BIBLIOTHEQUE NATIONALE DU CANADA DE REPRODUIRE, PRETER, DISTRIBUER OU VENDRE DES COPIES DE SA THESE DE QUELQUE MANIERE ET SOUS QUELQUE FORME QUE CE SOIT POUR METTRE DES EXEMPLAIRES DE CETTE THESE A LA DISPOSITION DES PERSONNE INTERESSEES.

THE AUTHOR RETAINS OWNERSHIP OF THE COPYRIGHT IN HIS/HER THESIS. NEITHER THE THESIS NOR SUBSTANTIAL EXTRACTS FROM IT MAY BE PRINTED OR OTHERWISE REPRODUCED WITHOUT HIS/HER PERMISSION.

L'AUTEUR CONSERVE LA PROPRIETE DU DROIT D'AUTEUR QUI PROTEGE SA THESE. NI LA THESE NI DES EXTRAITS SUBSTANTIELS DE CELLE-CI NE DOIVENT ETRE IMPRIMES OU AUTREMENT REPRODUITS SANS SON AUTORISATION.

ISBN 0-612-01356-1

Canada

Name JAGDISH PATEL

Dissertation Abstracts International is arranged by broad, general subject categories. Please select the one subject which most nearly describes the content of your dissertation. Enter the corresponding four-digit code in the spaces provided.

MECHANICAL — 0548 — U·M·I

SUBJECT TERM — SUBJECT CODE

Subject Categories

THE HUMANITIES AND SOCIAL SCIENCES

COMMUNICATIONS AND THE ARTS
Architecture 0729
Art History 0377
Cinema 0900
Dance 0378
Fine Arts 0357
Information Science 0723
Journalism 0391
Library Science 0399
Mass Communications 0708
Music 0413
Speech Communication 0459
Theater 0465

EDUCATION
General 0515
Administration 0514
Adult and Continuing 0516
Agricultural 0517
Art 0273
Bilingual and Multicultural 0282
Business 0688
Community College 0275
Curriculum and Instruction 0727
Early Childhood 0518
Elementary 0524
Finance 0277
Guidance and Counseling 0519
Health 0680
Higher 0745
History of 0520
Home Economics 0278
Industrial 0521
Language and Literature 0279
Mathematics 0280
Music 0522
Philosophy of 0998
Physical 0523
Psychology 0525
Reading 0535
Religious 0527
Sciences 0714
Secondary 0533
Social Sciences 0534
Sociology of 0340
Special 0529
Teacher Training 0530
Technology 0710
Tests and Measurements 0288
Vocational 0747

LANGUAGE, LITERATURE AND LINGUISTICS
Language
- General 0679
- Ancient 0289
- Linguistics 0290
- Modern 0291

Literature
- General 0401
- Classical 0294
- Comparative 0295
- Medieval 0297
- Modern 0298
- African 0316
- American 0591
- Asian 0305
- Canadian (English) 0352
- Canadian (French) 0355
- English 0593
- Germanic 0311
- Latin American 0312
- Middle Eastern 0315
- Romance 0313
- Slavic and East European 0314

PHILOSOPHY, RELIGION AND THEOLOGY
Philosophy 0422
Religion
- General 0318
- Biblical Studies 0321
- Clergy 0319
- History of 0320
- Philosophy of 0322

Theology 0469

SOCIAL SCIENCES
American Studies 0323
Anthropology
- Archaeology 0324
- Cultural 0326
- Physical 0327

Business Administration
- General 0310
- Accounting 0272
- Banking 0770
- Management 0454
- Marketing 0338

Canadian Studies 0385
Economics
- General 0501
- Agricultural 0503
- Commerce-Business 0505
- Finance 0508
- History 0509
- Labor 0510
- Theory 0511

Folklore 0358
Geography 0366
Gerontology 0351
History
- General 0578
- Ancient 0579
- Medieval 0581
- Modern 0582
- Black 0328
- African 0331
- Asia, Australia and Oceania 0332
- Canadian 0334
- European 0335
- Latin American 0336
- Middle Eastern 0333
- United States 0337

History of Science 0585
Law 0398
Political Science
- General 0615
- International Law and Relations 0616
- Public Administration 0617

Recreation 0814
Social Work 0452
Sociology
- General 0626
- Criminology and Penology 0627
- Demography 0938
- Ethnic and Racial Studies 0631
- Individual and Family Studies 0628
- Industrial and Labor Relations 0629
- Public and Social Welfare 0630
- Social Structure and Development 0700
- Theory and Methods 0344

Transportation 0709
Urban and Regional Planning 0999
Women's Studies 0453

THE SCIENCES AND ENGINEERING

BIOLOGICAL SCIENCES
Agriculture
- General 0473
- Agronomy 0285
- Animal Culture and Nutrition 0475
- Animal Pathology 0476
- Food Science and Technology 0359
- Forestry and Wildlife 0478
- Plant Culture 0479
- Plant Pathology 0480
- Plant Physiology 0817
- Range Management 0777
- Wood Technology 0746

Biology
- General 0306
- Anatomy 0287
- Biostatistics 0308
- Botany 0309
- Cell 0379
- Ecology 0329
- Entomology 0353
- Genetics 0369
- Limnology 0793
- Microbiology 0410
- Molecular 0307
- Neuroscience 0317
- Oceanography 0416
- Physiology 0433
- Radiation 0821
- Veterinary Science 0778
- Zoology 0472

Biophysics
- General 0786
- Medical 0760

EARTH SCIENCES
Biogeochemistry 0425
Geochemistry 0996
Geodesy 0370
Geology 0372
Geophysics 0373
Hydrology 0388
Mineralogy 0411
Paleobotany 0345
Paleoecology 0426
Paleontology 0418
Paleozoology 0985
Palynology 0427
Physical Geography 0368
Physical Oceanography 0415

HEALTH AND ENVIRONMENTAL SCIENCES
Environmental Sciences 0768
Health Sciences
- General 0566
- Audiology 0300
- Chemotherapy 0992
- Dentistry 0567
- Education 0350
- Hospital Management 0769
- Human Development 0758
- Immunology 0982
- Medicine and Surgery 0564
- Mental Health 0347
- Nursing 0569
- Nutrition 0570
- Obstetrics and Gynecology 0380
- Occupational Health and Therapy 0354
- Ophthalmology 0381
- Pathology 0571
- Pharmacology 0419
- Pharmacy 0572
- Physical Therapy 0382
- Public Health 0573
- Radiology 0574
- Recreation 0575
- Speech Pathology 0460
- Toxicology 0383

Home Economics 0386

PHYSICAL SCIENCES

Pure Sciences
Chemistry
- General 0485
- Agricultural 0749
- Analytical 0486
- Biochemistry 0487
- Inorganic 0488
- Nuclear 0738
- Organic 0490
- Pharmaceutical 0491
- Physical 0494
- Polymer 0495
- Radiation 0754

Mathematics 0405
Physics
- General 0605
- Acoustics 0986
- Astronomy and Astrophysics 0606
- Atmospheric Science 0608
- Atomic 0748
- Electronics and Electricity 0607
- Elementary Particles and High Energy 0798
- Fluid and Plasma 0759
- Molecular 0609
- Nuclear 0610
- Optics 0752
- Radiation 0756
- Solid State 0611

Statistics 0463

Applied Sciences
Applied Mechanics 0346
Computer Science 0984

Engineering
- General 0537
- Aerospace 0538
- Agricultural 0539
- Automotive 0540
- Biomedical 0541
- Chemical 0542
- Civil 0543
- Electronics and Electrical 0544
- Heat and Thermodynamics 0348
- Hydraulic 0545
- Industrial 0546
- Marine 0547
- Materials Science 0794
- Mechanical 0548
- Metallurgy 0743
- Mining 0551
- Nuclear 0552
- Packaging 0549
- Petroleum 0765
- Sanitary and Municipal 0554
- System Science 0790

Geotechnology 0428
Operations Research 0796
Plastics Technology 0795
Textile Technology 0994

PSYCHOLOGY
General 0621
Behavioral 0384
Clinical 0622
Developmental 0620
Experimental 0623
Industrial 0624
Personality 0625
Physiological 0989
Psychobiology 0349
Psychometrics 0632
Social 0451

CONCORDIA UNIVERSITY

SCHOOL OF GRADUATE STUDIES

This is to certify that the Thesis prepared,

By: Jagdish PATEL

Entitled: "A Silicon Micromachined Subminiature Condenser Microphone: Analysis, Design, Fabrication and Testing"

and submitted in partial fulfillment of the requirements for the Degree of

Master of Applied Science

complies with the regulations of this University and meets the accepted standards with respect to originality and quality.

Signed by the Final Examining Committee:

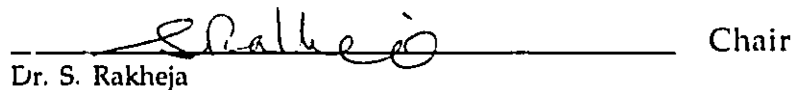

Dr. S. Rakheja — Chair

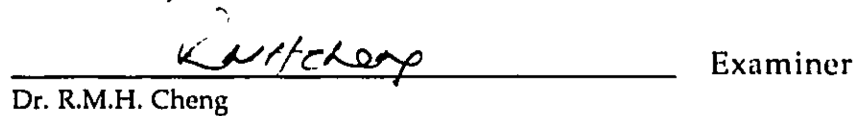

Dr. R.M.H. Cheng — Examiner

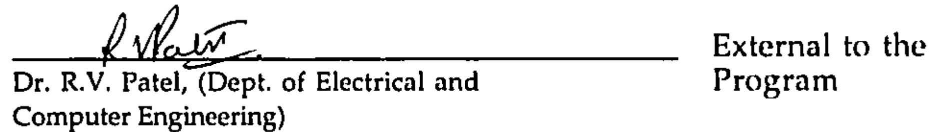

Dr. R.V. Patel, (Dept. of Electrical and Computer Engineering) — External to the Program

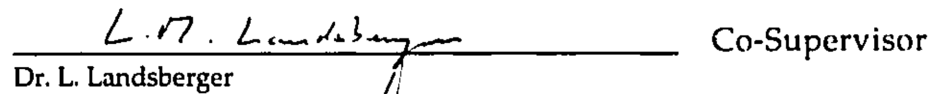

Dr. L. Landsberger — Co-Supervisor

Dr. I. Stiharu — Co-Supervisor

Approved by:

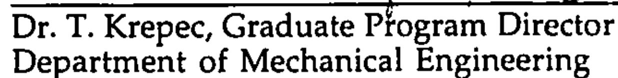

Dr. T. Krepec, Graduate Program Director
Department of Mechanical Engineering

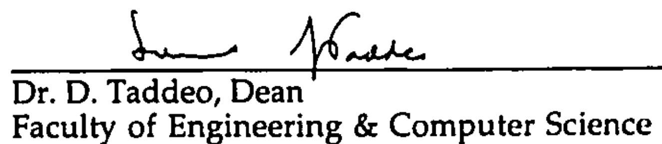

Dr. D. Taddeo, Dean
Faculty of Engineering & Computer Science

March [illegible], 1995

ABSTRACT

A Silicon Micromachined Subminiature Condenser Microphone: Analysis, Design, Fabrication and Testing

Jagdish Patel

Microphones are ordinary pressure sensors with an optimum behavior in a certain pressure and frequency range. The fundamental elements of a condenser microphone comprises of a diaphragm, backplate, airgap, and rear volume cavity. In order to analyze any system for its response behavior due to a particular loading, it is essential to obtain the characteristic properties of the system in terms of the natural frequencies, mode shapes and damping. This is done by solving a free vibration problem. Both the Rayleigh-Ritz Method and Finite Element Method were used in the present study to obtain the natural frequencies and normal modes of the plates (diaphragm). The natural frequencies and mode shapes of the diaphragm of square and circular shapes including those with cutouts (openings) and abrupt changes in thickness are obtained. The results show that the natural frequencies increase as the size of cutout increases, and also when the abrupt change in thickness increases. But, the increase due to abrupt change in thickness is very small when compared that of the plate with cutout.

In the present investigation, silicon micromachining technology is used to fabricate the condenser microphone. The condenser microphone is fabricated from two wafer chips, one containing the silicon membrane and the other the Pyrex glass (#7740) which forms the backplate. Between the

membrane and the backplate there is an airgap which completes the capacitance circuit. Lithographic techniques are used to manufacture the condenser microphone with specially shaped backplates which contain the airgap and side volume cavity. An Anodic bonding technique is used to bond the silicon membrane with the backplate. The silicon diaphragm is used as the moving electrode and the Pyrex glass backplate is made into a back electrode by a thin deposition of metal on it. The fabricated microphone is tested for its frequency response and sensitivity.

The introduction of silicon micromachining technology allows accurate control of dimensions, a high degree of miniaturization, and batch fabrication of microphones at low cost and with good reproducibility.

TO

RUPA & KARAN

Acknowledgments

The author wishes to express deep sense of gratitude and appreciation to his supervisors Dr. I. Stiharu and Dr. L. Landsberger for their continued support and encouragement, invaluable guidance and great patience during the course of this work.

Special thanks are due to Dr. R. B. Bhat for his continued help in various stages of this work. Helpful suggestions by Dr. C. Rajalingham, Dr. M. Kahrizi and Dr. A. Kaushal are greatly appreciated.

The author is also greatful for the help and assistance provided by Danny Juras, Joseph Hulet, Gegi George, Catalin Miu and Joseph Saruf. Thanks are also due to Jacques Lajoie and Gianni Ferrari of Ecole Polytechnique de Montreal for providing their facility during the course of chromium deposition of the fabrication process.

The financial support by the Mechanical Engineering and Electrical and Computer Engineering Departments of the Concordia University is acknowledged.

Sincerest thanks are due to my wife, Bharti, for her constant emotional and moral support during the pursuit of this project. Special thanks are due to my parents, brother and father-in-law for their emotional support and understanding, and to my friends for their abundant moral support all along.

TABLE OF CONTENTS

i. List of Figures. xi
ii. List of Tables xiv
iii. List of Acronyms and Symbols xv

CHAPTER 1

Introduction and Literature Review

1.1 Introduction 1
1.2 History 3
1.3 Scope of the Present Investigation 4
1.4 Literature Review 8
1.4.1 Vibration of Plates 8
1.4.2 Condenser Microphones 11

CHAPTER 2

Condenser Microphone

2.1 Condenser Microphone Principle 15

CHAPTER 3

Vibration Analysis of Plates

3.1 General 19
3.2 Rayleigh Ritz Method 22
3.3 Orthogonal Polynomials 24
3.3.1 General 24

3.3.2 Generation of Single Variable Orthogonal Polynomials. . 24
3.3.3 Generation of Two Variable Orthogonal Polynomials. . . 26
3.4 Analysis of the Rectangular Plate 28
3.4.1 Rectangular Plate 28
3.4.2 Rectangular Plate with Opening 31
3.4.3 Rectangular Plate with Abrupt Change in Thickness . . . 33
3.5 Analysis of the Circular Plate 35
3.5.1 Circular Plate 36
3.5.2 Annular Plate 38
3.5.3 Circular Plate with Abrupt Change in Thickness 40
3.6 Finite Element Method 43
3.6.1 General 43
3.6.2 Ansys Finite Element Program 43
3.6.3 Modal Analysis 45
3.7 Results and Discussion 47
3.7.1 General 47
3.7.2 Natural Frequencies of a Square Plate 47
3.7.3 Natural Frequencies of a Circular Plate 49
3.7.4 Natural Frequencies of a Hexagonal Plate 51
3.8 Summary 74

CHAPTER 4

Design of Condenser Microphone

4.1 Introduction 75
4.2 Design Considerations 76
4.3.1 Diaphragm Design Considerations 76
4.3.2 Backplate Design Considerations 78
4.3 Capacitance for Circular and Square Structures 80
4.3.1 Circular Diaphragm 80
4.3.2 Square Diaphragm 81
4.4 Sensitivity of the Microphone 82
4.5 Process Design of the Microphone 86

CHAPTER 5

Fabrication of Condenser Microphone

5.1 Introduction 87
5.2 Fabrication Process 87
5.2.1 Backplate Etching Process 95
5.2.2 Backplate Metalization Process 98
5.2.3 Silicon Membrane 99
5.2.4 Bonding of Silicon with Glass 99
5.3 Experimental Results and Summary 100

CHAPTER 6

Characterization of Condenser Microphone

6.1 Capacitive Measurement 102
6.1.1 Experimental Procedure. 103
6.1.2 Results and Discussion 104
6.2 Sensitivity and Frequency Response. 106
6.2.1 Experimental Setup 107
6.2.2 Experimental Procedure. 108
6.2.3 Results and Discussion 109
6.3 Summary 135

CHAPTER 7

Conclusions and Future Work

7.1 Overview 138
7.2 Conclusions for Plate Analysis 139
7.3 Conclusions for Subminiature Condenser Microphone 141
7.4 Recommendations for Future Work 144

APPENDIX

A Metalization and Chromium Deposition 146
B Lithography 148
C Anodic Bonding 151
D Wet Etching 154
E Frequency Response Function 155

Bibliography 165

LIST OF FIGURES

2.1 Condenser Microphone Basic Principle.. 16

3.1 Rectangular Plate 29
3.2 Rectangular Plate with Opening 31
3.3 Rectangular Plate with Abrupt Change in Thickness. 33
3.4 Circular Plate 36
3.5 Annular Plate 38
3.6 Circular Plate with Abrupt Change in Thickness 41
3.7 Ansys Program Organization. 44
3.8 Comparison of Frequency Parameter of Square Plate with Opening 62
3.9 Comparison of Second Frequency Parameter of Square Plate with Opening. 62
3.10 Comparison of Frequency Parameter of Square Plate with Abrupt Change in Thickness ($\beta = 1.5$). 63
3.11 Comparison of Frequency Parameter of Square Plate with Abrupt Change in Thickness ($\beta = 2.0$). 63
3.12 Comparison of Frequency Parameter of Annular Plate 64
3.13 Comparison of Second Frequency Parameter of Annular Plate . . 64
3.14 Comparison of Frequency Parameter of Circular Plate with Abrupt Change in Thickness ($\beta = 1.5$). 65
3.15 Comparison of Frequency Parameter of Circular plate with Abrupt Change in Thickness ($\beta = 2.0$). 65
3.16 Mode Shapes of a CCCC Square Plate 66
3.17 Mode Shapes of a CCCC Square Plate with Square Openings (0.2 X0.2) 67
3.18 Mode Shapes of a CCCC Square Plate with Square Openings (0.5 X0.5) 68
3.19 Mode Shapes of a CCCC Square Plate with Abrupt Change in Thickness ($\beta = 1.5$). 69
3.20 Mode Shapes of a Clamped Circular Plate. 70
3.21 Mode Shapes of a Clamped Annular Plate 71

3.22 Mode Shapes of a Circular Plate with Abrupt Change in Thickness ($\beta = 1.5$) 72
3.23 Mode Shapes of a Hexagonal Plate 73

4.1 Cross-Section of a Microphone Structures 76
4.2 Electrode Pattern and C/S of a Square and Circular Structures . . 79
4.3 The Condenser Microphone with Preamplifier 83

5.1 Linear Expansion Coefficients as a Function of Temperature for Several Commercial Glass Substrates and Silicon 88
5.2 Flexible Silicon Membrane 89
5.3 Fabrication Process for the Condenser Microphone 90
5.4 Mask # 1 for Etching of Side Cavity 92
5.5 Mask # 2 for Etching of Airgap Cavity 93
5.6 Mask # 3 for Metalization and Contact 94
5.7 Photograph of Airgap and Side Cavity of Square Diaphragm . . 96
5.8 Photograph of Airgap and Side Cavity of Circular Diaphragm . . 97
5.9 Advantages of Negative Photoresist 97

6.1 Experimental Setup for Capacitive Measurement 103
6.2 The Measurement Setup 107
6.3 Frequency of the B&K 4155 Standard Microphone 110
6.4(a) Dual Channel Autospectra for the Standard Microphone . . . 114
6.4(b) Frequency Response of the Standard Microphone 115
6.4(c) Coherence Between the Standard Microphones 116
6.5(a) Autospectra for the Fabricated (circular: dia = 1.2 mm) and Reference Microphones 117
6.5(b) Frequency Response of the Fabricated (circular: dia = 1.2 mm) Microphone 118
6.5(c) Coherence Between the Fabricated (circular: dia = 1.2 mm) and Reference Microphones 119
6.6(a) Autospectra for the Fabricated (circular: dia = 1mm) and Reference Microphones 120
6.6(b) Frequency Response of the Fabricated (circular: dia = 1mm) Microphone 121

6.6(c) Coherence Between the Fabricated (circular: dia = 1mm) and Reference Microphones 122
6.7(a) Autospectra for the Fabricated (square: side = 1mm) and Reference Microphones 123
6.7(b) Frequency Response of the Fabricated (square: side = 1mm) Microphone 124
6.7(c) Coherence Between the Fabricated (square: side = 1mm) and Reference Microphones 125
6.8(a) Autospectra for the Fabricated (square: side = 0.8 mm) and Reference Microphones 126
6.8(b) Frequency Response of the Fabricated (square: side = 0.8 mm) Microphone 127
6.8(c) Coherence Between the Fabricated (square: side = 0.8 mm) and Reference Microphones 128
6.9(a) Autospectra for the Fabricated (triangular: side = 0.7 mm) and Reference Microphones 129
6.9(b) Frequency Response of the Fabricated (triangular: side = 0.7 mm) Microphone 130
6.9(c) Coherence Between the Fabricated (triangular: side = 0.7 mm) and Reference Microphones. 131
6.10(a) Autospectra for the Fabricated (Hexagonal: side = 0.5 mm) and Reference Microphones 132
6.10(b) Frequency Response of the Fabricated (Hexagonal: side = 0.5 mm) Microphone 133
6.10(c) Coherence Between the Fabricated (Hexagonal: side = 0.5 mm) and Reference Microphones 134
6.11 Noise Level of Fabricated and Reference Microphone 135

A1 Chromium Deposition Setup 145
B1 A Lithographic Cycle 149
C1 Anodic Bonding 150
E1 System with Input/Output Signals in Time Domain and Frequency Domain 154
E2 Simplified Block Diagram of the Analysis in Dual Channel Averaging Mode 155

LIST OF TABLES

3.1 Processors Available in the ANSYS program. 45
3.2 Frequency Parameter of Clamped Square Plate. 52
3.3 Comparison of Frequency Parameter of a CCCC Square Plate . . 52
3.4 Frequency Parameter of Square Plate with Cutout. 53
3.5 Frequency Parameter of Square Plate with Abrupt Change in Thickness (β=1.5) 54
3.6 Frequency Parameter of Square Plate with Abrupt Change in Thickness (β=2.0). 55
3.7 Comparison of Frequency Parameter of Square Plate with Cutout 56
3.8 Comparison of Frequency Parameter of Square Plate with Different Cutout. 56
3.9 Comparison of Frequency Parameter of Square Plate with Abrupt Change in thickness (β=1.5). 56
3.10 Frequency Parameter of Circular Plate 57
3.11 Comparison of Frequency Parameter of Circular Plate 57
3.12 Frequency Parameter of Annular Plate 58
3.13 Frequency Parameter of Circular plate with Abrupt Change in Thickness (β=1.5).. 59
3.14 Frequency Parameter of Circular plate with Abrupt Change in Thickness (β=2.0).. 60
3.15 Comparison of Natural Frequency Coefficients of Clamped Annular Plate 61
3.16 Comparison of Natural Frequency Coefficients of Regular Hexagonal Plate 61
4.1 Fundamental Frequencies of Diaphragms 77
4.2 Diaphragm Parameters 78
6.1 Analytical and Measured Capacitance 104
6.2 Simulated and Measured Capacitance 105
6.3 Summary of Results for the Microphone Characterization. . . . 112
6.4 Estimated Volume and Constant K 113
E1 Advantages and Disadvantages of Different Measuring Techniques 161
E2 Best choice of FRF Estimator for Different Measurement Situations 163

NOMENCLATURE

a,b	Dimensions of a rectangular plate in x and y direction, outer and inner radius of an annular plate
C	Capacitance
C_i	Preamplifier input capacitance
C_m	Microphone working capacitance
C_p	Parasitic capacitance
C_s	Stray capacitance $(C_p + C_i)$
D	Plate flexural rigidity $[Eh^3/12(1-\nu^2)]$
d	air gap of the microphone
E	Modulus of elasticity
E_a	Electric field strength
H_a	Gain of the amplifier
H_c	Capacitance signal attenuation
h	Plate thickness
h_l	Abrupt change in thickness of the plate
[K]	Stiffness matrix
M	Mass in grams per square centimeter of area
[M]	Mass matrix
m,n	Number of half waves in x and y direction, respectively
P	Sound pressure
Q	Quasi-constant charge
R	Radius of a circle
R_L	Load resistor
R_b	Bias resistor

S_e	Microphone electrical sensitivity
S_m	Microphone mechanical sensitivity
S_{meas}	Microphone measured sensitivity
S_{open}	Microphone open-circuit sensitivity
T	Tension in the membrane
T_{max}	Maximum Kinetic Energy
U_{max}	Maximum Potential Energy
V_o	Bias voltage (Polarizing voltage)
V_L	Output voltage
u	displacement vector
W	Transverse plate deflection
x	Dimensionless plate Cartesian coordinates [ξ/a]
y	Dimensionless plate Cartesian coordinates [η/b]
α	Plate aspect ratio
ε_o	Dielectric constant of air
ν	Poisson's ratio for the plate material
ρ	Mass density of plate material
ω	Natural frequency of plate vibration
λ	Non dimensional frequency parameter [$\rho h w^2 a^4/D$]
φ	Deflection shape of plate in x direction
ψ	Deflection shape of plate in y direction
ϕ	Deflection shape of plate in x and y directions
ξ,η	Cartesian coordinates
Δd	Change in airgap thickness
ΔP	Change in sound pressure
ΔV	Change in voltage

CHAPTER 1

Introduction and Literature Review

1.1 Introduction

A microphone is a transducer, which converts acoustic signals into electrical signals. Once this conversion has taken place, the sound information is freed from the normal acoustical constraints. Sound waves are inherently short lived and can travel only a relatively short distance before they are attenuated below the limits of audibility. Electric currents by contrast, can be amplified and sent along any required length of wire or they can be modulated onto high-frequency radio waves for 'wireless' transmission around the world and they can be recorded too.

Microphones are ordinary pressure sensors with an optimum behavior in a certain pressure and frequency range. Membranes are an integral part of microphones where the membrane deflects in response to external stimulation. Subminiature microphones need membranes of extremely small dimensions and consequently must have extremely thin membranes since the pressure levels of sound waves are, in general, several orders of magnitude lower than barometric pressures.

A basic performance criterion is the frequency response of the microphone in the acoustic range *i.e* from 0 - 20 kHz.. The size and the boundary

conditions of the diaphragm determine the natural frequency of the diaphragm. A good understanding of the fundamental frequency and modes of the diaphragm is very important in the microphone design, as a very high natural frequency of the diaphragm is desired in order to ensure a good frequency response of the microphone in the audible range of frequencies.

Microphones are normally fabricated with thin aluminum diaphragms using conventional machining techniques. During the last decade, a number of interesting and significant innovations have occurred in the field of acoustic sensors, a term now often used for modern microphones in the audio and ultrasonic ranges. Most prominent were the development in the use of silicon. In the case of subminiature microphones, silicon micromachining technology can be used to obtain the small and controlled air gap, and thin diaphragms. Silicon micromachining has emerged as an extension of integrated circuit (IC) technology. It is a combination of silicon IC technology and precise deep etching, deposition, bonding, interconnections and packaging. Silicon condenser (capacitor) microphones are generally constructed from two wafer chips. One contains the membrane of the microphone and the other forms the backplate. The two wafers can be of silicon, or one of silicon which forms the membrane, and the other of glass wafer which forms the backplate. Between the membrane, which contains the top electrode and the backplate, which contains the back electrode, there is an air gap which completes the capacitor circuit.

1.2 History

The word "Microphone" first appeared in 1827 in Wheatstone's description of an acoustic device. Alexander Graham Bell is generally credited with the invention of the first workable microphone in 1876. Bell's original design proved to be too insensitive but, within a year he had produced an improved magnetic model which can be seen as the basis for telephone ear pieces for the next three-quarters of a century. Other inventions built and patented alternative transducer designs during 1877. The inventions of vacuum tubes or 'valves' and other refinements led to regular radio broadcasting from about 1920 onwards and intensified microphone research. Numerous physical phenomena have been used to convert acoustic energy into electrical energy. These include electromagnetic induction, the piezoelectric effect, magnetostriction, variation in the capacitance in the condenser, and variation in the resistance of packed carbon granules. Carbon microphones are noisy, have limited dynamic range, and produce high levels of distortion. In 1917 Wente introduced a microphone which relied on electrostatic charges. It consisted of a thin conductive diaphragm and a back plate separated by a narrow air gap to form a capacitive (condenser) microphone. In the early years of this century the principle of magnetic induction was applied to moving coil and ribbon devices. Their refinement over the last seventy years has formed the basis of the present day microphone art. Piezo-electric effects in transducers are a relatively recent development, dating from work on Rochelle-salt crystals by Sawyer in 1931.

During the thirties the capacitor microphone thrived in Europe, and made a significant impact on American recording practice after the world war I. In

the late 1940's, capacitor microphones, because of their extended high frequency response, were used with the introduction of tape recording and long playing records because magnetic microphones had frequency response limitations. The 1950's and 1960's saw the introduction of numerous excellent magnetic devices with extended response, and today's microphone needs are drawn heavily from magnetic and capacitive microphone types. In the last ten years demands have increased for all types of microphones which resulted in improved mass production techniques and the development of better materials. Today microphones are everywhere. They are part of our day to day life, as every telephone has a microphone.

1.3 Scope of the Present Investigation

In the present study, a new silicon microphone concept based on a capacitive measurement principle with external bias and a diaphragm in monocrystalline silicon is described.

The objectives of the present investigation are:

1. To develop suitable models of different shapes of microphone diaphragms, and obtain their natural frequencies and mode shapes in order to analyze their responses as acoustic devices.
2. Design, Fabrication and Testing of micromachined silicon condenser microphone with the chosen configuration.

The fundamental elements of a condenser microphone comprise a diaphragm, backplate, airgap, and rear cavity. The diaphragm may be modelled to be working either in the membrane mode or a plate mode, with tensile force and bending forces that determine the sensitivity to sound pressure. In our investigations, the diaphragm is considered to be working in the plate mode, since a stress free diaphragm is used in the fabrication of the condenser microphone.

One of the basic characteristics of the microphone is the cut-off frequency. A very high natural frequency of the diaphragm is desired in order to ensure a good frequency response of the microphone in the acoustic range of frequencies. The size of the membrane, its boundary conditions, the air gap losses and the structure of the backplate, determine the cut-off frequency. In order to analyze any system for its response behavior due to a particular loading, it is essential to obtain the characteristic properties of the system in terms of the natural frequencies, mode shapes and damping. This is done by solving a free vibration problem. In the case of plates, exact natural frequencies and normal modes information are available only for plates which are simply supported at least on one pair of opposite edges. When this is not true, approximate techniques such as the Rayleigh Ritz method or Finite Element Method must be used to obtain the natural frequency and normal modes. Since the normal modes affect the resulting response significantly, considerable effort is devoted in this thesis in developing techniques that obtain better approximation for the natural frequencies and normal modes for plate type structures considered in the study. Both the Rayleigh Ritz method and the Finite Element Method are used in the present study. Square, circular and Hexagonal plate frequency parameters and mode shapes are

presented. Also presented are the analysis for the above plates with cutout and abrupt change in thickness as a preliminary study for the optimization of the backplate electrode in future considerations. Results from these methods are used to find the fundamental frequency of the silicon diaphragm. The fundamental frequency of the diaphragm should be more than the audible frequency range of 20 kHz.

Silicon micromachining techniques are applied to design the fabrication process for the condenser microphone. Lithographic techniques along with deep etching, metalization and anodic bonding are used to manufacture the condenser microphone with specially shaped backplates. The designed fabrication process consists of three masking steps only. Different shapes and sizes of condenser microphone are fabricated by having the depth of air gap and side volume cavity constant. The fabricated microphone is tested for its frequency response and sensitivity and investigates the effect of different shapes of fabricated microphone on the frequency response, sensitivity and coherence. The introduction of silicon technology allows accurate control of dimensions, a high degree of miniaturization, and batch fabrication of microphones at low cost and with good reproducibility.

Chapter 2, presents the condenser microphone principle. It explains the fundamental elements of the condenser microphone and the principle of capacitance.

Chapter 3, presents the free vibrational analysis of the plates. Square circular and Hexagonal plate frequency parameters and mode shapes are presented. Also presented are the analysis for the above plates with cutout

and abrupt change in thickness. The analytical results are compared with existing literature results. As stated earlier Rayleigh Ritz and Finite Element Methods are used to obtain the natural frequency and mode shapes. Results from this methods are used to find the fundamental frequency of the silicon diaphragm.

Chapter 4, presents the design of the condenser microphone. The effect of the diaphragm thickness, diaphragm size, airgap, back electrode shape and volume of rear cavity for capacitive measurement and sensitivity are discussed.

Chapter 5, presents the sequenca of the process required for the fabrication of the condenser microphone. The condenser microphone is fabricated using micromachining techniques.

Chapter 6, presents the characterization of the fabricated condenser microphone. The frequency response and sensitivity of the different shapes of fabricated condenser microphone are obtained experimentally and compared with those of similar condenser microphone from the technical literature.

Chapter 7, presents the conclusions and suggestions for future work.

Appendix A-E presents the description of the Metalization process, lithographic techniques, anodic bonding process, wet chemical etching, and frequency response functions respectively.

1.4 Literature Review

1.4.1 Literature Review for the Vibration of Plates

The flexural vibration of rectangular plates by using beam vibration mode shapes as admissible functions in both the Rayleigh and Rayleigh-Ritz methods of analysis has been treated extensively by Young [1], Leissa [2], and Dickinson [3]. There is no exact solution for the vibration problem of rectangular plates unless at least two opposite edges of the plate are simply supported and hence approximate methods are adopted. Rayleigh-Ritz is one such method where using assumed shaped functions satisfying the boundary conditions, the system of equations is reduced to an eigenvalue problem. The solution of this problem provides the natural frequency coefficients and natural modes. The convergence and accuracy of the Rayleigh-Ritz method has been discussed by various authors including Trefftz [4], Courant [5], and Colatz [6].

While the Rayleigh-Ritz method is well known, it is not been used as much as might be expected for plate vibration problems. This is probably due, at least in part, to a great amount of computational labour which is required both to set up and solve the necessary equations. The amount of computation involved depends upon the set of functions that are used to represent the plate deflection. For these functions, some investigators have used combinations of the characteristic functions which define the normal modes of vibration of a uniform beam. Gorman [7] obtained a general analytical solution for the vibration of rectangular plates supported on their lateral surface by symmetrically distributed point supports. Bassily and Dickinson

[8] used degenerated beam functions to study flexure problems concerning static deflections or free vibration of plates involving free edges. An alternate set of admissible functions, derived from the mode shapes of vibration of plates having two parallel edges simply supported and boundary conditions on the other two edges appropriate for the plate under considerations, was suggested by Dickinson and Li [9]. Even though these functions, which were called "the simply supported plate functions" provided superior results for plates supported in some manner along all four edges, they did not yield satisfactory results when some of the plate edges were free. Laura [10] used 'polynomials co-ordinate functions" to approximate the fundamental natural frequencies of systems. Goldfracht and Rosenhouse [11] used a bipolynomial series to approximate the deflection shapes of plates and obtained the natural frequencies and mode shapes of plates with clamped boundaries with partial rotational flexibility of the edges employing Garlekin's method. They provided explicit algebraic expressions for the first nine modes. Bhat [12] proposed a set of beam characteristic orthogonal polynomials that can be used as plate deflection functions to obtain the natural frequencies and mode shapes of rectangular plates in Rayleigh-Ritz method. He showed that the use of these orthogonal polynomials yields excellent results for the natural frequencies of several example plates having various boundary conditions. The excellence of the functions was further established by Dickinson and DiBlasio [13] who conducted a convergence study of the method. They included the effect of special orthotropy and in-plane loading in their studies. These orthogonal polynomials for the beam are constructed using the Gram-Schmidt process, the first member of the set satisfying both the geometrical and natural boundary conditions of the beam and all the rest satisfying the geometrical boundary conditions.

A finite element analysis of a clamped plate with different cut-out sizes, along with experiments using holographic interferometry, was carried out by Monahan et. al [14]. Paramasivam [15] used a finite difference approach after adopting a grid framework in analyzing the effects of openings on the fundamental frequencies in plates with simply supported and clamped boundary conditions. The dynamic characteristics of the rectangular plates with one and two cut-outs using a finite difference formulation based on variational principles are obtained by Aksu and Ali [16], along with experimental verifications. In the case of composite plates with cut-outs, Rajamani et. al [17] used an assumption that the cut-out is like a displacement dependent external loading. They studied both isotropic and anisotropic plates with varying cut-out sizes in the case of plates with simply supported and clamped boundary conditions. An analysis of plates with cut-out and abrupt change in thickness (added mass) by a modified Rayleigh Ritz method was utilized by Lam et. al [18] by dividing the total domain into smaller areas, where the boundary conditions of the segments were applied more exactly. Tham et. al [19] used the negative stiffness approach to study the free vibration and buckling of plates with abrupt change in thickness.

Exact solutions for the circular plates having classical boundary conditions for clamped, free, or simply supported were obtained in terms of Bessel functions by several investigators. Among these investigators were: Rajalingham et al [20], who obtained the natural frequency parameters and the mode shapes for fully clamped circular plates; Itao and Crandall [21], who obtained natural frequency and the mode shapes for free circular plates; and Leissa and Narita [22], who presented the natural frequency for simply supported circular plates. Approximate natural frequency were obtained by

numerical approaches by Sato [23], Narita [24], and Kim and Dickinson [25] for completely free circular plates, Wah [26], Jones [27], John [28], and Kim and Dickinson [25] for simply supported circular plates, Jones [27], John [28], Rajalingham et al [29] and Kim and Dickinson [25] for fully clamped circular plates. Single variable orthogonal polynomials were used in Rayleigh Ritz method by Rajalingham et al [29] for clamped circular plates and Kim and Dickinson [25] for thin circular and annular plates. Vogel and Skinner [30] obtained exact solutions for the natural frequency parameter of isotropic annular plates with various combinations of the classical boundary conditions. A coordinate transformation for the analysis of axisymmetric vibration of annular plates was studied by Vijaykumar and Ramaiah [31].

In the present study, vibration of square plates with square cut-outs, circular plates with circular cut-outs (annular plates), square and circular plates with abrupt change in thickness, is studied by assuming boundary characteristic orthogonal polynomials functions proposed by Bhat [12, 32], and Lam [33] as assumed plate deflections shape functions satisfying the boundary conditions along the plate outer edges. Results from this methods are used to find the fundamental frequency of the silicon diaphragm.

1.4.2 Literature Review for the Condenser Microphone

During the last decade, a number of interesting and significant innovations have occurred in the field of acoustic sensors, a term now often used for

modern microphones in the audio and ultrasonic ranges. Most prominent development has been the use of micromachined silicon in microphones.

The progress in the field of silicon transducers can be attributed to a systematic application of the methods of micromechatronics to the production of tiny sensor structures. Acoustic silicon sensors are made with the methods of silicon technology, as they are customary for the production of micro electronic components [34]. Among these methods are doping, deposition, oxidation, and lithography processes and, as key technologies, anisotropic etching such as plasma etching or wet chemical etching. The utility of the wet-chemical methods is, among others, based on the fact that the etch rates of silicon dioxide or properly doped silicon are considerably smaller than those of silicon. The anisotropic etching methods allow one to produce holes, pits, recesses, membranes and cantilever beams. The method in their entirety, if used to make such structures, are referred to as micromachining. If micromachined sensors are combined with electronic components for signal processing on the same chip, integrated sensors are obtained.

The first microphone fabricated with silicon micromachining techniques was presented by Royer et al [35] in 1983. It has been followed successfully by others [36-51]. The silicon microphones are based on the piezoelectric [35-37], piezoresistive [38], and capacitive principles [39-51]. Most of the silicon microphones presented in the literature are based on the capacitive principle. The capacitive microphones can be divided into electret microphones [39-41], which are biased by a built-in charge, and condenser microphones [41-51] which have to be biased by an external voltage source.

A capacitive microphone usually consists of a thin flexible diaphragm mounted on a rigid back-plate. The backplate is provided with acoustic holes or a capillary vent on its side to allow air to flow in and out of the air gap. The backplate of conventional microphones is made of stainless steel, but in modern versions it is fabricated from glass [43,45] or from <100> silicon wafers [40-42,46-47]. In the latter case anisotropic etching in a KOH solution is used to form the air gap and the acoustic holes. Various methods have been applied for fabrication of diaphragm structures. The diaphragm of the silicon microphone of Sprenkles et al. [40] consists of a thin mylar foil, which is attached manually on the backplate and fixed by a polymer spray. Murphy et al [41] used a polyester diaphragm that was mounted on a separate support wafer before microphone assembly. In other microphones, the diaphragm and backplate are fabricated on separate wafers, which have to be bonded later on. Several bonding techniques have been investigated, like anodic bonding [43,45], bonding to silicon to oxide [50] or glueing [42,44,46]. In this way, thin film diaphragm materials can be used as a diaphragm. Homm and Hess [42] and Kuhmel and Hess [46] used 150 nm thick low pressure chemical Vapour Deposited (LPCVD) silicon nitride films as a diaphragm. Bergqvist et al. [43,50] fabricated silicon diaphragm by applying the electro-chemical etch-stop techniques, where as Bourouina et al [45] fabricated silicon diaphragm by using the p^+ etch-stop technique.

Bonding of diaphragm with backplate can be avoided by fabricating the microphones on a single wafer, this process is based on the well-known sacrificial layer technique. With this technique, the thickness of the air gap is determined by the thickness of the sacrificial layer, which is typically between 1 to 3 μm. This narrow air gap resulted in very high air streaming

resistance, thus causing a bad microphone sensitivity for audio frequencies [51]. Other authors have solved this problem by etching grooves or holes in the backplate with a large number of acoustic holes [45,50]. In our present investigations, silicon micromachining techniques are applied to design the fabrication process for the condenser microphone. The fabricated microphone is tested for its frequency response and sensitivity and investigates the effect of different shapes of fabricated microphone on the frequency response, sensitivity and coherence.

Chapter 2 discusses the principle of working of the condenser microphone.

CHAPTER 2

Condenser Microphone Principle

2.1 Condenser Principle

Condenser microphone consists of two parts which form the two electrodes, a thin diaphragm and the backplate, separated by a thin narrow air gap. The capacitance between these two electrodes varies as the thin diaphragm is deflected with respect to the fixed backplate electrode by acoustic pressure variations in air (Fig. 2.1). A quasi-constant charge Q is established when a polarizing voltage is applied across the two electrodes via a very high resistance R. The capacitance of the assembly is given by

$$C = \varepsilon_0 A/d \qquad (2.1)$$

where ε_0 is the dielectric constant of air, A is the effective diaphragm area and d is the electrode spacing (gap).

The voltage across the capacitor is given by

$$\begin{aligned} V &= Q/C \qquad (2.2) \\ &= (Q/\varepsilon_0 A)d \end{aligned}$$

When a sound wave impinges upon the diaphragm, the resulting displacement of the latter alters the electrical capacitance C of the microphone, causing a signal voltage V_L to appear across the load resistor R_L.

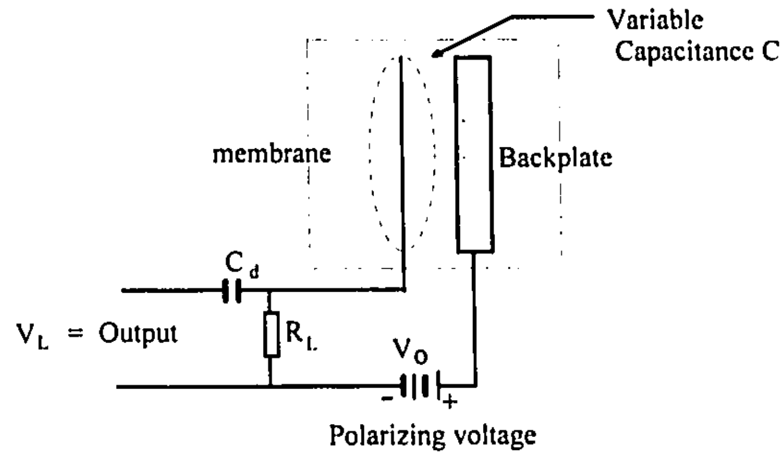

Fig. 2.1. Condenser Microphone basic principle.

Let us assume that the capacitance at any instant is given by

$$C = C_o + C_l \sin\omega t \tag{2.3}$$

where C_o is the capacitance in the absence of any applied pressure, and C_l is the amplitude of the change in capacitance resulting from the application of a sinusoidal pressure variation. In the above circuit of Fig. 2.1

$$V_o - iR_L = \frac{\int i dt}{C} \tag{2.4}$$

Substitution of equation (2.3) into equation (2.4) and differentiation with respect to time t gives

$$(C_o + C_l \sin\omega t)R_L \frac{di}{dt} + (1 + R_L C_l \omega \cos\omega t)i - V_o C_l \omega \cos\omega t = 0 \tag{2.5}$$

A series solution of this equation is most readily obtained by assuming

$$i = \sum A_n sin(n\omega t + \phi_n) \tag{2.6}$$

In all practical condenser microphones $C_1 << C_0$, even for very intense sounds, and consequently the amplitudes $A_2, A_3, A_4, \ldots$ of the higher harmonic overtones are negligible compared to A_1. Then

$$i \approx \frac{V_o C_1 \, sin(\omega t + \phi_1)}{C_o \sqrt{(1 / wC_o)^2 + R_L^{\,2}}} \tag{2.7}$$

where

$$tan\phi_1 = 1 / \omega C_o R_L \tag{2.8}$$

The voltage drop across the resistor R_L resulting from this current is

$$V_L = R_L i = \frac{V_o C_1 R_L \, sin(\omega t + \phi_1)}{C_o \sqrt{(1 / \omega C_o)^2 + R_L^{\,2}}} \tag{2.9}$$

Equation 2.9, indicates that a condenser microphone may be considered as equivalent to a generator having an open circuit voltage amplitude

$$V_L = \frac{V_o C_1}{C_o} \tag{2.10}$$

and an internal capacitance impedance $1 / j\omega C_o$.

When the diaphragm vibrates in response to the incident sound-pressure wave, the applied DC polarizing voltage will be effectively modulated by an AC component in linear relationship to the diaphragm vibrations. This AC

component is taken through the DC-blocking coupling capacitor C_d to provide the microphone's output signal. The use of a low-loss air dielectric and the basic simplicity of the generator mechanism make the condenser microphone a potentially quiet and linear transducer. The linear relationship between E and d means that it is a constant-amplitude device. The two factors, *viz.* the very narrow gap needed for adequate sensitivity and the very high impedance represented by the microphone capacitance of only 25-50 pF of conventional microphone [52], calls for high precision in fabrication. The high -impedance head amplifier located as close to the electrodes as possible, increases the cost and complexity of design. These two factors are ensured with the micromachining technology where the narrow gap needed is accomplished by the wet chemical etching process which is a high precision process, and the high-impedance amplifier head can be easily located near the electrodes. A field effect transistor (FET) can be used as head amplifier, which can directly be manufactured on to the silicon chip having the silicon diaphragm. Micromachining is batch manufacturing technology, which will provide a high uniformity of the integrated condenser microphones along with a high reliability at a very low cost.

Chapter 3 is on the vibration analysis of plates.

CHAPTER 3

Vibration Analysis of Plates

3.1 General

One of the basic characteristic of the microphones is the natural frequency of the whole structure. The size of the membrane and its boundary conditions determine the natural frequency of the membrane. A very high natural frequency of the membrane is desired in order to ensure a good frequency response in the acoustic range of frequencies. It is desirable to place the mechanical resonance well above the working frequency range, which is relatively simple in view of the low mass of the membrane. The cutoff frequency is directly related to the natural frequency and consequently related to the size and the boundary conditions provided for the vibrating membrane. The fundamental resonance frequency is placed at the upper limit of the frequency range of the condenser microphone. There is a possibility to use the diaphragm working either in the **plate mode** or the **membrane mode** with bending forces or tensile forces respectively, that determine the sensitivity to sound pressure.

Plates:

Circular Plates: The circular plates are assumed to be of uniform cross section, under no tension and are clamped . The fundamental frequency is given by [56],

$$f = \frac{0.469\,h}{R^2}\sqrt{\frac{E}{\rho(1-\nu^2)}} \qquad (3.1)$$

where

f = frequency in Hz

h = thickness of the plate, in centimeters,

R = radius of the plate up to clamping boundary, in centimeters,

ρ = density in grams per cubic centimeters

ν = Poison's ratio

E = Young's modulus in dynes per square centimeter.

Square plate: The fundamental frequency of a square plate clamped on its sides is given by [56]

$$f = \frac{1.6533h}{a^2}\sqrt{\frac{E}{\rho(1-\nu^2)}} \quad \text{(c/s)} \qquad (3.2)$$

where

a = side of the plate up to clamping boundary, in centimeters,

Membrane: The ideal membrane is assumed to be flexible and very thin in cross section , and stretched in all direction by a force which is not affected by the motion of the membrane.

Circular membrane: The fundamental frequency of a circular stretched membrane rigidly clamped at its circumference is given by [56]

$$f = \frac{0.382}{R}\sqrt{\frac{T}{M}} \qquad \text{(c/s)} \qquad (3.3)$$

where

M = mass, in grams per square centimeter of area,

R = radius of the membrane, in centimeters

T= tension, in dynes per centimeter.

The fundamental vibration is with the circumference as a node and a maximum displacement at the center of the circle.

Square membrane: The fundamental frequency of a square stretched membrane is given by [56]

$$f = \frac{0.705}{a}\sqrt{\frac{T}{M}} \qquad \text{(c/s)} \qquad (3.4)$$

where

M = mass, in grams per square centimeter of area,

a = length of a side, in centimeters

T = tension, in dynes per centimeter.

The square and circular plates with and without cutout, and also plates with abrupt change in thickness is studied using the energy method and finite element method. The natural frequencies and mode shapes of the plate with clamped boundary conditions for different cutout size and abrupt change in thickness are calculated and are compared with the available results.

3.2 Rayleigh Ritz Method

The Rayleigh-Ritz method is widely used to obtain the approximate values for the natural frequencies and mode shapes of structures [1]. The method is based on the conservation of energy in undamped structures undergoing vibration and provides upper bound values for the system natural frequencies. In this method, a deflection shape of the form

$$W(x,y) = \sum_{i=1}^{N} C_i \phi_i(x,y) \tag{3.5}$$

is assumed initially, where ϕ_i are admissible functions satisfying atleast the geometric boundary conditions and $C_1, C_2, \ldots\ldots\ldots C_i$, are arbitrary constant coefficients. The function ϕ_i must form a complete set to represent all the modes of vibration. In limiting this set to a finite number of functions, the analysis can be interpreted as approximating a continuous system into a multidegree of freedom discrete systems. The coefficients are adjusted by minimizing the frequency with respect to each of the coefficient. This results in N algebraic equations in terms of the N unknown coefficients, C_i, involving ω^2, the frequency of vibration. The solution of these equation then gives the natural frequencies and associated mode shapes of the system.

For a conservative system, the maximum kinetic energy in the system undergoing vibration is equal to the maximum strain energy. However since the assumed shape is not exact, the kinetic energy (T_{max}) will not be equal to strain energy (U_{max}), and hence the error can be taken as

$$F(C_i,\omega) = U_{max} - T_{max} \tag{3.6}$$

The coefficients C_i must be chosen so as to minimize the error and hence

$$\frac{dF}{dC_i} = \frac{d}{dC_i}(U_{max} - T_{max}) = 0 \tag{3.7}$$

$$\frac{\partial U_{max}}{\partial C_i} - \left[\omega^2 \frac{\partial T^*_{max}}{\partial C_i} + T^*_{max}\frac{\partial \omega^2}{\partial C_i}\right] = 0$$

where

$$T_{max} = \omega^2 T^*_{max}$$

Since ω^2 must be stationary with respect to C_i, we have $\frac{\partial \omega^2}{\partial C_i} = 0$, which gives

$$\frac{\partial U_{max}(C_i)}{\partial C_i} - \omega^2 \frac{\partial T^*_{max}(C_i)}{\partial C_i} = 0 \tag{3.8}$$

Equation (3.8) can also be written as

$$[K]\ \{C_i\} - \omega^2[M]\ \{C_i\} = 0$$

where

$$[M] = \frac{\partial T^*_{max}}{\partial C_i} = \text{Mass Matrix}$$

$$[K] = \frac{\partial U_{max}}{\partial C_i} = \text{Stiffness Matrix} \qquad i = 1,2 \ldots\ldots N$$

This is a standard eigenvalue problem and the solution yields the natural frequencies and the corresponding coefficients can be used in Eq.(3.5) to obtain the approximate mode shapes.

3.3 Orthogonal Polynomials

3.3.1 General

It is necessary to use shape functions satisfying at least the geometrical boundary conditions for the application of Rayleigh Ritz method. These shape functions when substituted in the kinetic and potential terms produce cross terms in the mass and stiffness matrices. The matrices become ill conditioned and pose numerical problem in solving for eigenvalues when more number of these terms are considered.

To overcome this problem, Bhat [12] and Lam [33] proposed a set of orthogonal polynomials for use in Rayleigh Ritz method as admissible function for dynamic and static problems of beams, rectangular plates with classical boundary condition.

3.3.2 Generation of Single Variable Orthogonal Polynomial

The orthogonal polynomial are generated along both in the x and y directions, by Gram-Schmidt process. Along x direction, given a polynomial $\varphi_1(x)$, an orthogonal set of polynomials in the interval $a \le x \le b$ can be generated using Gram-Schmidt process as follows [53].

$$\varphi_2(x) = (x - B_2)\varphi_1(x) \tag{3.9}$$

$$\varphi_k(x) = (x - B_k)\varphi_{k-1}(x) - C_k\varphi_{k-2}(x) \tag{3.10}$$

where

$$B_k = \frac{\int_a^b x f(x)\varphi_{k-1}^2(x)dx}{\int_a^b f(x)\varphi_{k-1}^2(x)dx}$$

$$C_k = \frac{\int_a^b x f(x)\varphi_{k-1}(x)\varphi_{k-2}(x)dx}{\int_a^b f(x)\varphi_{k-2}^2(x)dx}$$

where $f(x) =$ is the weighting function

The polynomials $\varphi_k(x)$,satisfy the orthogonality function

$$\int_a^b f(x)\varphi_k(x)\varphi_l(x)dx = 0 \quad if\ k \neq l \qquad (3.11)$$
$$= a_{kl} \quad if\ k = l$$

In the present application, since the plates are uniform, the weight function $f(x)$ is unity. The interval is from *0 - 1*, and the coefficients of the polynomial are chosen in such a way as to make the polynomials orthonormal.

$$\int_0^1 \varphi_k^2(x)dx = 1 \qquad (3.12)$$

The starting function $\varphi_1(x)$ is chosen as the simplest polynomial of the least degree that satisfies all the boundary condition of the beam problem accompanying the plate problem. Even though $\varphi_1(x)$ satisfies all the boundary conditions, both geometric and natural, the other members of the orthogonal set satisfy only the geometrical boundary conditions, which can be easily checked from the way the set is constructed by using Eqs. (3.9 and 3.10)

Procedure for the generation of the first member polynomial for a plate clamped on its sides (CCCC).

The boundary condition of the plate with all edges clamped:

$$W(0) = W'(0) = W(1) = W'(1) = 0 \tag{3.13}$$

Both the accompanying beam problems have the same boundary conditions. Assuming the beam deflection function as

$$W(x) = a_0 + a_1x+a_2x^2+a_3x^3+a_4x^4 \tag{3.14}$$

and applying the boundary condition of Eq.(3.13) gives the deflection shape as

$$W(x) = a_4\,(x^2-2x^3+x^4) \tag{3.15}$$

where a_4 is an arbitrary constant. The normalized mode function is obtained as

$$\varphi_0(x) = \frac{(x^2-2x^3+x^4)}{\left(\int_0^1 (x^2-2x^3+x^4)^2\,dx\right)^{1/2}} \tag{3.16}$$

3.3.3 Generation of Two Variable Orthogonal Polynomials:

The two orthogonal polynomial are generated along both in the x and y directions, by Gram-Schmidt process. Along x and y direction, given a polynomial $\phi_1(x,y)$, an orthogonal set of polynomials over the plate domain A can be generated using the recurrence formula [53]

$$\phi_m(x,y) = f_m(x,y)\phi_1(x,y) - \sum_{i-1}^{m-1}\psi_{m,i}\phi_i(x,y); \qquad m > 1. \tag{3.17}$$

where

$$\psi_{m,i} = \frac{\iint_A f_m(x,y)\varepsilon(x,y)\phi_1(x,y)\phi_i(x,y)dxdy}{\iint_A \varepsilon(x,y)\phi_i^2(x,y)dxdy}$$

in which $\varepsilon(x,y)$ denotes a weighting function and $f_m(x,y)$ is a generating function chosen to ensure that the higher order orthogonal plate functions satisfy at least the geometrical boundary conditions. The generated set of orthogonal plate functions satisfy the orthogonality condition.

$$\iint_A \varepsilon(x,y)\phi_i(x,y)\phi_j(x,y)dxdy \begin{cases} = 0, & i \neq j \\ = \delta_{ij}, & i = j \end{cases} \tag{3.18}$$

The weighting function is taken as unity in the present study.

Procedure for the generation of the first member polynomial for a circular plate clamped on its periphery.

For a plate with clamped periphery, the geometrical boundary conditions which need to be satisfied are

$$\phi_1(x,y) = 0, \qquad \frac{\partial \phi_1(x,y)}{\partial n} = 0 \tag{3.19}$$

Assuming the deflection function as

$$W(x) = a_0 + a_1x + a_2y + a_3x^2 + a_4xy + a_5y^2 \ldots\ldots \tag{3.20}$$

and applying the boundary condition of Eq.(3.19) gives the starting function as

$$\phi_1(x,y) = (1-x^2-y^2)^2 \tag{3.21}$$

3.4 Analysis of the Rectangular Plate

The maximum kinetic and potential energies of a thin plate during small amplitude, simple harmonic vibration are given by [1]

$$T_{max} = \frac{1}{2}\rho h\omega^2 \iint_A W^2(x,y)dxdy \tag{3.22}$$

$$U_{max} = \frac{1}{2} D \iint_A \left\{ \left(\frac{\partial^2\omega}{\partial x^2} + \frac{\partial^2\omega}{\partial y^2} \right)^2 - 2(1-\upsilon)\left[\frac{\partial^2\omega}{\partial x^2} + \frac{\partial^2\omega}{\partial y^2} - \left(\frac{\partial^2\omega}{\partial x \partial y} \right)^2 \right] \right\} dxdy \tag{3.23}$$

respectively, where ρ is the density of the plate material, h is the thickness of the plate, D is the flexural rigidity of the plate, E is the modulus of elasticity, and ν is the Poisson's ratio, ω is the angular frequency of vibration, $W(x,y)$ is the deflection shape function of the plate, and the integration is carried over the entire plate domain A.

3.4.1 Rectangular Plate

The deflection of the rectangular plate as shown in Fig. 3.1 undergoing flexural vibration can be described by the product of beam characteristic orthogonal polynomials in separable form [12].

$$W(x,y) = \sum_m \sum_n A_{mn}\varphi_m(x)\psi_n(y) \tag{3.24}$$

Geometrical boundary conditions are satisfied by the admissible function φ_m and ψ_n. The functions φ_m and ψ_n must form a complete set to represent all the mode of vibrations. A_{mn} are the arbitrary constants coefficients. The lengths along the coordinate axes ξ and η are normalized with respect to its lengths as, $x=\xi/a$ and $y=\eta/b$.

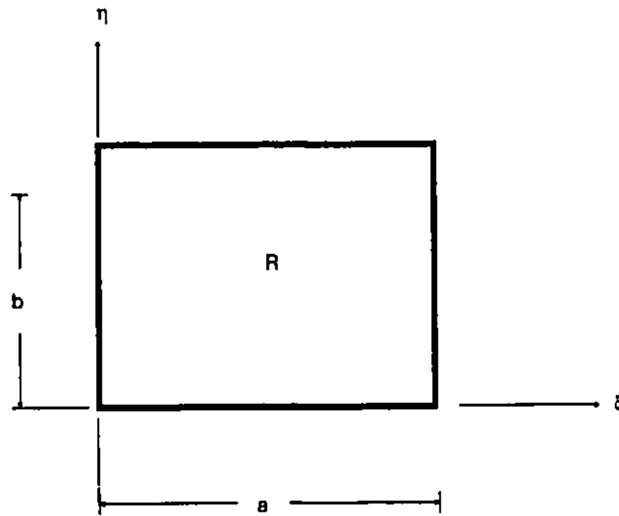

Fig. 3.1 Rectangular plate

The kinetic and potential energy expressions of the plate is given by [1]

$$T_{max} = \frac{1}{2}\rho hab\omega^2 \iint_R W^2(x,y)dxdy \tag{3.25}$$

$$U_{max} = \frac{1}{2}Dab\iint_R [W^2{}_{xx} + \alpha^4 W^2{}_{yy} + 2\nu\alpha^2 W_{xx}W_{yy} + 2(1-\nu)\alpha^2 W^2{}_{xy}]dxdy \tag{3.26}$$

where α is the side ratio a/b, The subscripts x etc., refer to the differentiation with respect to the variable x etc., and the number of times the subscript appears denotes the order of differentiation, and the integration is carried over the entire plate domain R.

Substituting the deflection function (Eq. 3.24) in the kinetic and potential energy expressions for the plate, the Rayleigh's quotient is obtained as $\omega^2 = U_{max} / T^*_{max}$ where $T_{max} = \omega^2 T^*_{max}$. Minimizing the Rayleigh quotient with respect to the undetermined coefficient A_{mn} yields an eigenvalue equation,

$$\sum_m \sum_n [K_{mnij} - \lambda M_{mnij}] A_{mn} = 0 \tag{3.27}$$

where

$$K_{mnij} = E^{(2,2)}_{mi} F^{(0,0)}_{nj} + \alpha^4 E^{(0,0)}_{mi} F^{(2,2)}_{nj} + \nu\alpha^2 [E^{(0,2)}_{mi} F^{(2,0)}_{nj} + E^{(2,0)}_{mi} F^{(0,2)}_{nj}] + 2(1-\nu)\alpha^2 E^{(1,1)}_{mi} F^{(1,1)}_{nj}$$

$$M_{mnij} = E^{(0,0)}_{mi} F^{(0,0)}_{nj}$$

$$E^{(r,s)}_{mi} = \int_0^1 (d^r\varphi_m / dx^r)(d^s\varphi_i / dx^s)dx$$

$$F^{(r,s)}_{nj} = \int_0^1 (d^r\psi_n / dy^r)(d^s\psi_j / dx^s)dy$$

$\alpha = a/b$, $\quad m,n,i,j = 1,2,3,........,$ $\quad \lambda = \rho h\omega^2 a^4/D,$ $\quad r,s = 0,1,2$

The solution of the eigenvalue equation will yield the natural frequency coefficients (λ) and mode shape (A_{mn}) of the plate.

3.4.2 Rectangular Plate with Opening

The kinetic and potential energy expression of a rectangular plate with opening as shown in figure 3.2 are given by

$$T_{max} = \frac{1}{2}\rho hab\omega^2 \iint_{R_l} W^2(x, y)dxdy \tag{3.28}$$

$$U_{max} = \frac{1}{2}Dab\iint_{R_l} [W^2{}_{xx} + \alpha^4 W^2{}_{yy} + 2\nu\alpha^2 W_{xx}W_{yy} + 2(1-\nu)\alpha^2 W^2{}_{xy}]dxdy \tag{3.29}$$

where the integration is carried over the plate domain R_l

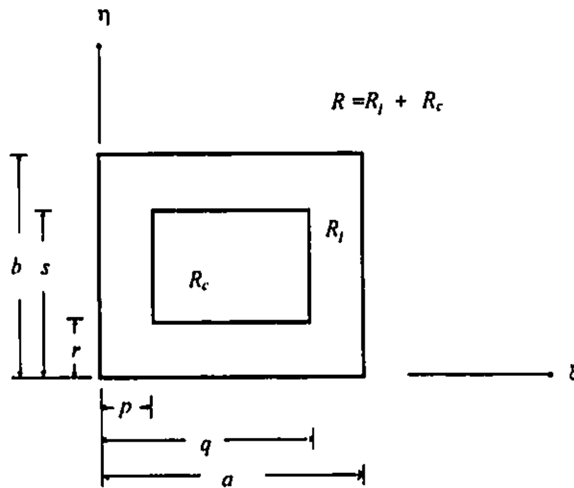

Fig. 3.2 Rectangular Plate with Opening.

The deflection of the plate with cutout undergoing flexural vibration can be expressed in separable form as given by the Eq.(3.24). Substituting the deflection function in the kinetic and potential energy expressions, and minimizing the Rayleigh quotient with respect to the coefficient A_{mn} yields an eigenvalue equation,

$$\sum_m \sum_n [K_{mnij} - \lambda M_{mnij}] A_{mn} = 0 \tag{3.30}$$

where

$$K_{mnij} = K^{(1)}_{mnij} - K^{(2)}_{mnij}$$
$$M_{mnij} = M^{(1)}_{mnij} - M^{(2)}_{mnij}$$
$$K^{(1)}_{mnij} = E^{1(2,2)}_{mi} F^{1(0,0)}_{nj} + \alpha^4 E^{1(0,0)}_{mi} F^{1(2,2)}_{nj} + \nu\alpha^2 [E^{1(0,2)}_{mi} F^{1(2,0)}_{nj} + E^{1(2,0)}_{mi} F^{1(0,2)}_{nj}] + 2(1-\nu)\alpha^2 E^{1(1,1)}_{mi} F^{1(1,1)}_{nj}$$
$$K^{(2)}_{mnij} = E^{2(2,2)}_{mi} F^{2(0,0)}_{nj} + \alpha^4 E^{2(0,0)}_{mi} F^{2(2,2)}_{nj} + \nu\alpha^2 [E^{2(0,2)}_{mi} F^{2(2,0)}_{nj} + E^{2(2,0)}_{mi} F^{2(0,2)}_{nj}] + 2(1-\nu)\alpha^2 E^{2(1,1)}_{mi} F^{2(1,1)}_{nj}$$

$$M^{(1)}_{mnij} = E^{1(0,0)}_{mi} F^{1(0,0)}_{nj}$$
$$M^{(2)}_{mnij} = E^{2(0,0)}_{mi} F^{2(0,0)}_{nj}$$

$$E^{1(P,Q)}_{mi} = \int_0^1 (d^P \varphi_m / dx^P)(d^Q \varphi_i / dx^Q) dx$$
$$F^{1(P,Q)}_{nj} = \int_0^1 (d^P \psi_n / dy^P)(d^Q \psi_j / dx^Q) dy$$

$$E^{2(P,Q)}_{mi} = \int_p^q (d^P \varphi_m / dx^P)(d^Q \varphi_i / dx^Q) dx$$
$$F^{2(P,Q)}_{nj} = \int_r^s (d^P \psi_n / dy^P)(d^Q \psi_j / dx^Q) dy$$

$\alpha = a/b$, $\quad m,n,i,j = 1,2,3,........$, $\quad \lambda = \rho h \omega^2 a^4/D$, $\quad P,Q = 0,1,2$

The solution of the eigenvalue equation will yield the natural frequency coefficients (λ) and mode shape (A_{mn}) of the plate. The kinetic and potential energies of the plate were calculated by subtracting the energies of the plate calculated over the plate domain R_c from the energies of the plate calculated over the entire plate domain R respectively. R_c is the region of the opening and R is the region of the entire plate without any opening.

3.4.3 Rectangular Plate with Abrupt Change in Thickness

The kinetic and potential energies of the rectangular plate are given by Eqs. 3.25 and 3.26 respectively. For simplicity, expressing these equations in short form

$$T_{max} = \iint_R U dxdy \tag{3.31}$$

$$U_{max} = \iint_R T dxdy \tag{3.32}$$

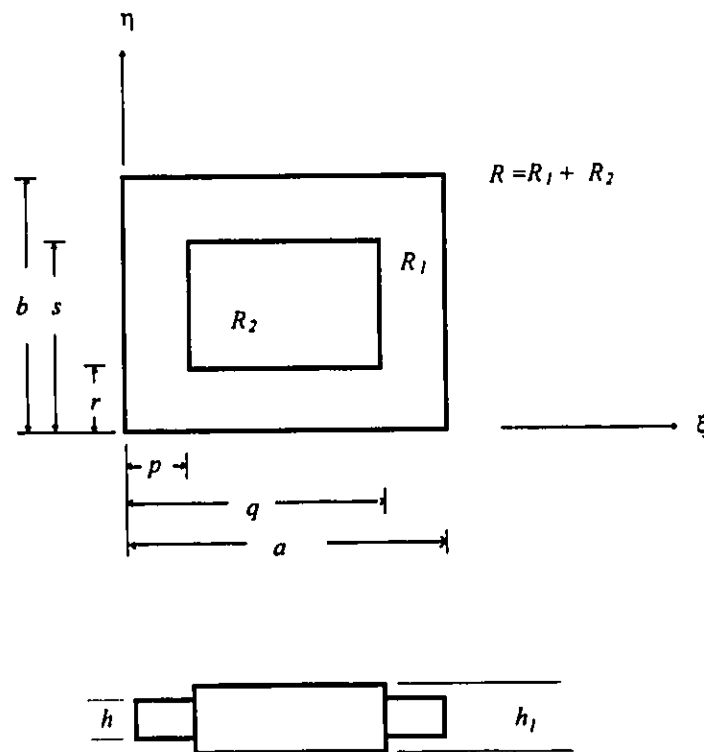

Fig. 3.3 Rectangular Plate with abrupt change in thickness

Then the kinetic and potential energy expression of a plate with abrupt change in thickness are given by

$$
\begin{aligned}
T_{max} &= \iint_{R_1} U dxdy + \iint_{R_2} U_2 dxdy \\
&= \iint_{R} U dxdy + \iint_{R_2} (U_2 - U) dxdy \\
&= \iint_{R} U dxdy + \iint_{R_2} (\beta^3 - 1) U dxdy
\end{aligned}
\tag{3.33}
$$

$$
\begin{aligned}
U_{max} &= \iint_{R} T dxdy \\
&= \iint_{R} T dxdy + \iint_{R_2} (T_2 - T) dxdy \\
&= \iint_{R} T dxdy + \iint_{R_2} (\beta - 1) T dxdy
\end{aligned}
\tag{3.34}
$$

Where R_2 is the region of the abrupt change in thickness and R is the region of the entire plate without any abrupt change in thickness.

The deflection of the plate with abrupt change in thickness undergoing flexural vibration can be expressed in separable form as given by Eq.(3.24) Substituting the deflection function in the kinetic and potential energy expressions, and minimizing the Rayleigh quotient with respect to the coefficient A_{mn} yields an eigenvalue equation,

$$
\sum_{m} \sum_{n} [K_{mnij} - \lambda M_{mnij}] A_{mn} = 0 \tag{3.33}
$$

where

$$K_{mnij} = K_{mnij}^{(1)} - (\beta^3 - 1) K_{mnij}^{(2)}$$

$$M_{mnij} = M_{mnij}^{(1)} - (\beta - 1) M_{mnij}^{(2)}$$

$$K^{(1)}_{mnij} = E^{1(2,2)}_{mi} F^{1(0,0)}_{nj} + \alpha^4 E^{1(0,0)}_{mi} F^{1(2,2)}_{nj} + \nu\alpha^2 [E^{1(0,2)}_{mi} F^{1(2,0)}_{nj} + E^{1(2,0)}_{mi} F^{1(0,2)}_{nj}] + 2(1-\nu)\alpha^2 E^{1(1,1)}_{mi} F^{1(1,1)}_{nj}$$

$$K^{(2)}_{mnij} = E^{2(2,2)}_{mi} F^{2(0,0)}_{nj} + \alpha^4 E^{2(0,0)}_{mi} F^{2(2,2)}_{nj} + \nu\alpha^2 [E^{2(0,2)}_{mi} F^{2(2,0)}_{nj} + E^{2(2,0)}_{mi} F^{2(0,2)}_{nj}] + 2(1-\nu)\alpha^2 E^{2(1,1)}_{mi} F^{2(1,1)}_{nj}$$

$$M^{(1)}_{mnij} = E^{1(0,0)}_{mi} F^{1(0,0)}_{nj}$$

$$M^{(2)}_{mnij} = E^{2(0,0)}_{mi} F^{2(0,0)}_{nj}$$

$$E^{1(P,Q)}_{mi} = \int_0^1 (d^P\varphi_m / dx^P)(d^Q\varphi_i / dx^Q)dx$$

$$F^{1(P,Q)}_{nj} = \int_0^1 (d^P\psi_n / dy^P)(d^Q\psi_j / dx^Q)dy$$

$$E^{2(P,Q)}_{mi} = \int_p^q (d^P\varphi_m / dx^P)(d^Q\varphi_i / dx^Q)dx$$

$$F^{2(P,Q)}_{nj} = \int_r^s (d^P\psi_n / dy^P)(d^Q\psi_j / dx^Q)dy$$

$\alpha = a/b, \quad m,n,i,j = 1,2,3,\ldots\ldots, \quad \lambda = \rho h\omega^2 a^4/D, \quad P,Q = 0,1,2 \quad \beta = h_1/h$

The solution of the eigenvalue equation will yield the natural frequency coefficients (λ) and mode shape (A_{mn}) of the plate.

3.5 Analysis of the Circular Plate

The circular plate under consideration lies in the *x-y* plane having dimensions of $2a$ X $2a$. For a free vibration of plate vibrating harmonically with amplitude $W(x,y)$ and radian frequency ω, the maximum Kinetic and Potential energies of the plate is given by Eqns. 3.22 and 3.23 respectively.

3.5.1 Circular Plate

The expression for the maximum values of kinetic and potential energy of the circular plate as shown in Fig 3.4 are given by [56]

$$T_{max} = \frac{1}{2} m a^2 \omega^2 \iint_R W^2 dxdy \tag{3.34}$$

$$U_{max} = \frac{1}{2} \frac{D}{a^2} \iint_R [\{W_{xx} + W_{yy}\}^2 - 2(1-\nu)\{W_{xx} + W_{yy} - W^2_{xy}\}] dxdy \tag{3.35}$$

where h is the thickness of the plate, D is the flexural rigidity of the plate, E is the modulus of elasticity, ν is the Poisson's ratio and integration is carried over the entire plate domain R. The subscripts x and y refer to the differentiation with respect to the given subscript, and the number of times the subscript appears denotes the order of differentiation. The lengths along the coordinate axes ξ and η are normalized with respect to its diameters as, $x = \xi / a$ and $y = \eta / a$.

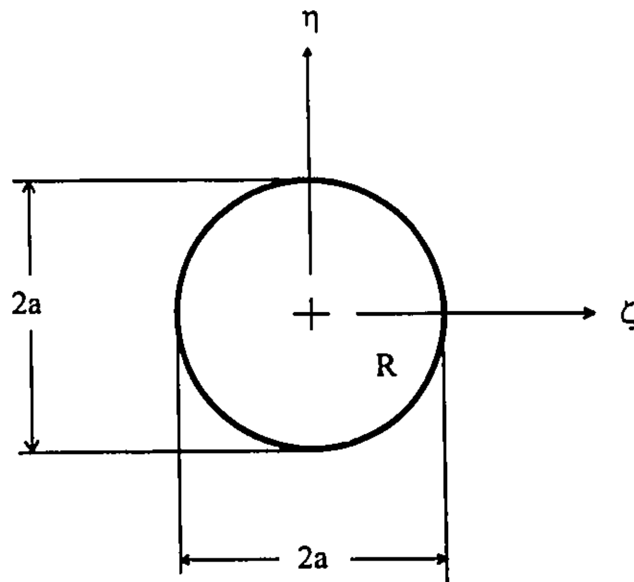

Fig. 3.4 Circular plate

The deflection of the circular plate undergoing flexural vibration can be described by the orthogonal plate functions

$$W(x,y) = \sum_{i=1}^{m} C_i \phi_i(x,y) \tag{3.36}$$

Geometrical boundary conditions are satisfied by the admissible function ϕ_i. C_i are the arbitrary constants coefficients to be minimized. The functions ϕ_i must form a complete set to represent all the mode of vibrations.

Substituting the above deflection function (Eq. 3.36) in the kinetic and potential energy expressions for the circular plate, and minimizing the Rayleigh quotient with respect to the coefficient C_i yields an eigenvalue equation,

$$\sum_{j=1}^{m} [K_{ij} - \lambda M_{ij}] C_i = 0 \tag{3.37}$$

where

$$K_{ij} = C_{ij}^1 + C_{ij}^2 + \nu [C_{ij}^3 + C_{ij}^4] + 2(1-\nu) C_{ij}^5$$
$$M_{ij} = \iint_R \phi_i(x,y)\phi_j(x,y)\,dxdy$$

in which

$$C_{ij}^1 = \iint_R \frac{\partial^2 \phi_i(x,y)}{\partial x^2} \frac{\partial^2 \phi_j(x,y)}{\partial x^2}\,dxdy$$
$$C^2_{ij} = \iint_R \frac{\partial^2 \phi_i(x,y)}{\partial y^2} \frac{\partial^2 \phi_j(x,y)}{\partial y^2}\,dxdy$$
$$C^3_{ij} = \iint_R \frac{\partial^2 \phi_i(x,y)}{\partial y^2} \frac{\partial^2 \phi_j(x,y)}{\partial x^2}\,dxdy$$
$$C^4_{ij} = \iint_R \frac{\partial^2 \phi_i(x,y)}{\partial x^2} \frac{\partial^2 \phi_j(x,y)}{\partial y^2}\,dxdy$$

$$C'_{ij} = \iint_R \frac{\partial^2\phi_i(x,y)}{\partial x\partial y}\frac{\partial^2\phi_j(x,y)}{\partial x\partial y}dxdy$$

$$i = 1,2,3,.....m, \qquad \lambda = \rho h\omega^2 a^4/D$$

The natural frequency and mode shape of the circular plate are obtained by solving the equation (3.37).

3.5.2 Annular Plate

The expression for the maximum values of kinetic and potential energy of an annular plate as shown in Fig 3.5 are given by

$$T_{max} = \frac{1}{2}ma^2\omega^2 \iint_{R_1} W^2 dxdy \tag{3.38}$$

$$U_{max} = \frac{1}{2}\frac{D}{a^2}\iint_{R_1}[\{W_{xx}+W_{yy}\}^2 - 2(1-\nu)\{W_{xx}+W_{yy}-W^2_{xy}\}]dxdy \tag{3.39}$$

where the integration is carried over the annular plate domain R_1.

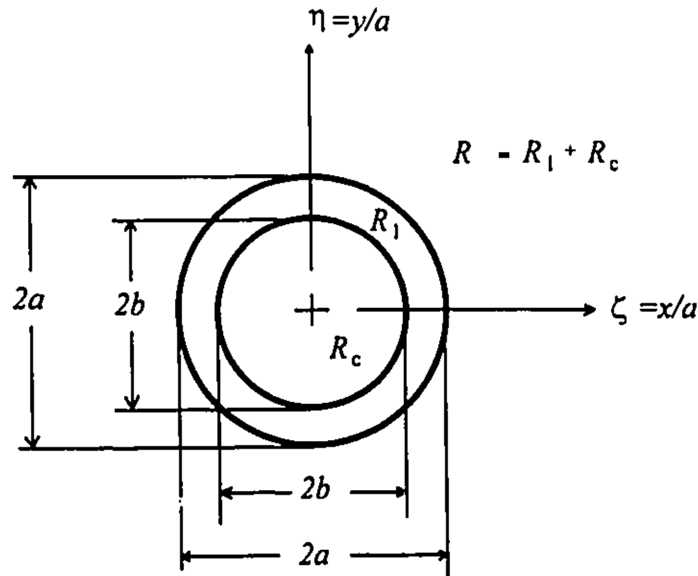

Fig. 3.5 Annular plate

The deflection of the annular plate undergoing flexural vibration can be described by the orthogonal plate function as given by the equation (3.36). Substituting the deflection function in the kinetic and potential energy expressions, and minimizing the Rayleigh quotient with respect to the coefficient C_i yields an eigenvalue equation,

$$\sum_{j=1}^{m}[K_{ij} - \lambda(M_{ij})]C_i = 0 \tag{3.40}$$

where

$$K_{ij} = K^1{}_{ij} - K^2{}_{ij}$$
$$M_{ij} = M^1{}_{ij} - M^2{}_{ij}$$

$$K^1{}_{ij} = C^{1,1}{}_{ij} + C^{1,2}{}_{ij} + \nu[C^{1,3}{}_{ij} + C^{1,4}{}_{ij}] + 2(1-\nu)C^{1,5}{}_{ij}$$
$$K^2{}_{ij} = C^{2,1}{}_{ij} + C^{2,2}{}_{ij} + \nu[C^{2,3}{}_{ij} + C^{2,4}{}_{ij}] + 2(1-\nu)C^{2,5}{}_{ij}$$

$$M^1{}_{ij} = \iint_R \phi_i(x,y)\phi_j(x,y)dxdy$$
$$M^2{}_{ij} = \iint_{R_c} \phi_i(x,y)\phi_j(x,y)dxdy$$

in which

$$C^{1,1}{}_{ij} = \iint_R \frac{\partial^2\phi_i(x,y)}{\partial x^2}\frac{\partial^2\phi_j(x,y)}{\partial x^2}dxdy$$
$$C^{1,2}{}_{ij} = \iint_R \frac{\partial^2\phi_i(x,y)}{\partial y^2}\frac{\partial^2\phi_j(x,y)}{\partial y^2}dxdy$$
$$C^{1,3}{}_{ij} = \iint_R \frac{\partial^2\phi_i(x,y)}{\partial y^2}\frac{\partial^2\phi_j(x,y)}{\partial x^2}dxdy$$
$$C^{1,4}{}_{ij} = \iint_R \frac{\partial^2\phi_i(x,y)}{\partial x^2}\frac{\partial^2\phi_j(x,y)}{\partial y^2}dxdy$$
$$C^{1,5}{}_{ij} = \iint_R \frac{\partial^2\phi_i(x,y)}{\partial x\partial y}\frac{\partial^2\phi_j(x,y)}{\partial x\partial y}dxdy$$

$$C^{2,1}{}_{ij} = \iint_{R_c} \frac{\partial^2\phi_i(x,y)}{\partial x^2}\frac{\partial^2\phi_j(x,y)}{\partial x^2}dxdy$$

$$C^{2,2}_{ij} = \iint_{R_c} \frac{\partial^2\phi_i(x,y)}{\partial y^2}\frac{\partial^2\phi_j(x,y)}{\partial y^2}dxdy$$
$$C^{2,3}_{ij} = \iint_{R_c} \frac{\partial^2\phi_i(x,y)}{\partial y^2}\frac{\partial^2\phi_j(x,y)}{\partial x^2}dxdy$$
$$C^{2,4}_{ij} = \iint_{R_c} \frac{\partial^2\phi_i(x,y)}{\partial x^2}\frac{\partial^2\phi_j(x,y)}{\partial y^2}dxdy$$
$$C^{2,5}_{ij} = \iint_{R_c} \frac{\partial^2\phi_i(x,y)}{\partial x\partial y}\frac{\partial^2\phi_j(x,y)}{\partial x\partial y}dxdy$$

$$i = 1,2,3,\ldots..m, \qquad \lambda = \rho h\omega^2 a^4/D$$

The natural frequency and mode shape of the annular plate are obtained by solving the equation (3.40). The kinetic and potential energies of the annular plate were calculated by subtracting the energies of the circular plate calculated over the plate domain R_c from the energies of the circular plate calculated over the entire plate domain R respectively. R_c is the region of the circular opening and R is the region of the entire circular plate without any opening.

3.5.3 Circular Plate with Abrupt change in Thickness

Following the procedure explained in section 3.4.3 for the rectangular plate with abrupt change in thickness, the kinetic and potential energy expression of a circular plate with abrupt change in thickness as shown in the figure 3.6 can be given by equations (3.33) and (3.34) respectively. Where R_2 is the region of the abrupt change in thickness and R is the region of the entire circular plate without any abrupt change in thickness.

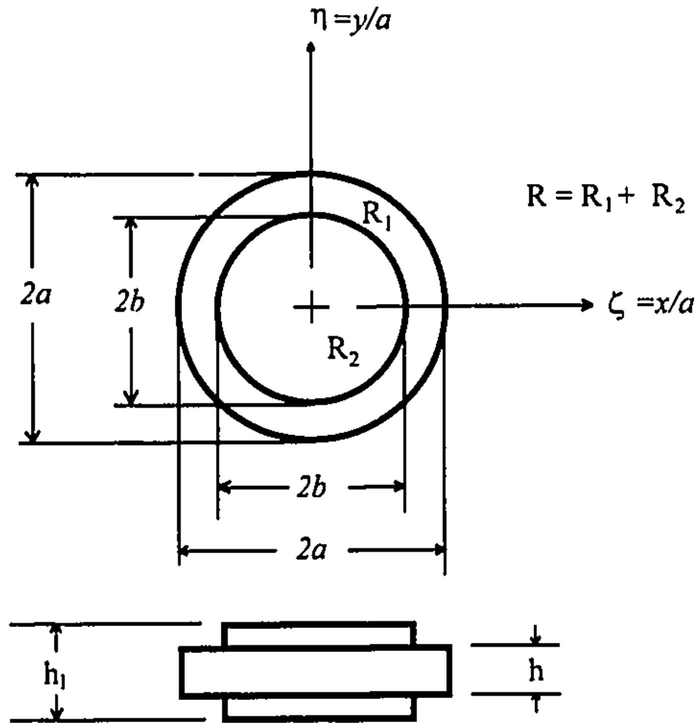

Fig. 3.6 Circular Plate with abrupt change in thickness

The deflection of the plate with abrupt change in thickness undergoing flexural vibration c n be described by the orthogonal plate function as given by the equation (3.36). Substituting the deflection function in the kinetic and potential energy expressions, and minimizing the Rayleigh quotient with respect to the coefficient C_i yields an eigenvalue equation,

$$\sum_{j=1}^{m}[K_{ij} - \lambda(M_{ij})]C_i = 0 \tag{3.41}$$

where

$$K_{ij} = K^1{}_{ij} - (\beta^3 - 1)K^2{}_{ij}$$
$$M_{ij} = M^1{}_{ij} - (\beta - 1)M^2{}_{ij}$$

$$K^1_{ij} = C^{1,1}_{ij} + (a/b)^2 C^{1,2}_{ij} + \nu(a/b)^2[C^{1,3}_{ij} + C^{1,4}_{ij}] + 2(1-\nu)(a/b)^4 C^{1,5}_{ij}$$
$$K^2_{ij} = C^{2,1}_{ij} + (a/b)^2 C^{2,2}_{ij} + \nu(a/b)^2[C^{2,3}_{ij} + C^{2,4}_{ij}] + 2(1-\nu)(a/b)^4 C^{2,5}_{ij}$$

$$M^1_{ij} = \iint_R \phi_i(x,y)\phi_j(x,y)dxdy$$
$$M^2_{ij} = \iint_{R_2} \phi_i(x,y)\phi_j(x,y)dxdy$$

in which

$$C^{1,1}_{ij} = \iint_R \frac{\partial^2\phi_i(x,y)}{\partial x^2}\frac{\partial^2\phi_j(x,y)}{\partial x^2}dxdy$$
$$C^{1,2}_{ij} = \iint_R \frac{\partial^2\phi_i(x,y)}{\partial y^2}\frac{\partial^2\phi_j(x,y)}{\partial y^2}dxdy$$
$$C^{1,3}_{ij} = \iint_R \frac{\partial^2\phi_i(x,y)}{\partial y^2}\frac{\partial^2\phi_j(x,y)}{\partial x^2}dxdy$$
$$C^{1,4}_{ij} = \iint_R \frac{\partial^2\phi_i(x,y)}{\partial x^2}\frac{\partial^2\phi_j(x,y)}{\partial y^2}dxdy$$
$$C^{1,5}_{ij} = \iint_R \frac{\partial^2\phi_i(x,y)}{\partial x\partial y}\frac{\partial^2\phi_j(x,y)}{\partial x\partial y}dxdy$$

$$C^{2,1}_{ij} = \iint_{R_2} \frac{\partial^2\phi_i(x,y)}{\partial x^2}\frac{\partial^2\phi_j(x,y)}{\partial x^2}dxdy$$
$$C^{2,2}_{ij} = \iint_{R_2} \frac{\partial^2\phi_i(x,y)}{\partial y^2}\frac{\partial^2\phi_j(x,y)}{\partial y^2}dxdy$$
$$C^{2,3}_{ij} = \iint_{R_2} \frac{\partial^2\phi_i(x,y)}{\partial y^2}\frac{\partial^2\phi_j(x,y)}{\partial x^2}dxdy$$
$$C^{2,4}_{ij} = \iint_{R_2} \frac{\partial^2\phi_i(x,y)}{\partial x^2}\frac{\partial^2\phi_j(x,y)}{\partial y^2}dxdy$$
$$C^{2,5}_{ij} = \iint_{R_2} \frac{\partial^2\phi_i(x,y)}{\partial x\partial y}\frac{\partial^2\phi_j(x,y)}{\partial x\partial y}dxdy$$

$$i = 1,2,3,.....m, \qquad \lambda = \rho h\omega^2 a^4/D$$

The natural frequency and mode shape of the circular plate with abrupt change in thickness are obtained by solving the equation (3.41).

3.6 Finite Element Method

3.6.1 General

The finite element method (FEM) is one of the most popular method of representing distributed mass structures. The method divides the structure of interest into sub sections of finite size, called a finite element. These elements are connected to adjacent element at various points on their boundaries, called nodes. Once this procedure is finished, the distributed mass structure is represented by a finite number of nodes and element refereed to as a finite grid or mesh.

The displacement of each element is approximated by a function of the spatial variable between nodes. The next step in the finite element analysis (FEA) is to calculate the energy in each element as a function of the displacement. The total energy of the structure is then expressed as the sum of the energy in each element. External forces are included by using the principle of virtual work to derive forces per element. Lagrange's equations are then applied to the total energy of the structure, which yields the approximate equation of motion.

3.6.2 ANSYS Finite Element Analysis Program

The ANSYS finite element program [54] is a large scale general purpose program which has the capabilities for a simple linear static analysis to a

complex non-linear transient dynamic analysis. "General Purpose" refers to the fact that the program can be used in all disciplines of engineering - structural, mechanical, electrical, electromagnetic, electronic, thermal, fluid, and biomedical. It utilizes the matrix displacement method for the analysis and the wavefront method for the matrix reduction and solution. The program contains many routines which are all inter-related. An extensive element library makes it feasible to analyze two or three dimensional structures.

The ANSYS program is organized into two basic levels: Begin level and Processor (or Routine) level. The begin level is the gateway to begin and end the Ansys program. It is also used for certain global program controls such as defining the jobname, clearing the database, and making copies of the binary files. At the processor level, several routines are available, each serving a specific purpose. Table 3.1., lists each processor, its function, the command to enter it and the Ansys prompt.

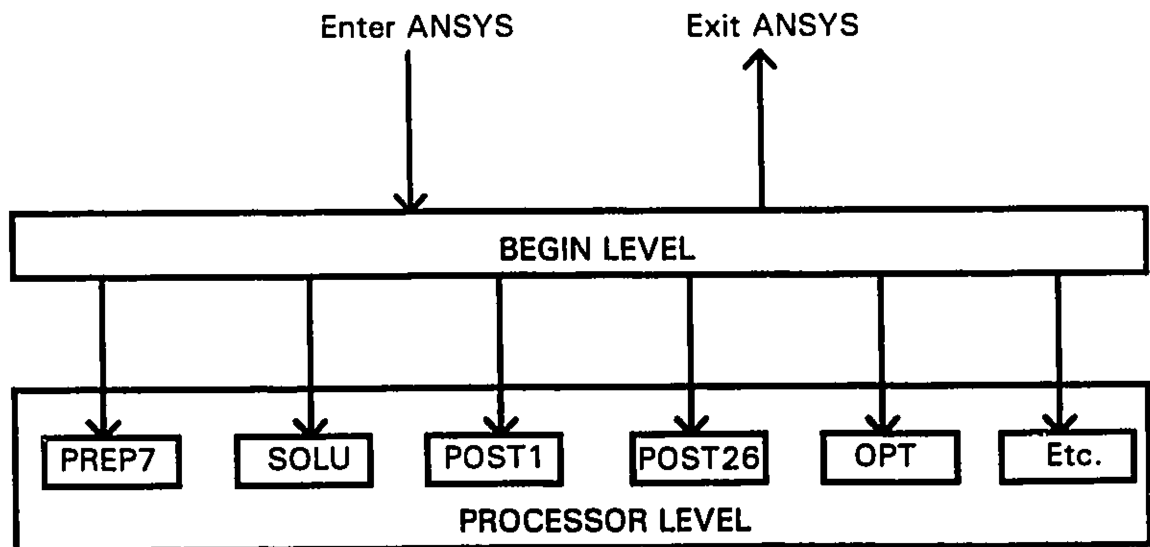

Fig. 3.7 ANSYS Program Organization

Table 3.1. Processors (routines) available in the ANSYS program

Processor	Function	Command	Prompt
PREP7	General preprocessing - to build the model (geometry,materials,coupling and constraints equations,etc.)	/PREP7	PREP7:
SOLUTION	Loading and solving - to apply loads and obtain the finite element solution	/SOLU	SOLU_LSn
POST1	General postprocessing - to review the results over the entire model	/POST1	POST1:
POST26	Time-history postprocessing - to review results at specific points in the model overtime	/POST26	POST26:
OPT	Design optimization	/OPT	OPT:
AUX2	Binary file utility - to dump binary files in readable form	/AUX2	AUX2:
AUX12	Radiation matrix generation - to calculate radiation view factors and generate a radiation matrix	/AUX12	AUX12:
AUX15	File translation - to translate files from CAD or FEA program	/AUX15	AUX15:
RUNSTAT	Run-time statistics - to predict CPU time, wavefront requirements, etc.	/RUNST	RUNSTAT:

3.6.3 Modal Analysis Using Ansys

The procedure for a modal analysis consists of four main steps:

- Build the model
- Apply loads and obtain the solution
- Expand the modes
- Review the results

ANSYS Modal Analysis Program is a linear analysis program.

The governing equation for free undamped vibration is ,

$$[M]\{\ddot{u}\} + [K]\{u\} = 0 \qquad (3.42)$$

where $[M]$ and $[K]$ are the mass and stiffness matrices respectively, and $\{u\}$ is the displacement vector. For a linear structure undergoing free vibration the displacements are harmonic of the form,

$$\{u\} = \{U\}\ Cos\omega t \qquad (3.43)$$

substituting in Equation (3.42),

$$[K - \omega^2 M]\ \{U\} = 0 \qquad (3.44)$$

Where ω is the Natural frequency of the plate

Equation (3.44), is a standard eigenvalue problem. Many numerical methods are available to solve the above equation. The ANSYS program offers three methods: reduced (Householder) method, subspace method, and unsymmetric method. A fourth method called the damped method is available for a damped modal analysis. In the present study subspace method was used to solve the equation (3.44).

3.7 Results and Discussion

3.7.1 General

Natural frequencies of plate, plate with openings (cut-outs), plate with abrupt change in thickness with clamped boundary conditions at the periphery are obtained for square and circular plates. Analysis was done using the orthogonal polynomials in Rayleigh Ritz method and Ansys finite element method. Construction of orthogonal polynomials are discussed in sections 3.2.2 and 3.2.3. In the Ansys finite element method three dimensional structural solid element (SOLID45) was used in the three dimensional modeling of the solid plate.

3.7.2 Natural Frequencies of a Square Plate

The results obtained by the above two methods for the clamped (CCCC) square plate are tabulated in Table 3.2. Accuracy of the results was ensured by working with a sufficiently large number of terms until the first four frequency converge to atleast five significant digits. The results from successive approximation also give an indication of the rate of convergence. Six terms were required in the rectangular plate analysis which includes the rectangular plate with cutout and rectangular plate with abrupt change in thickness. Using six plate characteristic functions corresponding to six roots of the frequency equation on either side, 36 natural frequency are obtained using Rayleigh Ritz analysis of which the first ten natural frequency are given in Table 3.2. The results are also compared with those from reference [2,9]

in Table 3.3. The results are in good agreement for all the natural frequencies. It is noted that the Ansys gives a slightly lower fundamental frequency when compared with orthogonal polynomials in Rayleigh Ritz method.

The results for the case of square plate with square openings in the middle of the plate are shown in Table 3.4. The trends of the first natural frequency of ten different square openings are plotted in Fig. 3.8 for the orthogonal polynomials in Rayleigh Ritz method and Ansys finite element method. The fundamental frequency parameter reaches a value of ten times, when the plate square openings is 0.8. However the increase in the higher natural frequencies is smaller. The fundamental frequency decreases for the small initial square openings of 0.1 X 0.1 and gradually increases with the increase in square openings for the Ansys finite element method. It can be seen from table 3.4 for the Ansys finite element method, the higher frequencies decreases gradually till the cutout size reaches 0.4, but subsequently starts to increase with increase in cutout size. However, the Rayleigh Ritz analysis shows the higher frequencies increasing with increasing cutout size. The plot for the second frequency for both the method is shown in Fig. 3.9. The increase in the natural frequency with increase in cutout size suggest that the reduction in kinetic energy due to the cutout at the plate center is more significant as compared to reduction in potential energy. In Rayleigh Ritz method the deflection is expressed in terms of higher polynomials and hence, the strain energy in the region of the cutout is accounted for more accurately as compared to finite element method. Hence Rayleigh Ritz results are more likely to exhibit the right trend. The results are also compared with those from reference [15,18] in Tables 3.7 for square opening of 0.5. The results

are in good agreement with the above reference. The results for different square openings are in good agreement with reference [15] in Table 3.8.

The results for the square plate with abrupt change in thickness for various inner and outer ratios *(f/a)* and β *(h_l/h)* are presented in Table 3.5 and 3.6. The results are in good agreement with those obtained by reference [18,19]. The Rayleigh Ritz and finite element analysis shows that the frequencies are increasing with increasing inner and outer ratios. However, the first three natural frequencies decrease for the small initial inner and outer ratios and gradually increase with the increase in inner and outer ratios for the Ansys finite element method as seen in the Fig. 3.10 and 3.11. The increase in the frequency with increase in inner and outer ratios is not as significant as increase in the frequency with increase cut out size. The results for β=1.5874 and for different side ratio is compared with reference [18,19] in Table 3.9. The results are in good agreement with the reference.

The first four mode shapes of the square plate using Ansys are shown in Fig. 3.16, and the first six mode shapes of the square plate with square openings of 0.2 and 0.5 using Ansys are shown in Fig. 3.17 and Fig 3.18. The first five mode shapes of the square plate with abrupt change in thickness of inner and outer ratio of 0.5 using Ansys is shown in Fig. 3.19.

3.7.3 Natural Frequencies of a Circular Plate

Thirty six terms were required in the circular plate analysis which includes the annular plate and circular plate with abrupt change in thickness. In Table

3.10, the first ten natural frequency parameters are given, calculated by using 36 terms in series (Eq. 3.34) in the Rayleigh Ritz analysis, and using Ansys finite element method, for a circular plate having its periphery clamped. The results are also compared with those from reference [20,25] in Table 3.11, where the exact values are obtained by reference [20]. The results are in good agreement for all the natural frequencies. It is noted that Ansys gives slightly lower fundamental frequencies when compared with others in Table 3.11 as seen in the case of a square plate with its periphery clamped in Table 3.3.

The results for the case of annular plate are shown in Table 3.12. and are compared with those from reference [15,18] in Tables 3.15. The trends of the first natural frequency of ten different ratios of inner radius and outer radius (b/a) are plotted in Fig. 3.12 for the orthogonal polynomials in Rayleigh Ritz method and Ansys finite element method. The fundamental frequency decreases for the small initial ratios of inner radius and outer radius (b/a) of 0.1 and gradually increases with the increase in ratios of inner radius and outer radius (b/a) for the Ansys finite element method. It can be seen from Table 3.12 for the Ansys finite element method, the higher frequencies decreases gradually till the ratio (b/a) reaches 0.4, but subsequently starts to increase with increase in ratio (b/a). However, the Rayleigh Ritz analysis shows the higher frequencies increasing with increasing ratio (b/a). The plot for the second frequency for both the method is shown in Fig. 3.13. The increase in the natural frequency with increase ratio (b/a) suggest that the reduction in kinetic energy due to the cutout at the plate center is more significant as compared to reduction in potential energy. In Rayleigh Ritz method the deflection is expressed in terms of higher polynomials and hence,

the strain energy in the region of the cutout is accounted for more accurately as compared to finite element method. Hence Rayleigh Ritz results are more likely to exhibit the right trend. Also it can be seen from Table 3.12, that for ratio *(b/a)* greater than 0.5, the first three natural frequency are vary close for both the methods. The results for the circular plate with abrupt change in thickness for various inner and outer ratios *(b/a)* and β (h_1/h) are presented in Table 3.13 and 3.14. The Rayleigh Ritz and finite element analysis shows that the frequencies are increasing with increasing inner and outer ratios *(b/a)* for both β (h_1/h) of 1.5 and 2. The increase in the frequency with increase in inner and outer ratios is not as significant as increase in the frequency with increase ratios *(b/a)* for annular plates.

The first six mode shapes of the circular plate using Ansys are shown in Fig. 3.20, and the first six mode shapes of annular plate of ratio *(b/a)* 0.2 using Ansys is shown in Fig. 3.21. The first six mode shapes of the circular plate with abrupt change in thickness of inner and outer ratio *(b/a)* of 0.5 using Ansys is shown in Fig. 3.22.

3.7.4 Natural Frequencies of a Hexagonal Plate

In Table 3.16, the first ten natural frequency parameter are given, as calculated using Ansys finite element method, for a hexagonal plate having its periphery clamped. The results are also compared with those from reference [33,55] in the above mentioned table. Two dimensional modeling was used in the Ansys finite element analysis. Reference [33] used two dimensional orthogonal polynomials in Rayleigh Ritz method to calculate the

natural frequency parameter of a hexagonal plate. The results are in good agreement for all the natural frequencies. The first four modes of the hexagonal plate clamped at its periphery is shown in fig. 3.23.

TABLE 3.2. FREQUENCY PARAMETER ($\sqrt{\lambda}$) OF CLAMPED SQUARE PLATE		
MODE	ORTHOGONAL POLYNOMIALS	ANSYS
1	35.9855	35.947
2	73.3947	73.3926
3	73.3947	73.3926
4	108.2179	107.9990
5	131.7789	131.9469
6	132.4097	132.5959
7	165.1597	164.8391
8	165.1597	164.8391
9	211.7061	211.9902
10	211.7061	211.9902

$\lambda = [\rho h w^2 a^4 / D]$

Table 3.3. Comparison of Frequency Parameters ($\sqrt{\lambda}$) of a CCCC square plate.

Mode	Orthogonal Polynomials	Ansys	Beam Functions [2]	S.S Plate functions [9]
1	35.9855	35.947	35.992	35.988
2	73.3947	73.3926	73.413	73.406
3	73.3947	73.3926	73.413	73.406
4	108.2179	107.9990	108.27	108.25
5	131.7789	131.9469	131.64	131.62
6	132.4097	132.5959	132.24	132.23

$\lambda = [\rho h w^2 a^4 / D]$

TABLE 3.4. FREQUENCY PARAMETERS ($\sqrt{\lambda}$) OF SQUARE PLATE WITH CUT-OUTS								
Cut-out Size	0.1 x 0.1		0.2 x 0.2		0.3 x 0.3		0.4 x 0.4	
MODE	ORTHO. POLY	ANSYS	ORTHO. POLY	ANSYS	ORTHO. POLY	ANSYS	ORTHO. POLY	ANSYS
1	36.504	35.675	38.107	36.623	41.792	40.616	49.8970	49.110
2	73.414	72.854	73.627	69.560	73.980	64.950	74.7538	65.468
3	73.414	72.854	73.627	69.560	73.980	64.950	74.7538	65.468
4	107.353	106.534	105.472	103.662	104.339	100.065	105.044	98.967
5	130.651	129.697	128.441	126.688	127.725	118.193	130.103	105.139
6	134.807	130.947	144.140	126.688	163.013	155.433	162.586	147.869
7	165.113	163.478	164.514	159.661	163.013	155.433	162.586	147.869
8	165.113	163.478	164.514	159.661	163.357	162.024	184.117	179.342
9	211.706	207.195	213.459	195.745	220.336	204.032	236.451	222.363
10	211.706	207.196	213.459	195.745	220.336	204.032	239.795	232.660

$\lambda = [\rho h w^2 a^4 / D]$

TABLE 3.4. cont'd. FREQUENCY PARAMETERS ($\sqrt{\lambda}$) OF SQUARE PLATE WITH CUT-OUTS								
Cut-out Size	0.5 x 0.5		0.6 x 0.6		0.7 x 0.7		0.8 x 0.8	
MODE	ORTHO. POLY	ANSYS	ORTHO. POLY	ANSYS	ORTHO. POLY	ANSYS	ORTHO. POLY	ANSYS
1	65.7150	65.003	96.5901	95.587	164.627	162.375	359.945	351.044
2	81.6796	75.622	106.512	102.365	170.938	166.576	363.841	353.380
3	81.6796	75.622	106.512	102.365	170.938	166.576	363.841	353.380
4	110.857	101.225	132.755	117.331	192.039	174.498	372.502	356.988
5	135.879	105.731	148.178	128.789	194.579	189.835	386.237	373.993
6	166.360	143.223	179.343	155.034	224.717	206.633	402.809	383.322
7	166.360	143.223	179.343	155.034	224.717	206.633	402.809	383.322
8	197.702	183.651	214.349	195.305	260.261	232.537	431.555	396.620
9	236.187	202.348	246.800	196.542	280.660	244.007	436.220	416.625
10	264.560	245.826	284.088	245.412	321.902	278.804	475.433	437.040

$\lambda = [\rho h w^2 a^4 / D]$

TABLE 3.5. FREQUENCY PARAMETERS ($\sqrt{\lambda}$) OF SQUARE PLATE WITH ABRUPT CHANGE IN THICKNESS ($\beta = h_1/h = 1.5$)

Abrupt Change Size	0.1 x 0.1		0.2 x 0.2		0.3 x 0.3		0.4 x 0.4	
MODE	ORTHO. POLY	ANSYS	ORTHO. POLY	ANSYS	ORTHO. POLY	ANSYS	ORTHO. POLY	ANSYS
1	36.5031	35.9174	37.051	36.199	37.7774	36.885	38.8764	37.848
2	73.507	73.194	74.497	73.383	76.299	74.344	79.299	76.650
3	73.507	73.194	74.497	73.383	76.299	74.344	79.299	76.650
4	110.029	109.025	113.376	112.173	116.296	114.889	118.818	116.483
5	134.359	133.100	139.280	137.821	143.133	141.586	146.453	142.826
6	136.603	133.220	142.352	138.064	146.802	144.359	150.296	148.239
7	165.509	164.154	168.633	166.283	174.696	171.871	181.791	178.450
8	165.509	164.154	168.633	166.283	174.696	171.871	181.791	178.450
9	212.535	210.201	219.882	213.185	232.422	223.200	244.062	237.714
10	212.535	210.201	219.882	213.185	232.422	223.201	244.464	237.758

$\lambda = [\rho h w^2 a^4/D]$

TABLE 3.5. cont'd. FREQUENCY PARAMETERS ($\sqrt{\lambda}$) OF SQUARE PLATE WITH ABRUPT CHANGE IN THICKNESS ($\beta = h_1/h = 1.5$)

Abrupt Change Size	0.5 x 0.5		0.6 x 0.6		0.7 x 0.7		0.8 x 0.8	
MODE	ORTHO. POLY	ANSYS	ORTHO. POLY	ANSYS	ORTHO. POLY	ANSYS	ORTHO. POLY	ANSYS
1	39.7595	38.866	40.3155	39.772	40.9009	40.564	41.944	41.464
2	84.023	80.409	88.439	85.008	90.978	89.060	92.366	91.351
3	84.023	80.409	88.439	85.008	90.978	89.060	92.366	91.351
4	122.988	118.776	128.680	123.394	133.700	129.691	137.841	135.287
5	151.264	144.454	158.611	150.263	168.661	160.601	174.976	169.955
6	155.152	150.538	162.608	155.576	171.761	164.324	176.319	171.601
7	188.701	183.148	196.850	188.486	207.852	198.160	217.257	209.551
8	188.701	183.148	196.850	188.486	207.852	198.160	217.257	209.551
9	251.658	247.512	258.136	250.235	271.835	258.372	288.180	274.906
10	251.658	247.512	258.136	250.235	271.835	258.372	288.180	274.906

$\lambda = [\rho h w^2 a^4/D]$

TABLE 3.6. FREQUENCY PARAMETERS ($\sqrt{\lambda}$) OF SQUARE PLATE WITH ABRUPT CHANGE IN THICKNESS ($\beta=h_1/h=2.0$)

Abrupt Change Size	0.1 x 0.1		0.2 x 0.2		0.3 x 0.3		0.4 x 0.4	
MODE	ORTHO. POLY	ANSYS	ORTHO. POLY	ANSYS	ORTHO. POLY	ANSYS	ORTHO. POLY	ANSYS
1	37.175	35.640	37.631	35.661	39.171	36.533	41.955	38.266
2	73.738	73.152	75.648	73.095	78.027	73.752	83.162	76.254
3	73.738	73.152	75.648	73.095	78.027	73.752	83.162	76.254
4	112.782	110.273	119.715	117.048	126.041	123.619	130.735	126.022
5	138.991	132.603	151.263	140.732	160.030	154.423	165.194	157.918
6	142.965	134.721	152.391	144.273	162.262	154.423	170.367	165.690
7	166.196	164.221	173.470	167.933	186.096	178.840	201.416	193.801
8	166.196	164.221	173.470	167.933	186.096	178.840	201.416	193.801
9	214.299	209.920	231.064	212.867	252.735	227.330	270.156	254.343
10	214.299	209.920	231.064	212.870	253.237	227.330	276.485	254.343

$\lambda = [\rho h w^2 a^4/D]$

TABLE 3.6. cont'd. FREQUENCY PARAMETERS ($\sqrt{\lambda}$) OF SQUARE PLATE WITH ABRUPT CHANGE IN THICKNESS ($\beta=h_1/h=2.0$)

Abrupt Change Size	0.5 x 0.5		0.6 x 0.6		0.7 x 0.7		0.8 x 0.8	
MODE	ORTHO. POLY	ANSYS	ORTHO. POLY	ANSYS	ORTHO. POLY	ANSYS	ORTHO. POLY	ANSYS
1	44.040	40.629	45.479	43.236	46.978	45.679	48.6915	47.711
2	92.481	81.448	101.011	89.664	108.001	99.959	113.031	108.738
3	92.481	81.448	101.011	89.664	108.001	99.959	113.031	108.738
4	137.544	126.951	146.543	132.110	157.388	143.842	169.408	159.148
5	170.029	156.270	180.834	159.437	204.577	174.326	221.874	199.345
6	176.912	168.384	187.896	170.643	209.566	182.612	223.860	203.240
7	213.994	203.174	226.431	207.116	249.544	218.624	273.407	243.763
8	213.994	203.174	226.431	207.116	249.544	218.624	273.407	243.763
9	291.899	277.635	305.012	288.983	326.646	290.889	367.211	317.496
10	294.353	282.167	305.012	289.450	326.646	290.889	367.211	317.501

$\lambda = [\rho h w^2 a^4/D]$

Table 3.7. Comparison of Natural Frequency Coefficients ($\sqrt{\lambda}$) of a CCCC square plate with cutout.

Mode	Ortho. poly	Ansys	Rajamani [18]	Paramasivam [15]
1	65.7150	65.003	65.30	62.40
2	81.6976	75.622	77.30	68.55
4	110.8569	101.225	111.70	98.52
5	135.8793	105.731	128.40	143.95
6	166.3604	143.223	193.90	

cut out size = 0.5 X 0.5 $\lambda = [\rho h w^2 a^4 / D]$

Table 3.8. Comparison of Natural Frequency Coefficients ($\sqrt{\lambda}$) of a CCCC square plate with different cutout.

Cut Out Size	Ortho. poly	Paramasivam [15]
0.0000	35.9855	34.85
0.1667	37.4259	35.80
0.3333	43.8694	43.20
0.5000	65.7150	62.40

$\lambda = [\rho h w^2 a^4 / D]$

Table 3.9. Comparison of Natural Frequency Coefficients ($\sqrt{\lambda}$) of a CCCC square plate with abrupt change in thickness.

($DI = 4D$, $\beta = h_l/h = 1.5874$, $\nu = 0.0$, $\lambda = [\rho h w^2 a^4 / D]$)

Abrupt Change Size	Ortho. poly	Tham [19]	Lam [18]
0.25	57.62	57.28	57.46
0.50	58.55	58.50	58.40
0.75	51.49	52.11	51.22
1.00	35.9855	35.98	35.99

TABLE 3.10. FREQUENCY PARAMETERS ($\sqrt{\lambda}$) OF CIRCULAR PLATE		
MODE	RAYLEIGH RITZ	ANSYS
1	10.2158	10.2135
2	21.2603	21.2306
3	21.2603	21.2306
4	34.8771	34.7352
5	34.8771	34.8048
6	39.7711	39.7190
7	51.0319	50.7897
8	51.0319	50.7897
9	60.8320	60.6736
10	60.8320	60.6736

$\lambda = [\rho h w^2 a^4 / D]$

Table 3.11. Comparison of Frequency Parameters ($\sqrt{\lambda}$) of Circular plate.

Mode	Orthogonal Polynomials	Ansys	Rajalingam [20]	Kim [25]
1	10.2158	10.2135	10.2158	10.2158
2	21.2604	21.2306	21.2604	21.260
3	21.2604	21.2306	21.2604	21.260
4	34.8770	34.7352	34.8770	34.877
5	34.8770	34.8048	34.8770	34.877
6	39.7711	39.7190	39.7711	39.771
7	51.0319	50.7897	51.0300	51.030
8	51.0319	50.7897	51.0300	51.030
9	60.8320	60.6736	60.8287	60.829
10	60.8320	60.6736	60.8287	60.829

$\lambda = [\rho h w^2 a^4 / D]$

TABLE 3.12. FREQUENCY PARAMETERS ($\sqrt{\lambda}$) OF ANNULAR PLATES								
b/a	0.1		0.2		0.3		0.4	
MODE	ORTHO. POLY	ANSYS	ORTHO. POLY	ANSYS	ORTHO. POLY	ANSYS	ORTHO. POLY	ANSYS
1	10.3458	10.1732	10.7248	10.4162	11.6015	11.4263	13.6550	13.5947
2	21.2650	21.1731	21.3115	20.4389	21.2864	19.3593	20.9973	19.3950
3	21.2650	21.1731	21.3115	20.4389	21.2864	19.3593	20.9973	19.3950
4	34.5916	34.4763	33.9760	33.6751	33.6458	32.4977	34.0232	31.3159
5	34.5916	34.4763	33.9760	33.6751	33.6458	32.4977	34.0232	31.3159
6	40.5282	39.4557	43.7208	42.8329	49.6730	48.999	48.8938	46.8588
7	51.0009	50.9384	50.6253	50.4085	49.6730	49.9997	48.8938	46.8588
8	51.0009	50.9384	50.6253	50.4085	51.8641	51.3334	67.2568	66.1006
9	60.8978	59.6089	61.5372	55.9847	64.1459	58.7876	68.4199	66.1006
10	60.8978	59.6089	61.5372	55.9847	64.1459	58.7876	68.4199	66.2430

$\lambda = [\rho h w^2 a^4 / D]$

TABLE 3.12. cont'd. FREQUENCY PARAMETERS ($\sqrt{\lambda}$) OF ANNULAR PLATES								
b/a	0.5		0.6		0.7		0.8	
MODE	ORTHO. POLY	ANSYS	ORTHO. POLY	ANSYS	ORTHO. POLY	ANSYS	ORTHO. POLY	ANSYS
1	17.7280	17.6794	25.6799	25.5559	43.1461	42.6998	93.076	90.6329
2	22.4442	21.7998	28.8127	28.4504	45.3465	44.7159	94.2638	92.0027
3	22.4442	21.7998	28.8127	28.4504	45.3465	44.7159	94.2638	92.0027
4	35.1437	31.7458	38.5366	36.2839	51.9921	50.5734	99.3872	96.1136
5	35.1437	31.7458	38.5366	36.2839	51.9921	50.5734	99.3872	96.1136
6	49.4431	45.5338	52.1398	47.9391	62.6501	59.9145	106.924	102.979
7	49.4431	45.5338	52.1398	47.9391	62.6501	59.9145	106.924	102.979
8	67.9791	63.0695	70.9148	63.1044	81.3710	72.5286	120.063	112.647
9	67.9791	63.0695	70.9148	63.1044	81.3710	72.5286	120.063	112.647
10	89.0176	84.4748	90.1729	81.9337	99.6776	88.4392	140.789	125.215

$\lambda = [\rho h w^2 a^4 / D]$

TABLE 3.13. FREQUENCY PARAMETERS ($\sqrt{\lambda}$) OF CIRCULAR PLATE WITH ABRUPT CHANGE IN THICKNESS ($\beta=h_1/h=1.5$)

b/a	0.1		0.2		0.3		0.4	
MODE	ORTHO. POLY	ANSYS	ORTHO. POLY	ANSYS	ORTHO. POLY	ANSYS	ORTHO. POLY	ANSYS
1	10.3481	10.4221	10.4769	10.4596	10.6741	10.5729	10.9934	10.8144
2	21.2872	21.9063	21.5195	21.8137	21.9115	21.7994	22.7161	22.2150
3	21.2872	21.9063	21.5195	21.8137	21.9115	21.7994	22.7161	22.2150
4	35.5093	36.8992	36.7288	37.7875	37.7665	38.2190	38.4761	38.2483
5	35.5093	36.8996	36.7288	37.7875	37.7665	38.2239	38.4761	38.2483
6	41.246	42.2729	43.2545	43.4732	44.8433	45.1192	45.9578	45.8775
7	51.1085	54.4071	51.9271	54.4773	53.8147	54.8592	56.0210	56.2668
8	51.1085	54.4071	51.9271	54.4773	53.8147	54.8592	56.0210	56.2668
9	61.1757	65.2071	63.9230	64.8579	67.8871	66.6275	71.8338	70.0006
10	61.1757	65.2071	63.9230	64.8579	67.8871	66.6275	71.8338	70.0006

$\lambda = [\rho h w^2 a^4/D]$

TABLE 3.13. cont'd. FREQUENCY PARAMETERS ($\sqrt{\lambda}$) OF CIRCULAR PLATE WITH ABRUPT CHANGE IN THICKNESS ($\beta=h_1/h=1.5$)

b/a	0.5		0.6		0.7		0.8	
MODE	ORTHO. POLY	ANSYS	ORTHO. POLY	ANSYS	ORTHO. POLY	ANSYS	ORTHO. POLY	ANSYS
1	11.2214	11.1120	11.3609	11.3412	11.4443	11.4623	11.6368	11.5921
2	24.0615	23.2286	25.3001	24.6308	26.3406	25.9718	26.7289	26.6736
3	24.0615	23.2286	25.3001	24.6308	26.3406	25.9718	26.7289	26.6736
4	39.2905	38.5240	41.1916	39.7200	43.6958	42.1615	45.2835	44.6989
5	39.2905	38.4596	41.1916	39.7200	43.6958	42.2469	45.2835	44.8573
6	47.0028	46.2710	49.2604	47.3151	52.2006	49.9675	53.3186	52.7188
7	57.8517	57.6176	59.8379	58.6567	63.4117	61.1798	66.8523	65.5906
8	57.8517	57.6176	59.8379	58.6567	63.4117	61.1798	66.8523	65.5906
9	74.5462	73.6497	75.8764	74.3081	79.3815	75.7775	82.9001	80.6982
10	74.5462	73.6497	75.8764	74.3091	79.3815	75.7775	82.9001	80.6990

$\lambda = [\rho h w^2 a^4/D]$

TABLE 3.14. FREQUENCY PARAMETERS ($\sqrt{\lambda}$) OF CIRCULAR PLATE WITH ABRUPT CHANGE IN THICKNESS ($\beta=h_1/h=2.0$)

b/a	0.1		0.2		0.3		0.4	
MODE	ORTHO. POLY	ANSYS	ORTHO. POLY	ANSYS	ORTHO. POLY	ANSYS	ORTHO. POLY	ANSYS
1	10.5118	10.2851	10.5837	10.2258	10.9995	10.4059	11.6788	10.8679
2	21.3423	21.7527	21.7662	21.5815	22.2112	21.5514	23.6550	22.0069
3	21.3423	21.7527	21.7662	21.5815	21.2112	21.5514	23.6550	22.0069
4	36.5684	36.8222	39.2698	39.0368	41.4238	41.4622	42.6225	42.3954
5	36.5684	36.8222	39.2698	39.0374	41.4238	41.4661	42.6225	42.4076
6	43.4779	41.7969	46.6670	43.9091	50.1297	48.2885	53.1340	52.5557
7	51.2527	53.3639	53.3675	54.0126	57.3313	56.9849	61.8079	62.4139
8	51.2527	53.3639	53.3675	54.0126	57.3313	56.9859	61.8079	62.4139
9	61.8763	64.6023	67.6211	63.9087	73.0604	66.9348	81.1201	74.7166
10	61.8763	64.6023	67.6211	63.9087	73.0604	66.9348	81.1201	74.7166

$\lambda = [\rho h w^2 a^4 / D]$

TABLE 3.14. cont'd FREQUENCY PARAMETERS ($\sqrt{\lambda}$) OF CIRCULAR PLATE WITH ABRUPT CHANGE IN THICKNESS ($\beta=h_1/h=2.0$)

b/a	0.5		0.6		0.7		0.8	
MODE	ORTHO. POLY	ANSYS	ORTHO. POLY	ANSYS	ORTHO. POLY	ANSYS	ORTHO. POLY	ANSYS
1	12.1973	11.5693	12.7866	12.3397	13.1234	12.9566	13.3272	13.2457
2	25.7682	23.2859	28.1189	25.5593	31.2298	28.8222	32.5834	31.6994
3	25.7682	23.2559	28.1189	25.5593	31.2298	28.8222	32.5834	31.6994
4	43.6667	41.9061	46.9743	42.2408	51.2957	45.6229	55.5967	51.9328
5	43.6667	41.9061	46.9743	42.2815	51.2957	45.6938	55.5967	52.0835
6	54.6204	53.5280	57.8219	52.7732	62.5371	55.1779	66.5412	61.7847
7	65.5345	64.9773	68.9184	65.3120	74.6086	67.0763	81.4767	74.5589
8	65.5345	64.9773	68.9184	65.3120	74.6086	67.0763	81.4767	74.5589
9	89.3972	84.8306	91.8502	88.2296	91.0160	86.8575	102.721	92.4938
10	89.3972	84.8306	91.8502	88.2334	91.0160	86.8576	102.721	92.4938

$\lambda = [\rho h w^2 a^4 / D]$

Table 3.15. Comparison of Natural Frequency Coefficients ($\sqrt{\lambda}$) of a Clamped Annular plate.

Hole size b/a	Ortho. poly	Ansys	Vogel [30]	Vijay [31]
0.1	10.3458	10.1732	10.1614	10.2276
0.3	11.6015	11.4263	11.4172	11.4502
0.5	17.7280	17.6794	17.6793	17.7545
0.7	43.1461	42.6998	43.1243	43.2068

$\lambda = [\rho h w^2 a^4 / D]$

Table 3.16. Comparison of Natural Frequency Coefficients of a Regular Hexagonal plate

Mode	Ansys	Lam [33]	Irie [55]
1	5.1943	5.2886	5.212
2	10.7933	10.8525	10.85
3	10.8052	10.8567	10.88
4	17.6389	17.7528	17.73
5	17.6567	17.7816	17.75
6	20.2173	20.2331	20.13
7	24.5546	24.8543	24.80
8	26.7617	27.2217	27.14

$\lambda = [\rho h w^2 a^4 / D\pi^2]$
where a is the half distance across the two parallel sides

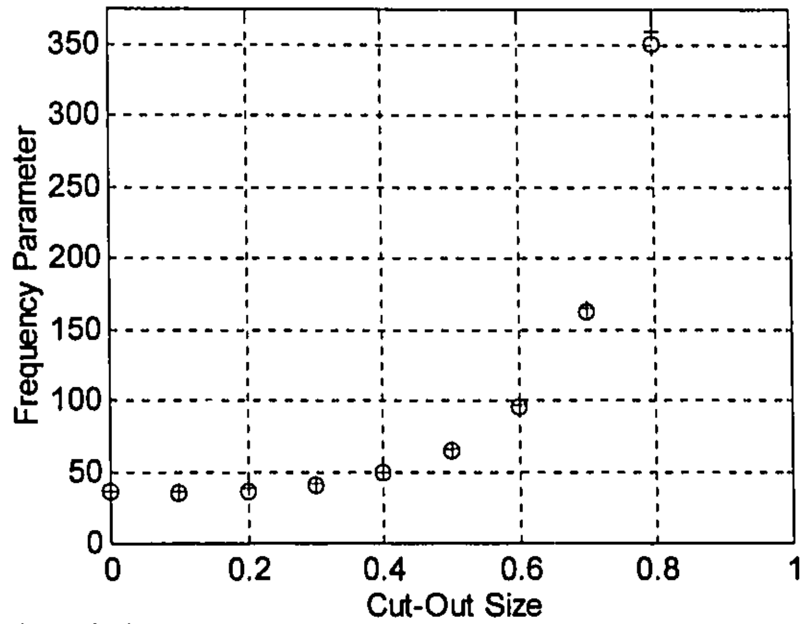

+ Rayleigh Ritz method
o Finite Element Method

Fig. 3.8 Comparison of frequency parameter of square plate with opening

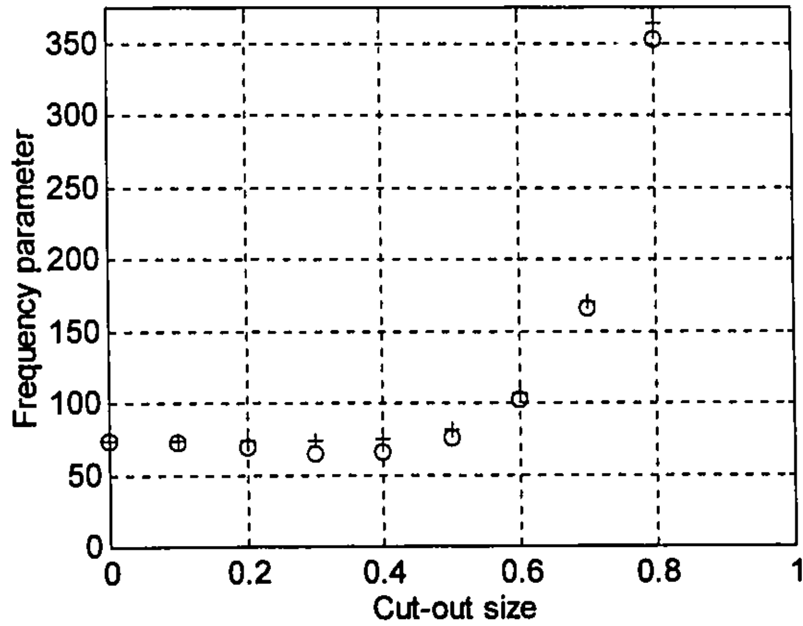

+ Rayleigh Ritz method
o Finite Element Method

Fig. 3.9 Comparison of second frequency parameter of square plate with opening

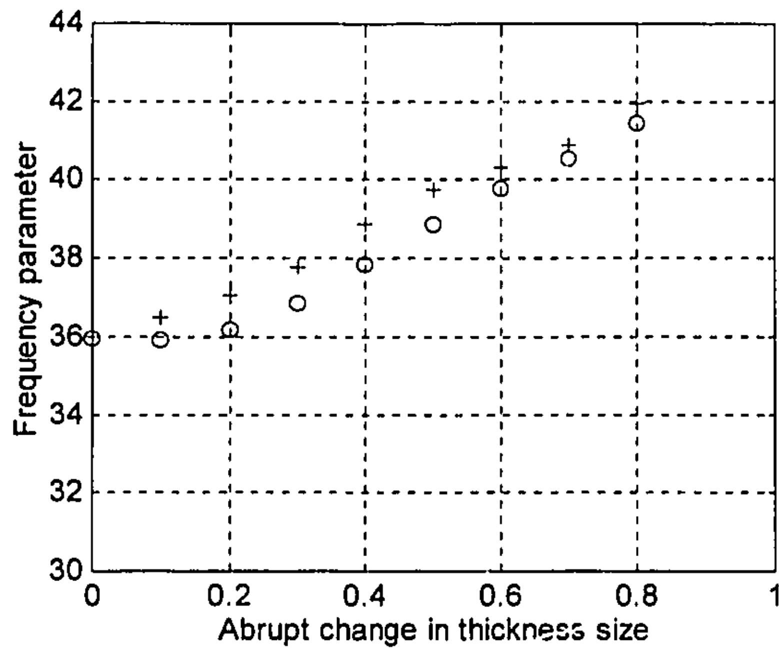

+ Rayleigh Ritz method
o Finite Element Method

Fig. 3.10 Comparison of frequency parameter of square plate with abrupt change in thickness ($\beta=h_1/h = 1.5$)

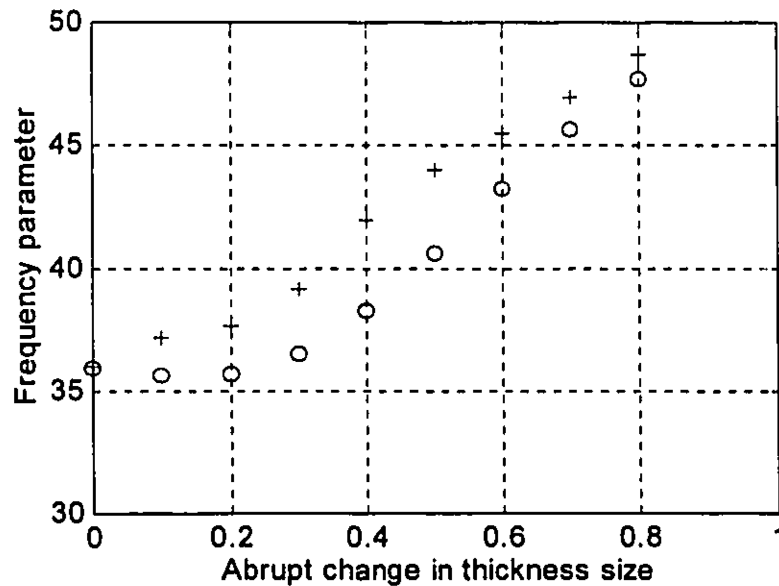

+ Rayleigh Ritz method
o Finite Element Method

Fig. 3.11 Comparison of frequency parameter of square plate with abrupt change in thickness ($\beta=h_1/h = 2$)

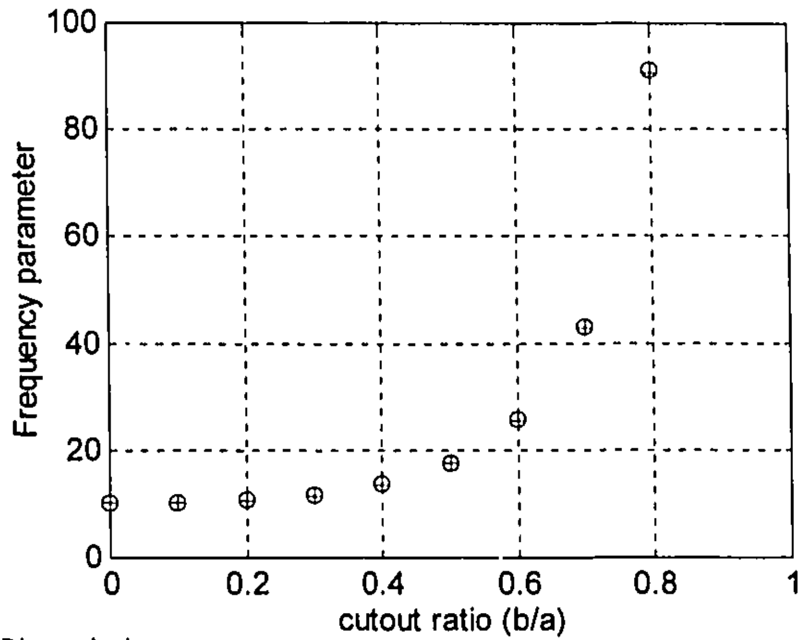

+ Rayleigh Ritz method
o Finite Element Method

Fig. 3.12 Comparison of frequency parameter of annular plate

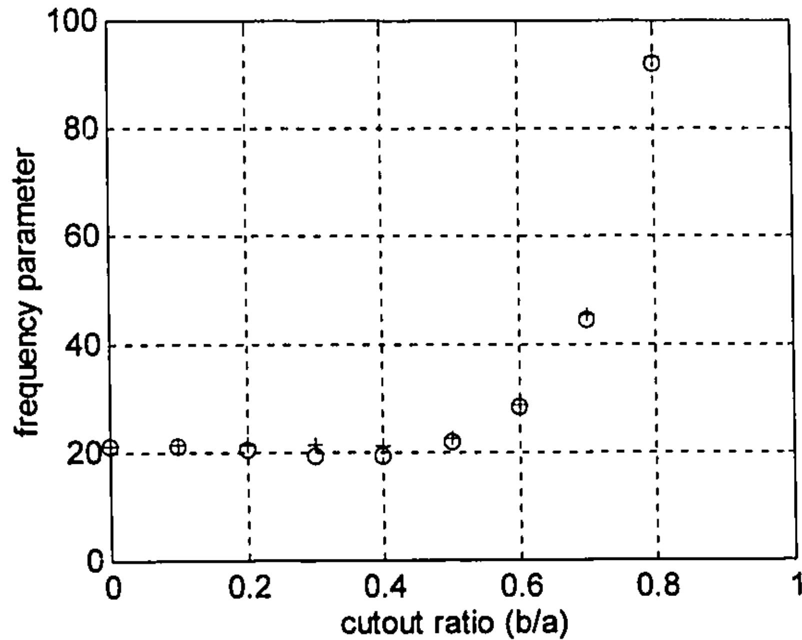

+ Rayleigh Ritz method
o Finite Element Method

Fig. 3.13 Comparison of second frequency parameter of annular plate

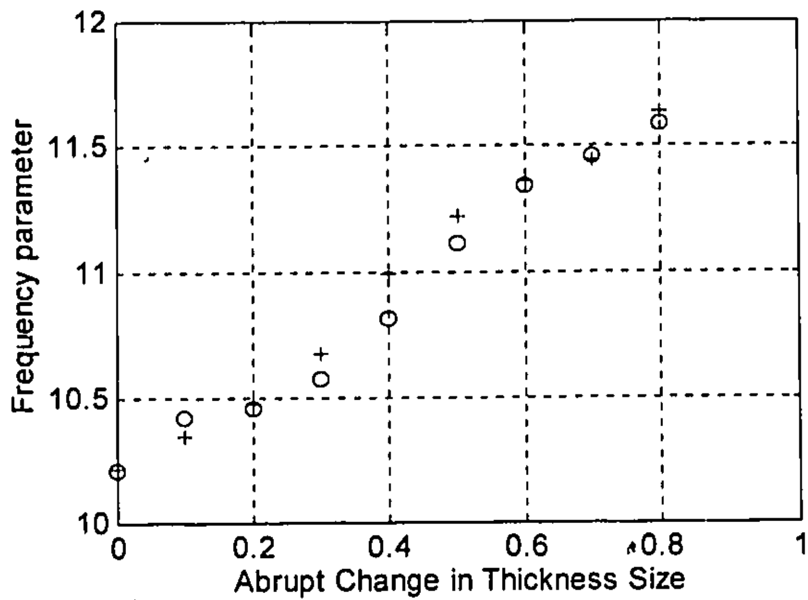

+ Rayleigh Ritz method
o Finite Element Method

Fig. 3.14 Comparison of frequency parameter of circular plate with abrupt change in thickness ($\beta = h_1/h = 1.5$)

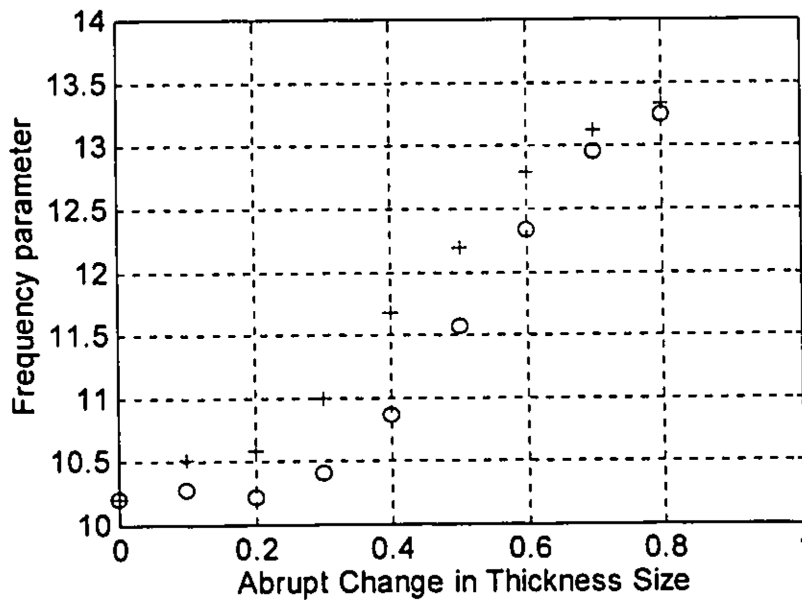

+ Rayleigh Ritz method
o Finite Element Method

Fig. 3.15 Comparison of frequency parameter of circular plate with abrupt change in thickness ($\beta = h_1/h = 2.0$)

First and Second mode shapes of a clamped square plate

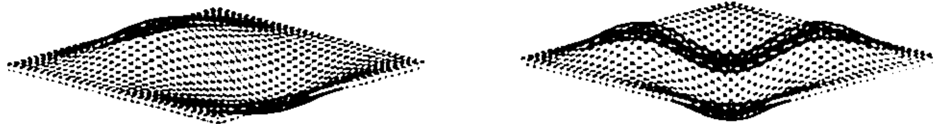

Third and Fourth mode shapes of a clamped square plate

Sixth mode shapes of a clamped square plate

Fig 3.16 Mode shapes of a square plate clamped at its periphery

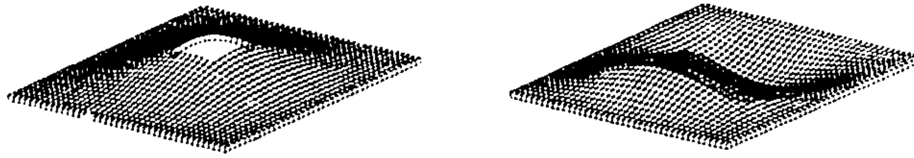

First and Second mode shapes of a square plate with cut-out

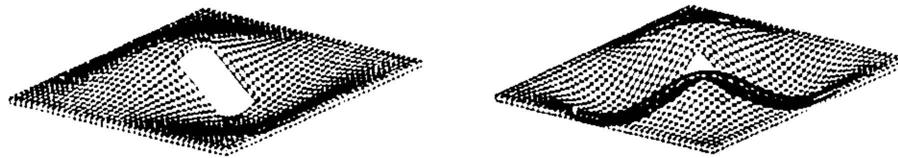

Third and Forth mode shapes of a square plate with cut-out

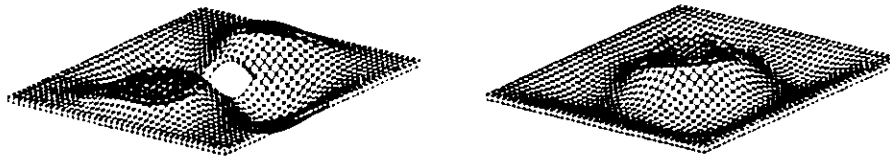

Fifth and Sixth mode shapes of a square plate with cut-out

Fig 3.17 Mode shapes of a clamped square plate with square opening
cutout size = 0.2 X 0.2

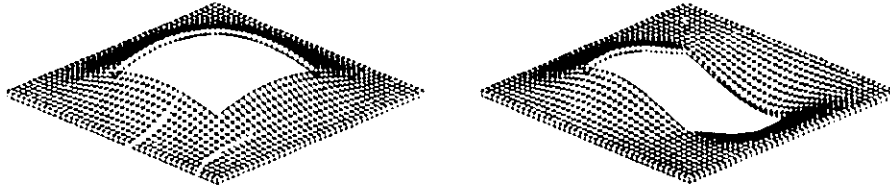

First and Second mode shapes of the plate with cut out size 0.5 X 0.5

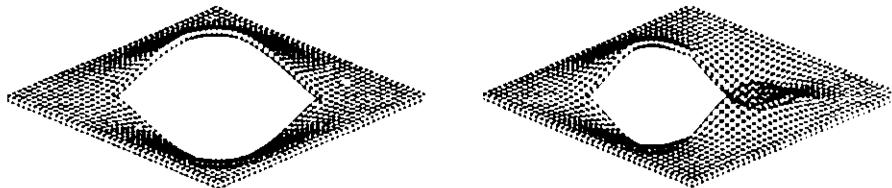

Third and Fourth mode shapes of the plate with cut out size 0.5 X 0.5

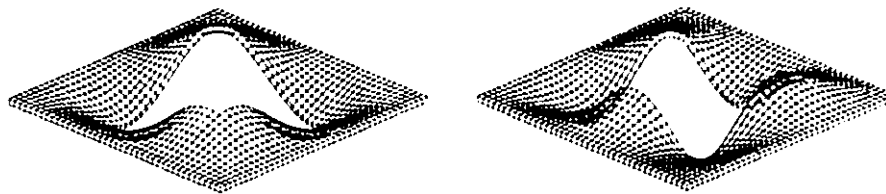

Fifth and Sixth mode shapes of the plate with cut out size 0.5 X 0.5

Fig 3.18 Mode shapes of a clamped square plate with square opening

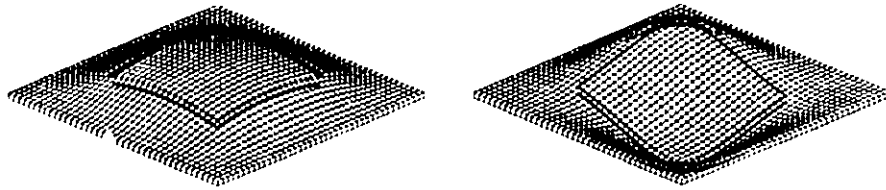

First and Second mode shapes of a square plate with abrupt change in thickness

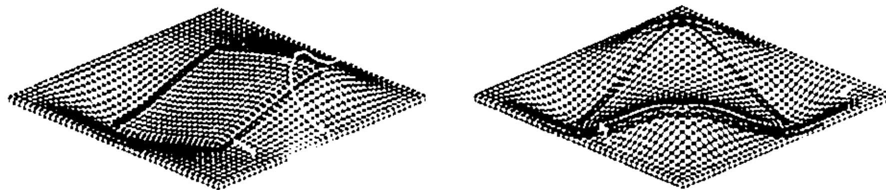

Third and Fourth mode shapes of a square plate with abrupt change in thickness

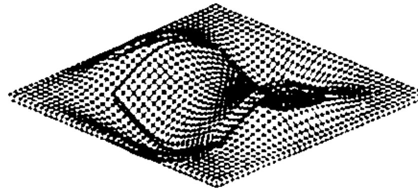

Fifth mode shape of a square plate with abrupt change in thickness

Fig 3.19 Mode shapes of a clamped square plate abrupt change in thickness (β=1.

First and Second mode shapes of a clamped circular plate

Third and Fourth mode shapes of a clamped circular plate

Fifth and Sixth mode shapes of a clamped circular plate

Fig. 3.20 Mode shapes of a clamped circular plate

First and Second mode shapes of an annular plate

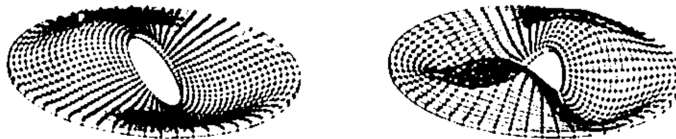

Third and Fourth mode shapes of an annular plate

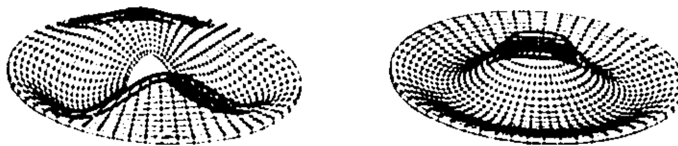

Fifth and Sixth mode shapes of an annular plate

Fig. 3.21 Mode shapes of a clamped annular plate

First and Second mode shapes

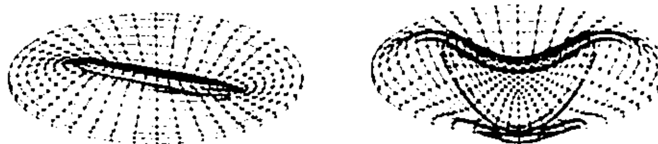

Third and Fourth mode shapes

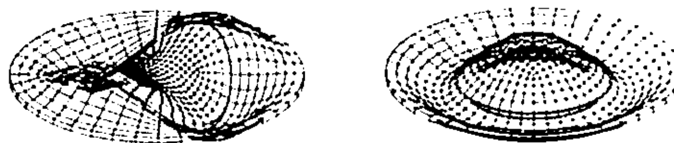

Fifth and Sixth mode shapes

Fig. 3.22 Mode shapes of a clamped circular plate with abrupt change in thickness ($\beta = 1.5$)

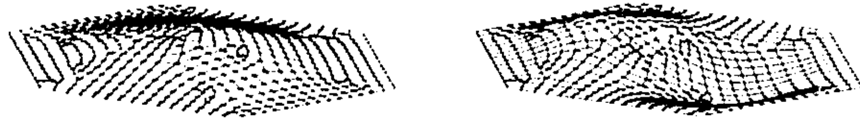

First and second mode shapes

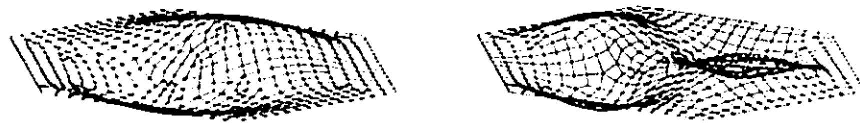

Third and Fourth mode shapes

Fig. 3.23 Mode shapes of a clamped Hexogonal Plate.

3.8 Summary

The Rayleigh Ritz method using orthogonal function provides a highly-accurate and computationally-efficient scheme of finding frequencies and mode shapes for the transverse vibration of plates. A simplification of the resulting eigenvalue problem and rapid convergence properties suitable for digital computers makes it a popular method. This was demonstrated by several authors cited in the reference for rectangular and polygon plates. The present analysis extends this lists to rectangular plates with cutout, rectangular plates with abrupt varying thickness, circular plates, annular plates, circular plates with abrupt varying thickness. The agreement of the results with those available in the literature confirm the power and efficiency of the method. This is expected since the orthogonal plate function can be accurately used to describe the deflected shape of rectangular and circular plates. This accurate numerical method for vibration of plates can be applied to any combination of clamped, simply supported and free boundaries. The results of the Rayleigh Ritz method using orthogonal polynomials was compared in detail with those of the Ansys Finite Element Method. The Ansys program is a large scale general purpose program which has the capabilities for a simple linear static analysis to a complex non-linear transient dynamic analysis.

CHAPTER 4

Design of Condenser Microphone

4.1 Introduction

Silicon subminiature microphones, can be manufactured with the methods of silicon technology, and have been designed and fabricated on the basis of piezoelectric, capacitive and piezoresistive principles. Capacitive sensors are normally constructed as two wafer realizations, where one wafer contains the back electrode and the other contains the membrane of the microphone. Between the membrane and the backplate there is an air gap whose acoustic behaviour influences the frequency characteristic and sensitivity of the microphone due to streaming resistances and compliances. A preliminary study of the dynamic characteristics of acoustic pressure sensors is necessary in order to provide a good quality design along with a consistent fabrication process. The shape and size of the sensitive membrane has a large impact on the acoustic characteristic of the sensor.

A simple design gives the advantage of an accurate prediction of the dynamic characteristic of the microphone. Therefore, a membrane bonded to a rigid support and a proper layout of the electrodes and the electronic circuitry are the primary requirements for fabrication of the microphone .

4.2 Design Considerations

The microphone consists of two parts, the silicon wafer forms the diaphragm and the pyrex glass wafer forms the back plate. A cross-sectional view of the structure is presented in Fig. 4.1. The air gap between the diaphragm and the backplate is a few microns, which results in a high nominal working capacitance.

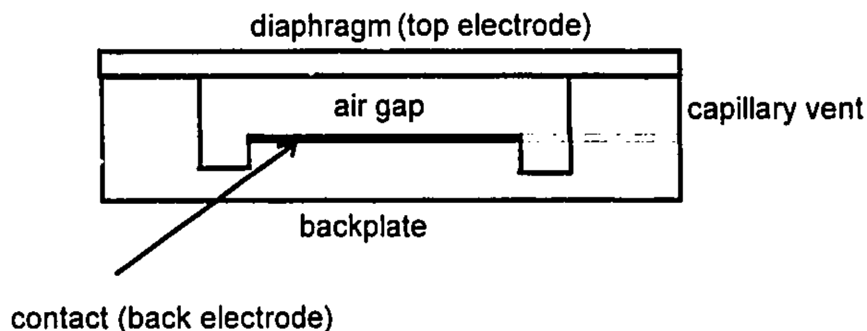

Fig. 4.1 . Cross section of microphone structure.

4.2.1 Diaphragm Design Considerations

One of the basic characteristics of the microphone is the cut-off frequency of the microphone. A very high natural frequency of the diaphragm is desired in order to ensure a good frequency response of the microphone in the acoustic range of frequencies. The size of the membrane, its boundary conditions, the air gap losses, and the structure of the backplate determine the cut-off frequency. The vibrational analysis results of Chapter 3, are used in

determining the natural frequency of the diaphragm. The natural frequencies of different shapes and sizes of microphones are calculated by using the fundamental frequency parameter (λ) results of clamped plates of different shapes of the diaphragm. The natural frequencies of different shapes and sizes of microphone are given in Table 4.1. The diaphragm parameters used in the calculations of the natural frequency are given in Table 4.2.

Table 4.1 Fundamental Frequencies of Diaphragms

Shape	**Size (μm)**	**Frequency (kHz)**
Square	1000	148.5
	900	183.4
	800	232.1
	700	303.2
Shape	**Dia (μm)**	**Frequency (kHz)**
Circle	1000	42.2
	900	52.1
	800	65.9
	700	86.0
Shape	**Width Across flat (μm)**	**Frequency (kHz)**
Hexagonal	1000	38.6
	900	47.3
	800	59.8
	700	78.7
Shape	**Side length (μm)**	**Frequency (kHz)**
Triangle (equilateral)	1000	40.1
	900	49.5
	800	62.6
	700	81.9

Table 4.2 Diaphragm parameters

Material	**Silicon**
Modulus of Elasticity	$1.64 * 10^{11}$ N/m^2
Density	2300 kg/m^3
Poison's Ratio	0.3
Diaphragm thickness	10 µm

The calculated natural frequency for different shapes of the diaphragm given in Table 4.1 are all substantially above the audible frequency range of 20 kHz. Therefore the natural frequencies of the microphone should not effect the performance of the microphone in the audible range. Therefore six designs using all four basic shapes were fabricated in Chapter 5, and the designed dimensions of the microphone are given in Chapter 6.

4.2.2 Backplate Design Considerations

The back-electrode area of conventional condenser microphone is normally structured in a special manner or perforated with holes to obtain favorable values of the acoustic air-gap elements. Unstructured or smooth back electrode areas can be used to produce high resonance frequencies of the microphone with smaller sensitivities [44]. A smooth back electrode combined with a very thin air gap can generate high values of streaming losses, so that the resistive cut-off frequency of the microphone is reduced to an unacceptable value [41,43].

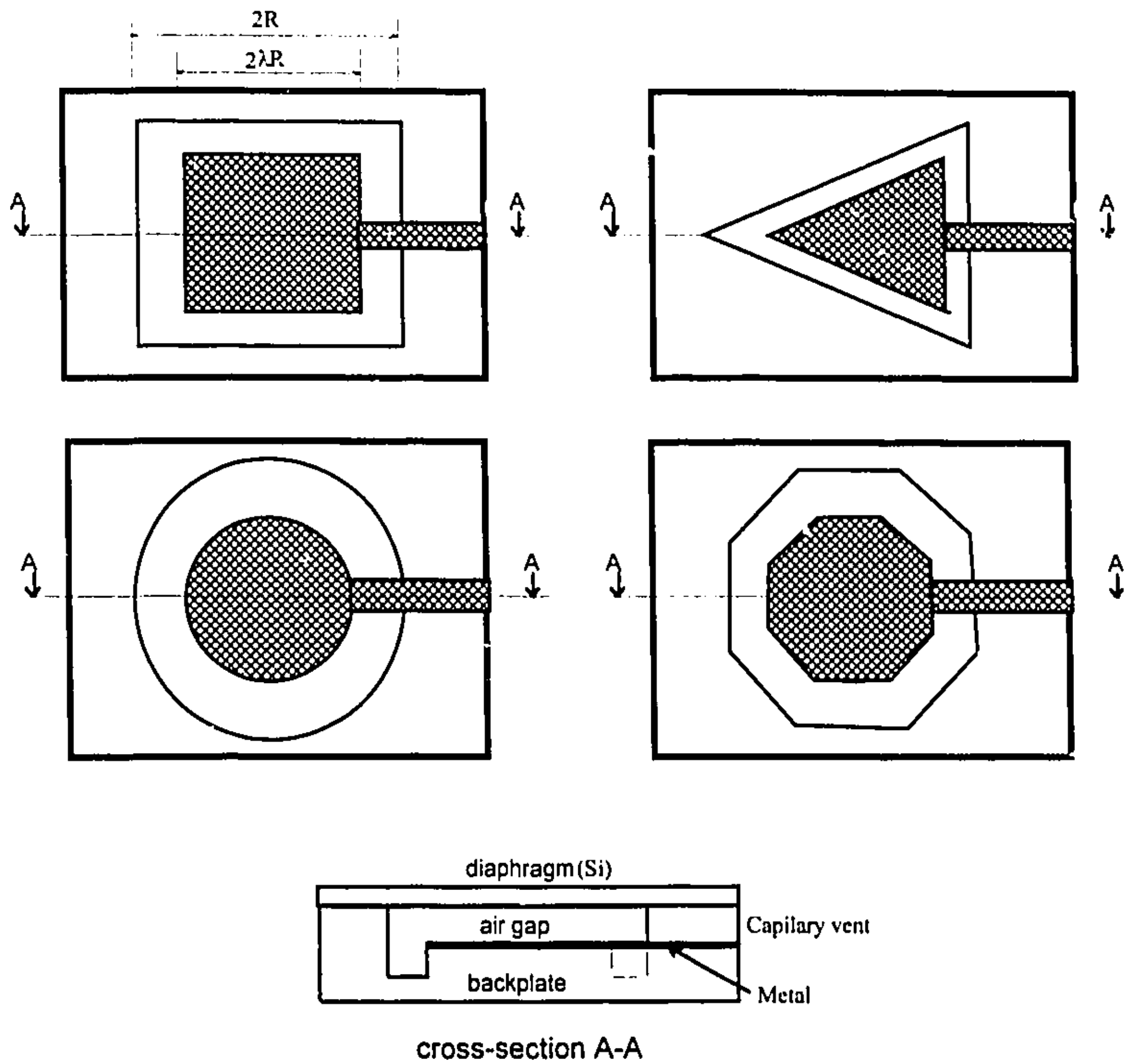

Fig. 4.2. Electrode pattern and cross-section of the square, circular, triangle and hexagonal structures

A back electrode with small lateral dimensions can be used if the capacitive variations of the microphone are detected by an active element [34]. Since the deflection near the edge of the diaphragm is very small, the part of the electrode in this area mainly contributes to the parasitic capacitance loading the microphone. Consequently, if this part of the electrode is omitted, the capacitive signal attenuation is reduced, thus increasing the sensitivity. The

dimensions of the microphone backplate required in this case can be made very small. Therefore, in the design, the size of the back electrode area is made smaller than the size of the diaphragm (Fig 4.2), and the air gap of the remaining back area is made larger for decreasing the air gap stiffness. Air gap losses which are caused by streaming resistances and which effect a high-frequency cut-off, therefore becomes negligibly small and the airgap stiffness, which decreases the sensitivity of the microphone, can be reduced to a minimum. These parasitic capacitance becomes more important with decreasing capacitance of the microphone.

4.3 Capacitance for Circular and Square Structures

The cross-section and the capacitor electrode pattern of the circular and square structure device are shown in Fig. 4.2. This figure shows the airgap between the top and bottom electrodes and also shows larger airgap around the periphery of the microphone diaphragm. It also indicates that the metalized pattern (area) of the back electrode is considerably smaller than the diaphragm area. The reason for larger airgap around the periphery and smaller metalized area at the backplate are discussed in section 4.2.

4.3.1 Circular Diaphragm

The deflection of the circular membrane shown in Fig. 4.2, can be expressed as [56]

$$w(r) = \frac{P}{64D}(R^2 - r^2)^2 \quad (4.1)$$

and the maximum deflection occurs at the center, which is given as

$$W_O = \frac{P}{64D} R^4 \quad (4.2)$$

For a circular diaphragm the expression for the capacitor is given as:

$$C = \int_0^{\lambda R} \frac{\varepsilon_o 2\pi r dr}{d - w(r)} \quad (4.3)$$

$$C = \frac{4\pi\varepsilon_o R^2}{\sqrt{64 W_o d}} ln\left[\frac{\frac{d}{W_o} + \lambda^2\sqrt{\frac{d}{W_o}} + \lambda^2 - 1}{\frac{d}{W_o} - \lambda^2\sqrt{\frac{d}{W_o}} + \lambda^2 - 1}\right] \quad (4.4)$$

where

ε_o = dielectric constant of air

R = radius of the diaphragm

d = air gap (zero pressure plate separation)

4.3.2 Square Diaphragm

The deflection of the square diaphragm shown in Fig. 4.2, can be expressed as [57]

$$w(x,y) = \frac{P(R^2 - x^2)(R^2 - y^2)}{49.6D} \quad (4.5)$$

and at the center

$$W_O = \frac{PR^4}{49.6D} \quad (4.6)$$

The shape of the deflection is quite similar to that of the circular diaphragm for the area not too close to the edges. Therefore, for simplicity, the square diaphragm will be approximated with a circular diaphragm that has a diameter of $2R$ (the length of the sides of the square), but has a center deflection determined by equation (4.6) instead of (4.2).

4.4 Sensitivity of the Microphone

Sensitivity is basically a straight forward characteristic and can best be described as; "within a specified frequency range of any particular condenser microphone, the sound input should create a change in output voltage that is a direct function of the sound pressure input". The ratio of the two, the signal output to the sound input, is known as either the response coefficient or sensitivity. The ratio of the logarithm of the magnitude of the response coefficient to the logarithm of the frequency, is called frequency characteristic. Ideally, this should be a flat (straight) line, constant with frequency. The frequency response of a microphone is either indicated by a graph over the full audio spectrum or expressed by two frequency limits in cycles per second (Hertz (Hz)), within which the microphone responds uniformly and with little variation of sensitivity.

Figure 4.3 shows the condenser microphone connected to an external bias voltage source V_o., loaded by a parasitic capacitance C_p. a bias resistor R_b. and a preamplifier with an input capacitance C_i.

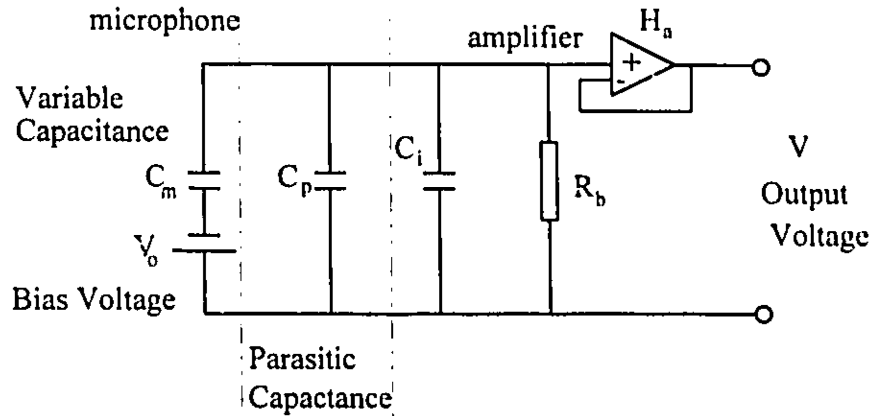

Fig 4.3 The condenser microphone with preamplifier

The open-circuit sensitivity of a condenser microphone is considered to consist of two components S_m and S_e *i.e.* the mechanical and electrical sensitivity of the microphone respectively [58].

The mechanical sensitivity is defined as the increase in the deflection of the microphone diaphragm, Δd , resulting from an increase in the pressure ΔP, acting on the diaphragm.

$$S_m = \frac{\Delta d}{\Delta P} \tag{4.7}$$

The electrical sensitivity is defined as the change in the voltage ΔV across the air gap resulting from the change in the air gap thickness Δd,

$$S_e = \frac{\Delta V}{\Delta d} \tag{4.8}$$

The microphone capacitance changes with the diaphragm movements as explained in Section 4.3. For fast diaphragm movements, and if the amplifier is ideal (input capacitance =0, infinite impedance) the charge on the plates of the microphone remains constant. Note that in the case of a piston diaphragm, the electric field strength E_a in the airgap is homogeneous. Since the charge is constant, the electrical field strength between the plates remains constant. The electrical sensitivity is then given by

$$S_e = E_a = \frac{V_o}{d} \tag{4.9}$$

where V_o is the bias voltage of the microphone and d is the air gap thickness

The quasi-static open circuit sensitivity S_{open} of a condenser microphone is defined as

$$S_{open} = S_m S_e \tag{4.10}$$

To measure the sensitivity, the microphone is connected to the preamplifier, which acts as an impedance converter. The most commonly used preamplifier is the source follower. It has a gain H_a, which is close to unity and an input capacitance C_i. The measured microphone sensitivity S_{meas} is equal to

$$S_{meas} = S_m S_e H_c H_a \tag{4.11}$$

Where H_c, is the capacitance signal attenuation due to the input capacitance of the preamplifier and the parasitic capacitance C_p. The parasitic capacitance is due to the bondpad of the microphone. [50]

$$H_c = \frac{C_m}{C_m + C_i + C_p} \tag{4.12}$$

where C_m is the microphone working capacitance

The air gap between the diaphragm and the backplate is a few microns, which results in a high nominal working capacitance. This increases microphone sensitivity according to [50]

$$S_{meas} = V_o \frac{\Delta C_m / C_m}{\Delta P} \frac{1}{(1 + C_s / C_m)} \qquad [\frac{V}{Pa}] \tag{4.13}$$

The small air gap d allows a low bias voltage V_o, since sensitivity is proportional to the ratio V_o/d according to

$$S_{meas} = \frac{V_o}{d} \frac{\Delta d}{\Delta P} \frac{1}{(1 + C_s / C_m)} \qquad [\frac{V}{Pa}] \tag{4.14}$$

Air moving in the narrow air gap leads to increased viscous damping as indicated by Skvor [59], and heat conduction effects as reported by Plantier and Bruneau [60]. This may result in serious damping of the high-frequency response and the damping leads to increasing Mechanical Johnson noise. Therefore, it is necessary to reduce the length of the narrow gap. The solution is to provide a rear volume cavity. A back chamber is provided on the periphery of the diaphragm as the rear volume cavity as shown in the Fig. 4.2. The different air gaps also serve to reduce microphone stray capacitance and thus increase sensitivity according to Eqn. (4.7). The stiffness of the air in the rear volume cavity will add to the diaphragm

stiffness and influence the sensitivity as well as the overall frequency response. A narrow slit (capillary vent) at the bond interface allow for equalization of the static pressure variations between the interior and the exterior of the microphone.

4.5 Process Design of the microphone

As mentioned in section 4.2, a condenser microphone consists of a two layer structure: a silicon layer and a glass layer. The sensitive electrode of the condenser microphone is a flat plate of monocrystalline silicon and the back plate is the Pyrex glass (# 7740). The fabrication design was carefully planned to satisfy the primary objectives of the geometrical size. The fabrication of the condenser requires three masking steps regardless of the geometrical parameters. The mask design takes into consideration the size and tolerance required for each masking step. The masks were prepared using photographic techniques as explained in Appendix B. The glass wafer which forms the back plate with air gap and side volume requires all the three masks. The mask drawings (X10 magnification) required for processing the backplate (glass) are presented in Figures 5.4 to 5.6. Mask 1 is used for etching the side volume cavity. Mask 2 is used to etch air gap cavity, and Mask 3 is used for making metallic contact for the back electrode. Once the three masking steps are completed on the glass wafer, anodic bonding is performed between the glass wafer and the silicon wafer as explained in Appendix C. The complete fabrication process of the condenser microphone is explained in detail in Chapter 5.

CHAPTER 5

Fabrication of Condenser Microphone

5.1 Introduction

The fabrication of micromechanical structures such as sensors on silicon substrates became possible with the employment of micromachining methods based on semiconductor technology. Improvements over the last few years in precision micromachining techniques, such as orientation-dependent etching in silicon, and the growing demand of high quality and high reliability sensors with reduced physical dimensions, has led to the development of many conventional sensors and transducers for pressure, temperature and other physical quantities. However, application of this technology for the development of acoustic silicon sensors is not prevalent.

5.2 Fabrication Process

Silicon and glass wafer are the materials used for the fabrication of the condenser microphone. The condenser microphone consists of two wafers, a membrane wafer and a backplate wafer. The membrane wafer is the silicon and the backplate wafer is the glass.

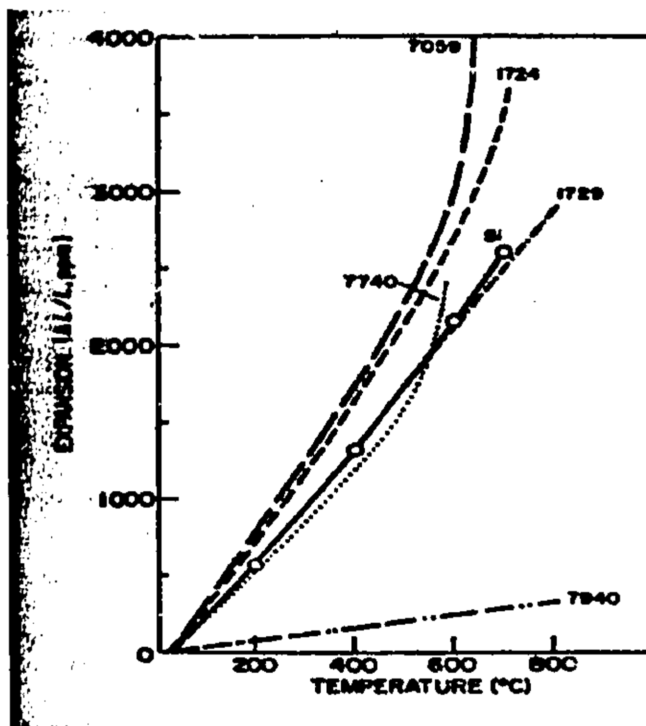

Fig. 5.1 Linear expansion coefficients as a function of temperature for several commercial glass substrates and silicon. [61]

Very thin commercially available (Virginia semiconductor*) p-type doped silicon wafer is used as the membrane element. Pyrex glass (# 7740) is used as the backplate. Pyrex glass is used because its thermal expansion coefficient is very close to that of silicon thermal expansion coefficient, as parts with the same thermal expansion coefficient are required during anodic bonding and also because of its excellent electrical insulation properties. Linear expansion coefficients as functions of temperature for several commercial glass substrates and silicon are shown in figure 5.1. As seen from the figure, throughout the temperature range between the bonding temperature and room temperature, the thermal expansion coefficients ($\Delta L/L$) difference is less than 100 ppm for the 7740 Pyrex glass and silicon.

* nicknamed "Virginia Slims"

Fig. 5.2 Flexible silicon membrane [62]

The thin silicon wafer is 10μm thick, with p-type (boron) doping concentration of 3 $*10^{19}$ cm $^{-3}$. The high doping concentration reduces the resistivity (≈ 0.002 Ω cm) in the silicon wafer. Thereby it can be used as an electrode. The wafers used are double-sided-polished and are extremely flexible because of the dominance of the elastic nature of single crystal silicon (Fig. 5.2). This dominance becomes evident when the ratio of surface to wafer thickness is very large, (larger the ratio, the more flexible the silicon wafer). Glass having a thickness of 760 μm and chemical composition of SiO_2-18%, H_2O_2-2%, B_2O_3-13% and Na_2O-4% is used as the backplate.

The fabrication of the condenser microphone requires two wafers: a silicon wafer and a pyrex glass wafer. The fabrication procedure of the condenser microphone is shown in Fig. 5.3. The backplate of the condenser microphone is prepared from a optically polished (surface roughness 400 Å) 760 μm thick pyrex glass (#7740).

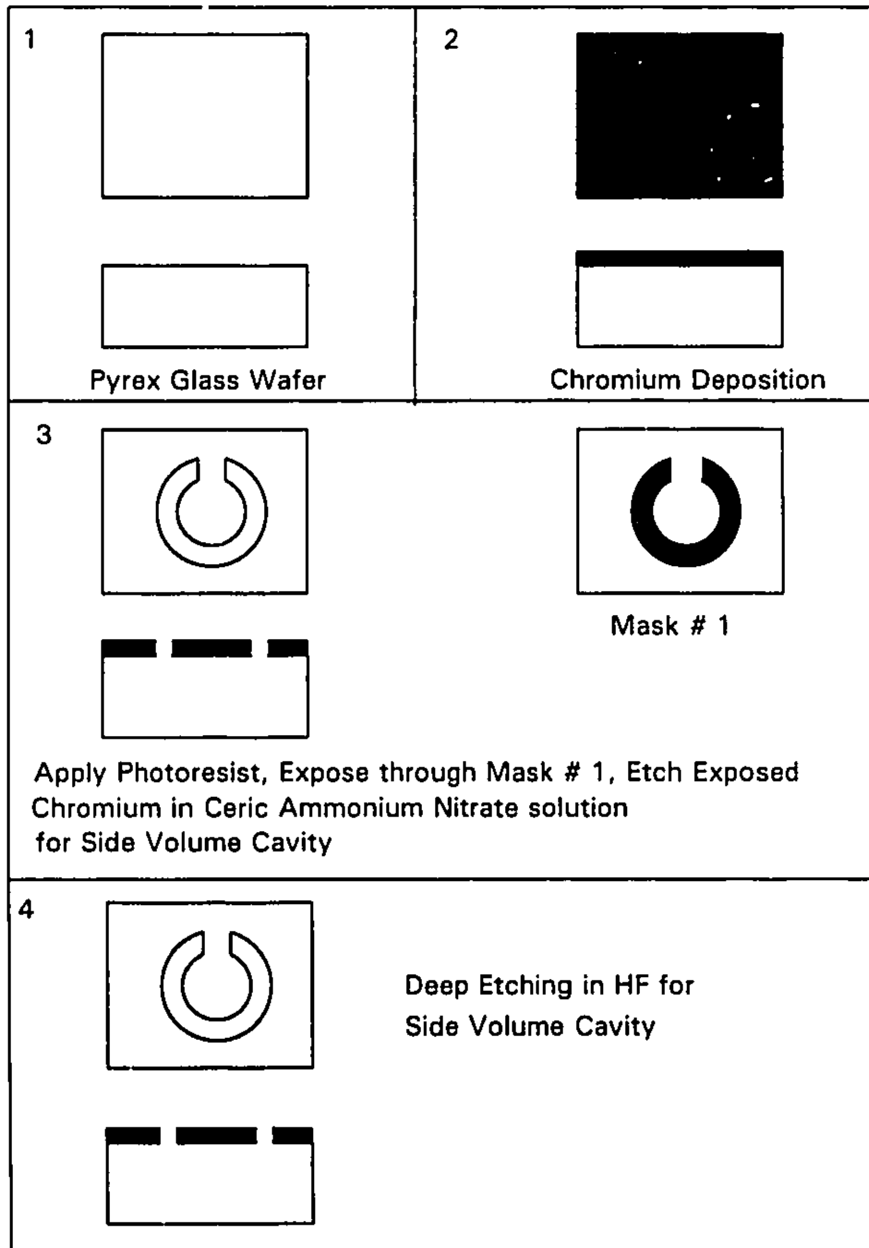

Fig. 5.3 Fabrication process for the Condenser Microphone.

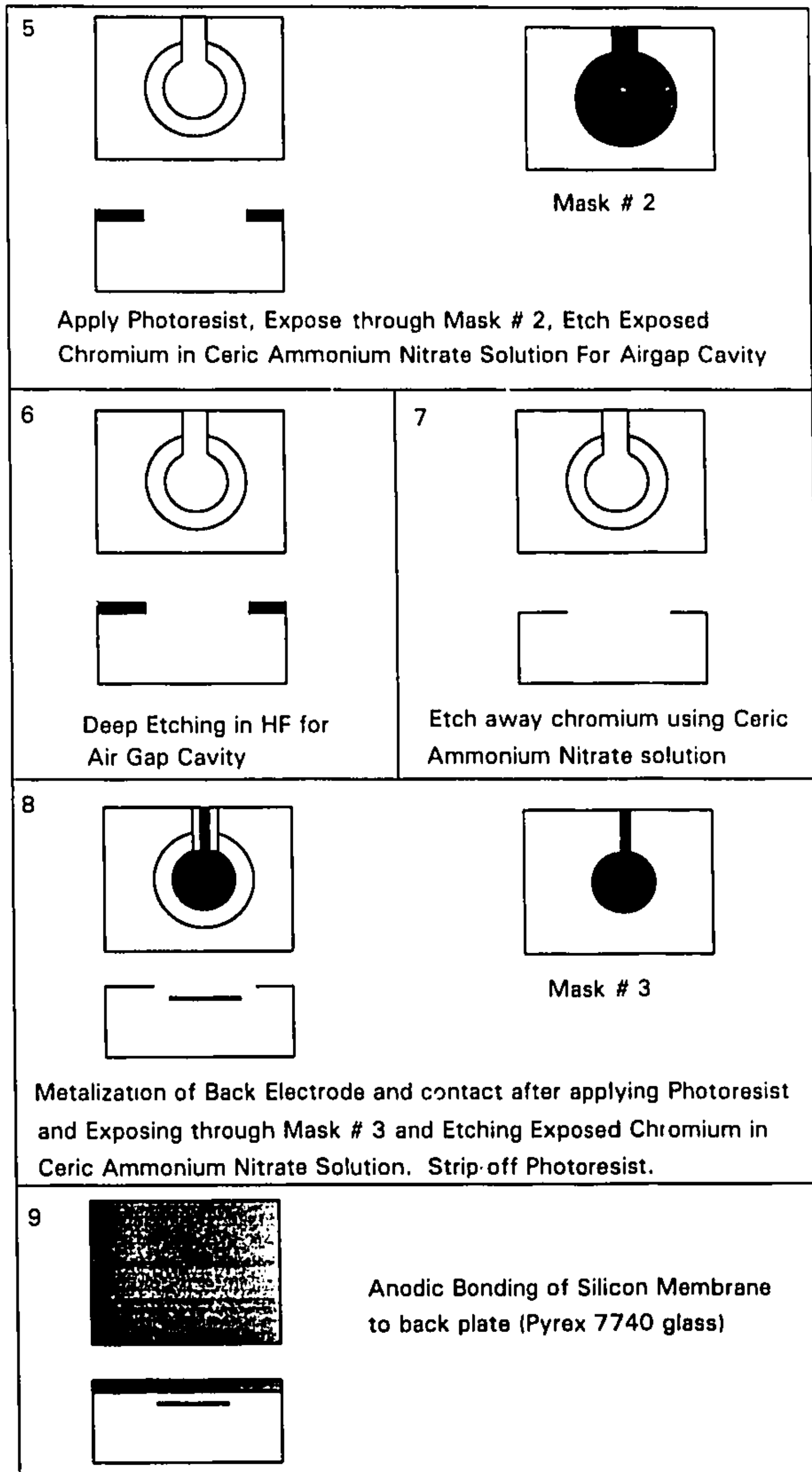

Fig. 5.3*(Cont'd)* Fabrication process for the Condenser Microphone.

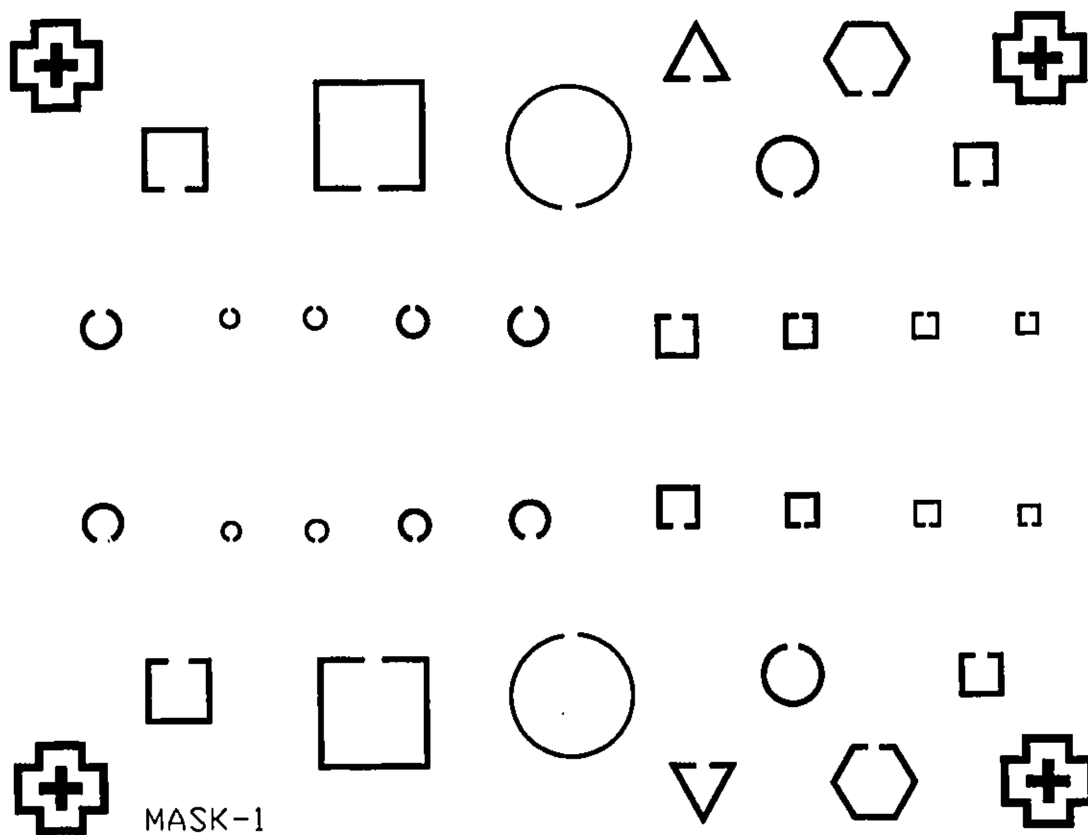

Fig. 5.4 Mask # 1 for etching the side volume cavity

The sizes of the square ranges from 1200 x 1200 μm^2 to 200 x 200 μm^2,
the sizes of the circle ranges from diameter 1300 μm to 150 μm,
the equilateral triangle is 700 μm each side, and
the size of the regular hexagon is 500 μm side length.

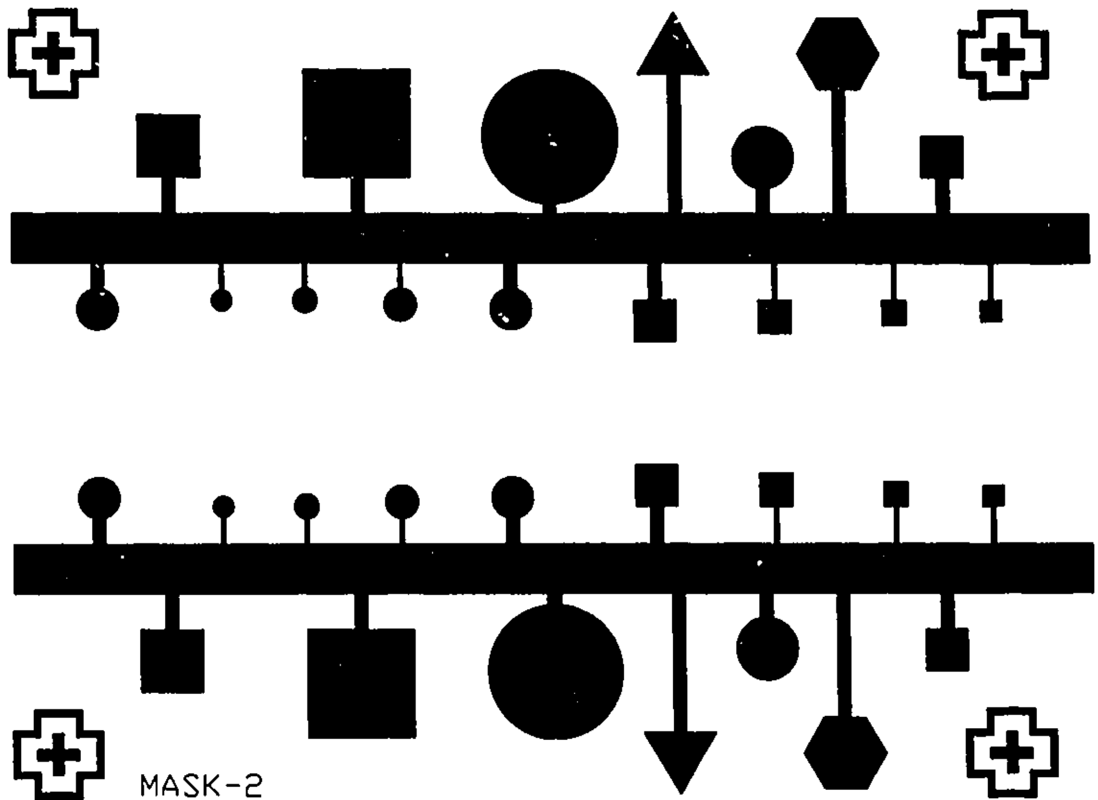

Fig. 5.5 Mask # 2 for etching the air gap cavity and capillary vent

The sizes of the square ranges from 1200 x 1200 μm^2 to 200 x 200 μm^2,
the sizes of the circle ranges from diameter 1300 μm to 150 μm,
the equilateral triangle is 700 μm each side, and
the size of the regular hexagon is 500 μm side length.

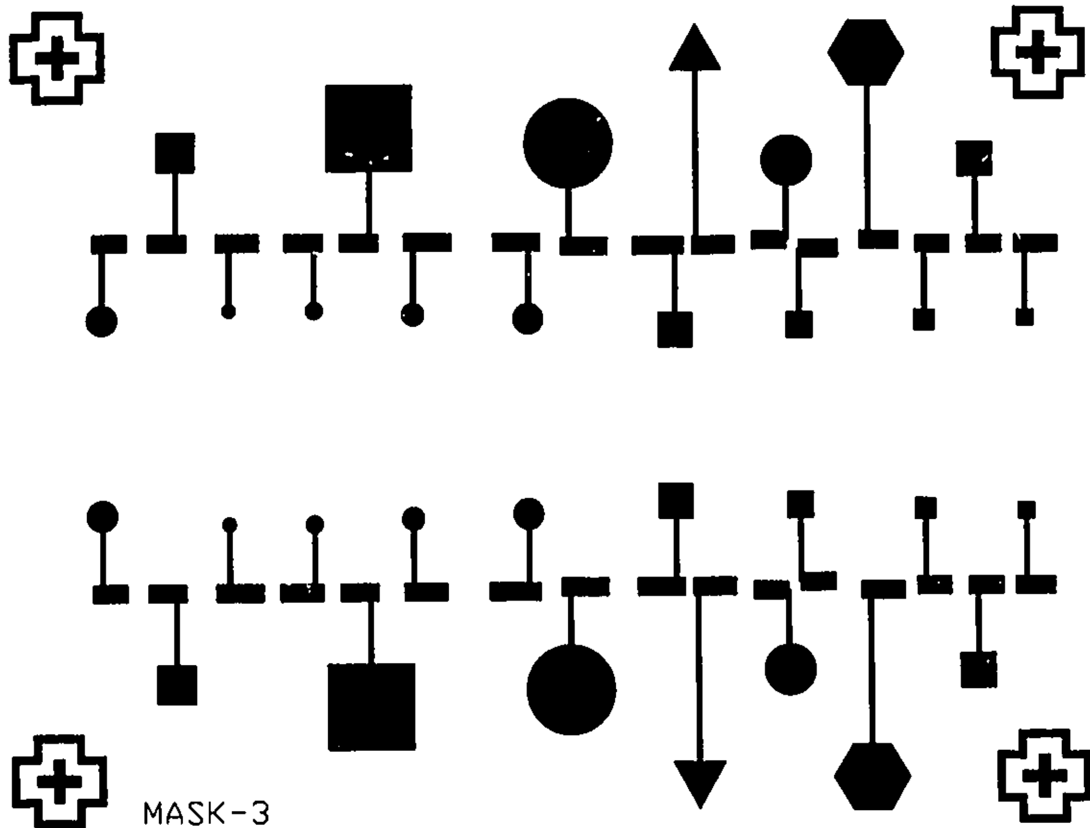

Fig. 5.6 Mask # 3 for metalization

The sizes of the square ranges 800 x 800 μm^2 to 100 x 100 μm^2,
the sizes of the circle ranges from diameter 900 µm to 100 µm,
the equilateral triangle is 500 µm each side, and
the size of the regular hexagon is 425 µm side length

5.2.1 Backplate Etching Process:

The first step is to deposit a layer of chromium on the glass wafer using the chromium deposition evaporator as explained in Appendix A. Chromium is deposited on the glass wafer to act as a mask during the etching of the rear volume and air gap cavity. The process of chromium deposition was carried out in a high vacuum (10^{-6} Torr.), where the chromium was heated up and vaporized to form a uniform thin film on the pyrex glass. After chromium deposition, the glass wafer is cleaned in de-ionized (DI) water. Using Mask 1, the photolithography process is performed, where the mask pattern is transferred onto the glass wafer as explained in Appendix B. Photolithography consists of applying photoresist to the substrate, softbaking it in an oven at temperature of 95°C for 20 min., exposing to UV light for 60 seconds through a mask, developing it using a negative photoresist developer to form the pattern, and hardbaking in an oven at a temperature of 145°C for 15 min. HF(49%) is used as the etchant for etching the rear volume cavity. Negative photoresist was used as the radiation sensitive material. The glass wafer now contains the mask pattern, where the chromium is exposed, which is the region where etching of the glass is required to form the side volume cavity. The exposed chromium is etched away in a solution of ceric ammonium nitrate (ceric ammonium nitrate - 150 gms + acetic acid - 35 ml + water - 1 litre) [63]. The etch rate of chromium using the above etchant is 1500 Å/min. The wafer is then dipped in concentrated HF (49%) to form the side volume cavity of required depth as shown in step 4 in Fig. 5.3. The etch rate of glass in HF is 9 μm/min approximately at room temperature. The negative photoresist is then stripped off using a negative photoresist remover. The process procedure of etching of the air gap cavity and capillary

vent (process done at the same time) is similar to the above procedure followed for the etching of side volume cavity, except that, mask 2 is used instead of 1, in the photolithography process. Care should be taken during the photolithography to align mask 2 on the aligner mark made by the Mask 1 pattern on the glass wafer. After completing the process, the wafer has a side volume cavity and an air gap cavity in the center as shown in step 6 in Fig. 5.3. The remaining chromium is etched away using ceric ammonium nitrate solution. Fig. 5.7 and 5.8 shows the side volume cavity and the air gap cavity of the circular and square shaped microphone backplate.

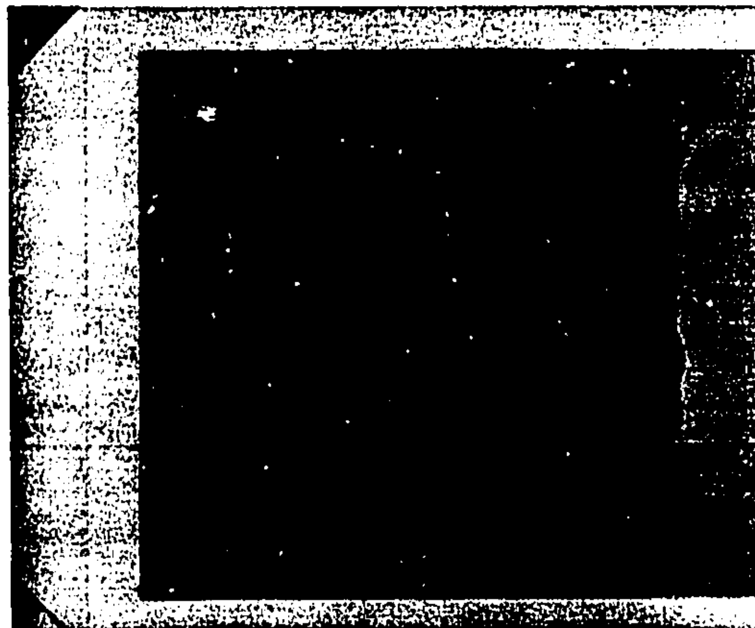

Fig. 5.7. The Photograph of the glass wafer showing the air gap cavity and the side volume cavity around the periphery for the square diaphragm.

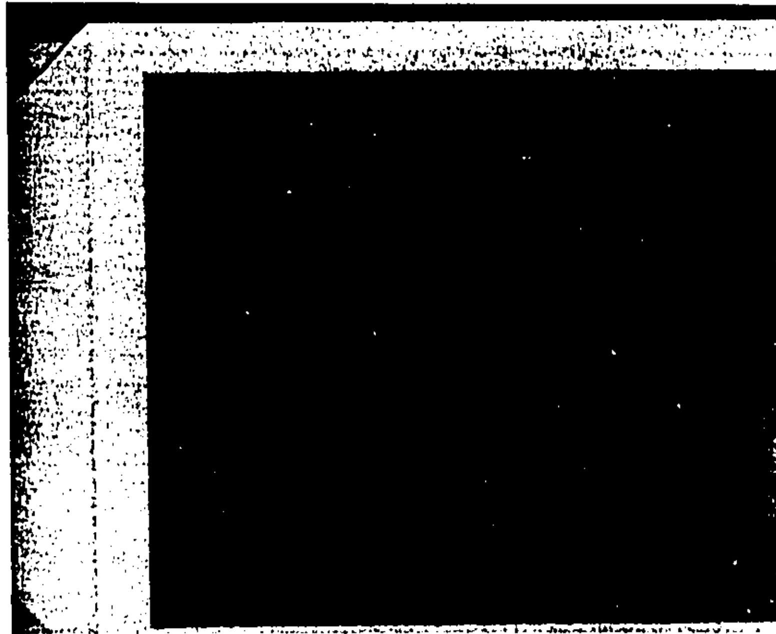

Fig. 5.8. The Photograph of the glass wafer showing the air gap cavity and the side volume cavity around the periphery for the circular diaphragm.

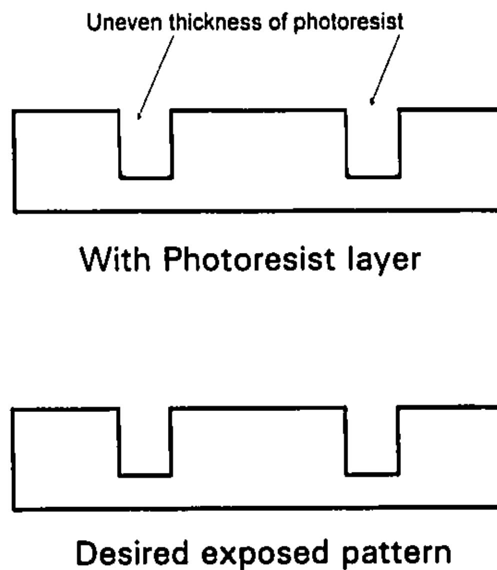

Fig 5.9 Advantages of Negative Photoresist

Negative photoresist was used because for accurate photolithography, it was desired to expose only regions of constant photoresist thickness to UV light. When negative resist is exposed to UV light, it becomes harder and is not removed during the development step. In this design, during step 5, the surface of the glass wafer has an etched cavity, and a highly variable thickness of resist will fill this cavity. If positive photoresist were used this would have been the regions which was exposed and removed. The penetration of UV light into this uneven layer would have been non uniform and the development step might not have removed the resist completely. Therefore negative photoresist was used, and the clear regions of the mask, exposed negative resist of a uniform thickness avoiding potential problems during the development process as shown in Figure 5.9.

5.2.2 Backplate Metalization Process:

The glass wafer with the electrical cavities is cleaned in DI water. Using Mask 3, photolithography process is performed. The mask 3 has to be aligned with the earlier mask pattern so that metalization can be done at the bottom of the air gap cavity. Metalization of the electrical contact is made in a chromium deposition evaporator as explained in Appendix A. 500 Å thick chromium is deposited on the glass wafer which forms the metal contact for the back electrode. The negative photoresist is then stripped off and the glass wafer with the metal contact and etch cavity is ready for Anodic bonding process.

5.2.3 Silicon Membrane

Very thin (10 µm thick) commercially available silicon membrane is used as the membrane for the condenser microphone. Using thin silicon membrane wafers reduces the micromachining steps of manufacturing a silicon membrane. Generally membranes are produced using anisotropic etching or surface micromachining (sacrificial layer) techniques. High dimensional tolerance is achieved (±0.1 µm) using thin silicon membranes. They also provide dimensional stability in flatness (±0.5 µm). The silicon membrane is cleaned by blowing nitrogen before the anodic bonding process. No other cleaning procedure is required before anodic bonding, as the membrane was cleaned from the factory and the dust particles were removed by blowing nitrogen on it. The membrane itself did not have any oxidation or patterning by photolithography process, as all the photolithography process was done on backplate which contains the side volume cavity, airgap cavity and back electrode.

5.2.4 Bonding of Silicon with Glass

The silicon and glass wafers are bonded using anodic bonding techniques as explained in Appendix C. Anodic bonding is a process of electrostatically bonding two dissimilar materials together to form a strong, hermetic seal. The bonding is performed by applying a voltage of 1000 V at temperature of 400°C.

5.3 Experimental Results and Summary

The achieved dimensions were very close to the designed dimensions. The achieved dimensions are given in Table 6.2 of Chapter 6. The designed air gap depth was 12 μm. By using the measuring instruments and its measurement accuracy, it was determined that the achieved devices dimensions are within ±5 μm in size and within ±.5 μm in the airgap depth. Except for the anodic bonding, all the fabrication techniques belong to the family of IC processes. However, the entire set of fabrication techniques belong to the class of microfabrication techniques. These techniques (microfabrication) are very powerful for sensor development and for a certain type of micromechanisms.

In our investigation, the electrical connections from the contact pads of the fabricated microphone to the preamplifier were made using silver paste commercially known as Electrodag 415. It is a dispersion of finely divided silver in a thermoplastic resin that rapidly dries in air to form a conductive shield on non-conductive substrates [64]. It exhibits excellent adhesion and provides controlled electrical properties in coatings as thin as 0.3 mil. It has a sheet electrical resistance of 0.04-0.07 Ω/□ @1 mil thickness. The surface to be coated must be clean, dry and free from dust. Proper stirring of the silver paste is necessary before the application of thin coating. The coated part is allowed to dry for 10 minutes approximately.

During anodic bonding, residual stresses develop in the diaphragm because of the little mismatch in the thermal expansion coefficients of the two materials

(Fig 5.1). The material are bonded at 350°C, when a potential of 1000 V is applied at that temperature for a few minutes.

The modulus of elasticity of a material is given by the equation

$$E = \frac{\sigma}{\varepsilon} \tag{5.1}$$

where E is the modulus of elasticity, σ is the stress and ε is the strain. From Fig 5.1, the strain for pyrex glass at 350°C is about 900 ppm and strain for silicon at the same temperature is about 1000 ppm. The difference between the two strains is about 100 ppm. Since this is the worst case scenario the actual strain will be less than 100 ppm. Using Eq. 5.1 and the material properties of silicon given in Table 4.2, the calculated stress in silicon during bonding is $\leq 1.64*10^7$ N/m^2. Other researchers have addressed the stresses in silicon membranes during anodic bonding at temperature similar to these used here (400°C), and have found similar results. In particular, Scheeper *et al* [51] found experimentally by a wafer bending method that the stresses in silicon membrane is $6*10^7$ N/m^2 and Bergqvist [70] predicted by multilayer multitemperature simulation of mechanical structure a stress on the diaphragm of $1.5*10^8$ N/m^2.

CHAPTER 6

Characterization of Condenser Microphone

As a sensor of sound, a microphone must fulfill three basic requirements: to provide an electrical signal well above the microphone self noise level, to provide undistorted output over a wide dynamic range, and, when used with associated equipment, to respond equally well to all frequencies produced by the sound source.

The experimental results presented in this chapter are based on the performance of the first few prototype condenser microphone fabricated for this project. Capacitive and frequency measurements were conducted, and their results are tabulated and compared with analytical results.

6.1 Capacitive Measurement

The capacitance of the microphone was measured at zero deflection using a setup as shown in Fig 6.1. The fabricated microphone chip is mounted on a probe box and is connected to a capacitive measurement instrument (precision LCR meter-HP 4284A) by means of calibrated leads. Shielded cables which minimize the effect of external fields are used to connect the microphone chip contacts with the measuring instrument. The measuring

instrument has a resolution of 0.5 fF and the fluctuations in the measurement can be minimized at high input frequency.

6.1.1 Experimental Procedure

The fabricated condenser microphone is placed on the testing platform of the probe box (black box). Vacuum pump is switched on to hold the condenser microphone to the base of the platform. Two probes, one connected to the bottom electrode and the other connected to the top electrode (membrane) is connected to the capacitance measurement instrument through the leads in the probe box. The zero pressure capacitance of one fabricated microphone was tested, at ambient conditions using the capacitance measurement instrument. It was observed that at low frequency the noise effect was too high and once the frequency was increased the stray effects were reduced and the capacitance value was stabilized. For frequencies above 800 kHz, the fluctuations reduced considerably and therefore the measurements of the capacitance was made at 1 MHz, for different shape and size of fabricated microphones.

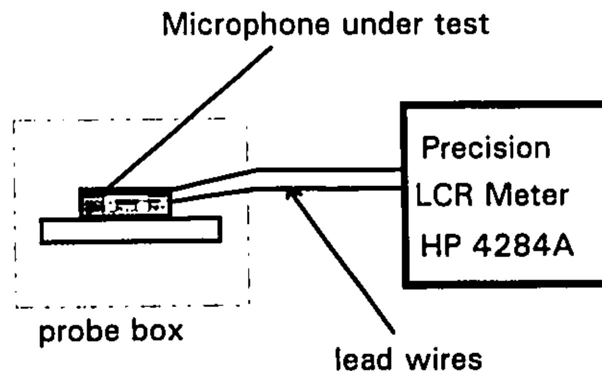

Fig. 6.1 Experimental Setup for Capacitive Measurement

6.1.2 Results and Discussion

Table 6.1 presents the theoretical and measured values for different condenser microphones. The theoretical value of the zero pressure capacitance of the microphones was calculated using Eqn. 2.1. It can be observed from the table that the variation of the zero pressure capacitance is less than 9% from theoretical results. This variation in capacitance may be due to the dimensional variation in the shape and size of the bottom electrode, and the depth of the airgap of each condenser microphones during the fabrication process.

Table 6.1 Analytical and Measured Capacitance

Microphone Shape	Designed Backplate electrode size (μm)	Designed Backplate electrode area (mm²)	Designed air gap thickness (μm)	Capacitance Analytical (pF)	Capacitance Measured (pF)
circle	dia = 900	.636	12	.469	.448
circle	dia = 750	.502	12	.326	.300
square	side = 800	.640	12	.472	.430
square	side = 600	.360	12	.266	.243
triangular	side = 500	.433	12	.319	.299
hexagonal	side = 425	.469	12	.346	.317

The achieved dimensions were very close to the designed dimensions. The achieved dimensions are given in Table 6.2. The designed air gap depth is

12 μm. Given the accuracy of the measuring instruments and measurement accuracy the achieved device dimensions are within ±5 μm in size and within ±0.5 μm in the airgap depth. The simulated values are given in Table 6.2. There is little variation of capacitance value for different size of backplate electrode area for a fixed airgap depth. Therefore computation of the capacitance value was done for change in airgap depth .

Table 6.2 Computed and Measured Capacitance

Microphone Shape	Achieved Backplate electrode size (μm)	Capacitance Analytical at 11 μm airgap (pF)	Capacitance Analytical at 12 μm airgap (pF)	Capacitance Measured (pF)
circle	dia = 900±5	.437 .428	.474 .463	.448
circle	dia = 750±5	.304 .296	.330 .321	.300
square	side = 800±5	.441 .430	.478 .466	.430
square	side = 600±5	.249 .241	.270 .261	.243
triangular	side = 500±5	.297 .291	.322 .316	.299
hexagonal	side = 425±5	.327 .312	.357 .337	.317

As seen from the Table 6.2, the computed capacitance at 11 μm airgap is very close to the measured capacitance. In all the cases, the measured capacitance is within the band of simulated values for airgap of 11.5±0.5 μm. A fully automated process would produce uniform and repeatable relation between designed and measured quantities.

6.2 Sensitivity and Frequency Response

Most condenser microphones are calibrated in terms of their open circuit voltage for a given sound pressure existing in a plane wave sound field before insertion of the microphone. Within the frequency range of any particular condenser microphone, the sound input should create an output voltage that is a direct function of the sound pressure input. The ratio of the two, the signal output to the sound input, is known as either the response coefficient or sensitivity. When plotting the logarithm of the magnitude of the response coefficient *vs* the logarithm of the frequency in a coordinate system, the result is the so called frequency response characteristic. Ideally, this should be a straight line, constant with frequency. The frequency response of a microphone is either indicated by a graph over the full audio spectrum or expressed by two frequency limits in cycles per second (Hz), within which the microphone responds uniformly and with little variation of sensitivity.

6.2.1 Experimental Setup

The sensitivity and frequency range of a condenser microphone can be measured using a Brüel and Kjaer 2619 preamplifier and a Brüel and Kjaer 2035 dual channel spectrum analyzer. The experimental setup is shown in Fig 6.2.

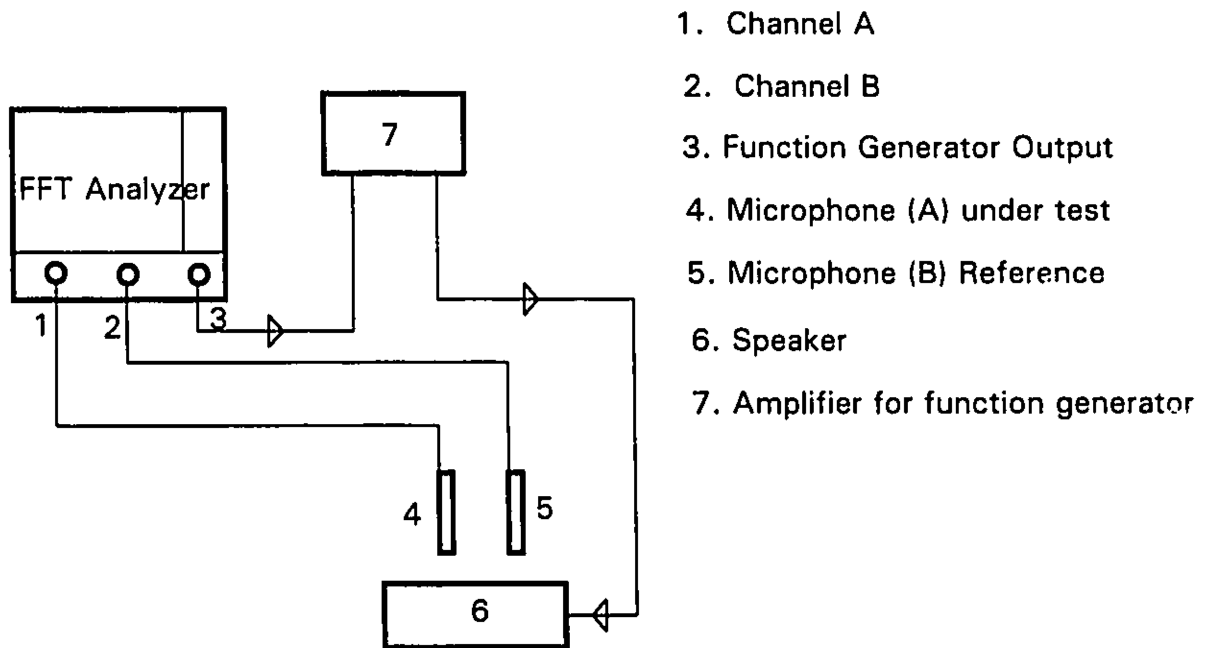

Figure 6.2 The measurement setup.

The back electrode contact of the condenser microphone is connected to the preamplifier input contact and the membrane contact of the condenser microphone is connected to the ground. The 2619 preamplifier has an input resistance of greater than 2.6 G Ω, and an input capacitance of 0.7 pF. The

standard (reference) microphone (B&K 4155) with the B&K 2615 preamplifier is connected to channel B and the fabricated microphone with the 2619 preamplifier is connected to the channel A. The broad band loudspeaker is connected to the amplifier and the amplifier is connected to the function generator (Module 3016), which is already available in the Brüel and Kjaer 2035 dual channel spectrum analyzer. A DC polarization voltage of 28V, required for the fabricated microphone is directly available from the B&K 2035 dual channel spectrum analyzer. The broad band loudspeaker excites the device under test and the reference microphone, which are all piloted by the B&K 2035 dual channel spectrum analyzer.

6.2.2 Experimental Procedure

The frequency response of a microphone is measured in an anechoic chamber, an enclosure which is carefully lined throughout with a highly absorbent material. The entire anechoic chamber arrangement is designed to enable a microphone to hear only the direct sound from a high-quality loudspeaker.

The dual channel spectrum analyzer (B&K 2035) excites the loudspeaker with 800 discrete and equally spaced frequencies between 0 and 25.6 kHz. There are several possible excitation signals, however in the present experimental analysis, pseudo random excitation signals were used. The advantages and disadvantages of the excitation signals are explained in Appendix E (Table E1). The loudspeaker reproduces sound electrical signals

supplied by an audio frequency signal generator and amplifier. Mounted next to the fabricated silicon microphone is a calibrated (reference) condenser microphone. Sensitivity of the microphone is calibrated by applying a sine excitation signal of 1 kHz at a sound pressure level of 94 dB (≈1 Pa).

The microphone under test and the reference microphone are pointed at the loudspeaker. Both the signals are fed into the analyzer (B&K 2035) for computation of the microphone transfer function, and its frequency response curve, the autospectrum, and the coherence (see Appendix E) is recorded in the dual channel spectrum analyzer (B&K 2035). The voltage output of the microphone will increase or decrease when its frequency response is not uniform. This results in the dips and peaks revealed by the curves, indicating the ability of the microphone to convert sound pressures into equal variations in voltage output.

6.2.3 Results and Discussions

Initially, two standard microphones, one B&K 4155, which has a sensitivity of 45.7 mV/Pa with 0 V polarization voltage and the other B&K 4138, which has a sensitivity of 16.5 mV/Pa with 200 V polarization voltage, were calibrated by a B&K Pistophone for their response, and they were also tested for their frequency response by using the procedure explained in section 6.2.2. The frequency response of the B&K 4155 standard microphone supplied by the manufacturer is shown in Fig. 6.3. The responses of the autospectrum, frequency response and coherence are given in Fig. 6.4 (a,b and c). The autospectrum response of both the standard microphones are

identical as seen from Fig. 6.4 a., when a sine excitation signal at 250 Hz was applied at a sound pressure level of 94 dB (≈1 Pa). This was done as the sensitivity of the standard microphone was calibrated at 250 Hz.

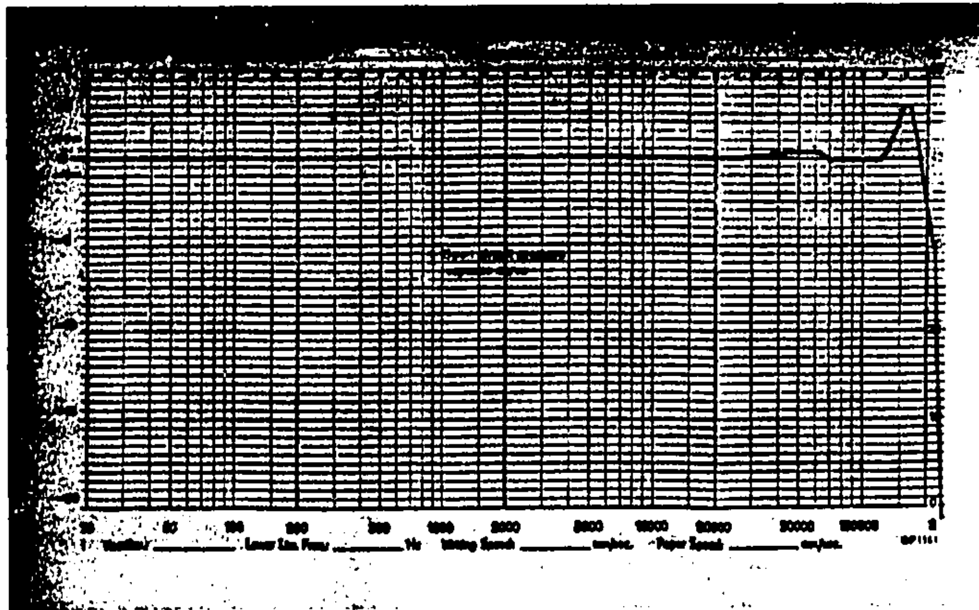

Fig. 6.3 Frequency response of the B&K 4155 standard microphone [65]

The flat frequency range of the standard microphone is in the range of 0-20 kHz as can be seen from the frequency response (H_1 and H_2) and coherence plots (Fig 6.4 b and c). The irregularities of the readings in the plots of frequency response (Fig. 6.4 b) are ±5 dB. Actually these response curves should be flat within ±1 dB as shown by the manufacturer frequency response given in Fig. 6.3. The fluctuations larger than this i.e >5-10 dB at 9-13 kHz were found to be due to the loudspeaker. In view of the ≈ ±5 dB variations of the standard microphone response throughout most of the

frequency range, a tolerance of ±5 dB will be used in determining the flat frequency range of the fabricated microphone. This test confirms that standard microphones are calibrated to the specifications and can be used as reference microphones in the experiment. B&K 4155 standard microphone was taken as the reference microphone for the experiment.

The standard (reference) microphone (B&K 4155) with the B&K 2615 preamplifier is connected to channel B and the fabricated microphone with the 2619 preamplifier is connected to channel A for the setup shown in Fig. 6.2. The fabricated microphones are calibrated by following the procedure explained in section 6.2.2. The autospectrum plots, frequency response plots and coherence plots for all the fabricated microphones are plotted in Figures 6.5 - 6.10 both inclusive.

The sensitivity and the flat frequency range of the different fabricated microphone are presented in Table 6.3. The sensitivity of the microphone was measured at 1 kHz. The flat frequency range of the fabricated microphone can be seen from the figures 6.5 - 6.10. All measurements were performed on complete wafers with microphones. From the autospectra and coherence measurements, it can be found that for all fabricated microphones there is an important difference for responses below 1 kHz. The tested microphones are more sensitive at low frequencies, which is why, the sensitivities were measured at 1 kHz. For the flat frequency range the response is reasonable.

The ambient noise of the room was 41 dB (A weighting). The noise was tested using a Modular Precision Sound level meter (B & K type: 231) .

Table 6.3 Summary of the Results for the Microphone Characterization.

Microphone Shape	Backplate electrode size (μm)	Flat Frequency Range (kHz)	Sensitivity (mV/Pa) @ 1 kHz	Frequency limit for > 0.85 coherence (kHz)
B & K	-	0-22	45.7*	0-22
circle	dia = 900	0.2-5.4	0.92	1-22
circle	dia = 750	0.2-5.2	0.73	2-22
square	side = 800	0.2-3.6	0.84	2-22
square	side = 600	0.2-5.2	0.53	2-22
triangular	side = 500	0.2-5.4	0.62	2-22
hexagonal	side = 425	0.2-5.3	0.67	2-22

* @ 250 Hz exception

The summary of the tests are presented in Table 6.3. For each fabricated microphone, the flat frequency response, the sensitivity and the coherence are presented. Fig 6.11 shows the noise level of the standard microphone and fabricated microphone, the noise level of the fabricated microphone is about 50 dB. the measured noise level corresponds well with the measurements of Bergqvist et al [50]. Because the noise of the microphone is dominated by microphone preamplifier, the signal to noise ratio of the silicon condenser microphone can only be optimized by increasing the sensitivity. The sensitivity of the microphone can be optimized by decreasing the diaphragm thickness. In order to maintain the same band width, the air streaming resistance should be decreased, which can be achieved by increasing the air gap thickness.

Analyzing the results from Table 6.3, the frequency range of the fabricated microphones lies between 0.2- 5.4 kHz. For all the shapes designed, the natural frequency of the diaphragm was found to be ≥ 38.6 kHz (Table 4.1), which is substantially above the audible frequency range. The cut-off frequency of the fabricated microphone varied between 3.6 kHz and 5.4 kHz. Furthermore, with the exception of 1 square microphone, all cut-off frequencies lie within a much tighter range of 5.2-5.4 kHz. Note that, even though the natural frequency of the diaphragm varies drastically for different shapes of the diaphragm (Table 4.1), the measured cut-off frequency does not. This is a very revealing result, since the cut-off frequency of the fabricated microphone appears to not vary significantly with membrane shape. Note that the theoretical fundamental frequencies calculated in Table 4.1 would predict considerable variation with shape. Thus it can be reasoned that the cutoff in the audible range is not due to shape, but due to some mechanism which does not vary significantly with shape.

Table 6.4 Estimated Volume and Constant K.

Microphone Shape	Diaphragm size (µm)	Diaphragm area (mm^2)	Estimated Volume (mm^3)	Constant K
circle	dia = 1000	.7854	0.00994	79.04
circle	dia = 800	.5027	0.00648	77.57
square	side = 1200	1.4400	0.01795	80.22
square	side = 1000	1.0000	0.01265	79.04
triangular	side = 700	.2122	0.00295	71.78
hexagonal	side = 500	.6495	0.00874	74.33

One such possible mechanism involves the total airgap volume. This mechanism has also been suggested by other researchers in references [59,60]. The airgap volume for the different shapes were estimated from the design and process and are given in Table 6.4. These estimates assume an airgap depth of 11.5 μm and a side volume depth of 19 μm. A constant K, which is the ratio of the airgap volume to the diaphragm area, is shown in Table 6.4. Note that this constant K does not vary significantly for the different shapes of the microphones. Therefore this is a possible cause for the invariance of cut-off frequencies of the fabricated microphone.

As seen from Table 6.3, the sensitivity lies between 0.53 - 0.92 mV/Pa. The measured sensitivities are roughly equal to the values presented by Bergqvist *et al* [43] and by Kuhnel and Hess [47] for their microphones with highly perforated backplates. Fabrication of the microphone by Bergqvist *et al* requires four wafer chip and seven masking steps and Kuhnel and Hess require two wafer chips and more than four masking steps. The present investigations requires two wafer chips and three masking steps to fabricate the microphone. The aim of the present investigation was to design a process that uses a minimum number of masking steps, since each masking steps require a critical and labor intensive mask alignment process. Any increase in masking steps increase the cost of production.

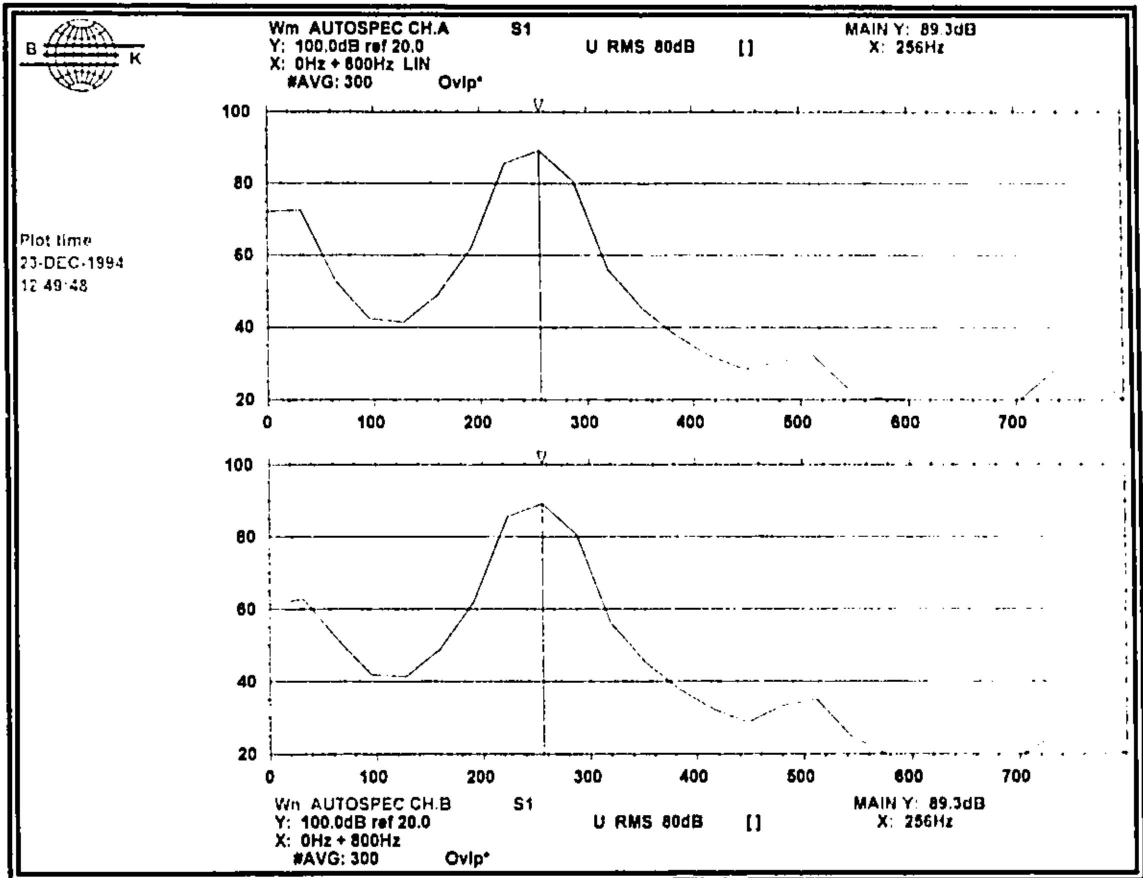

Figure 6.4 (a) Dual channel autospectra for the standard microphones

Channel A - B&K 4138 microphone
Channel B - B&K 4155 microphone

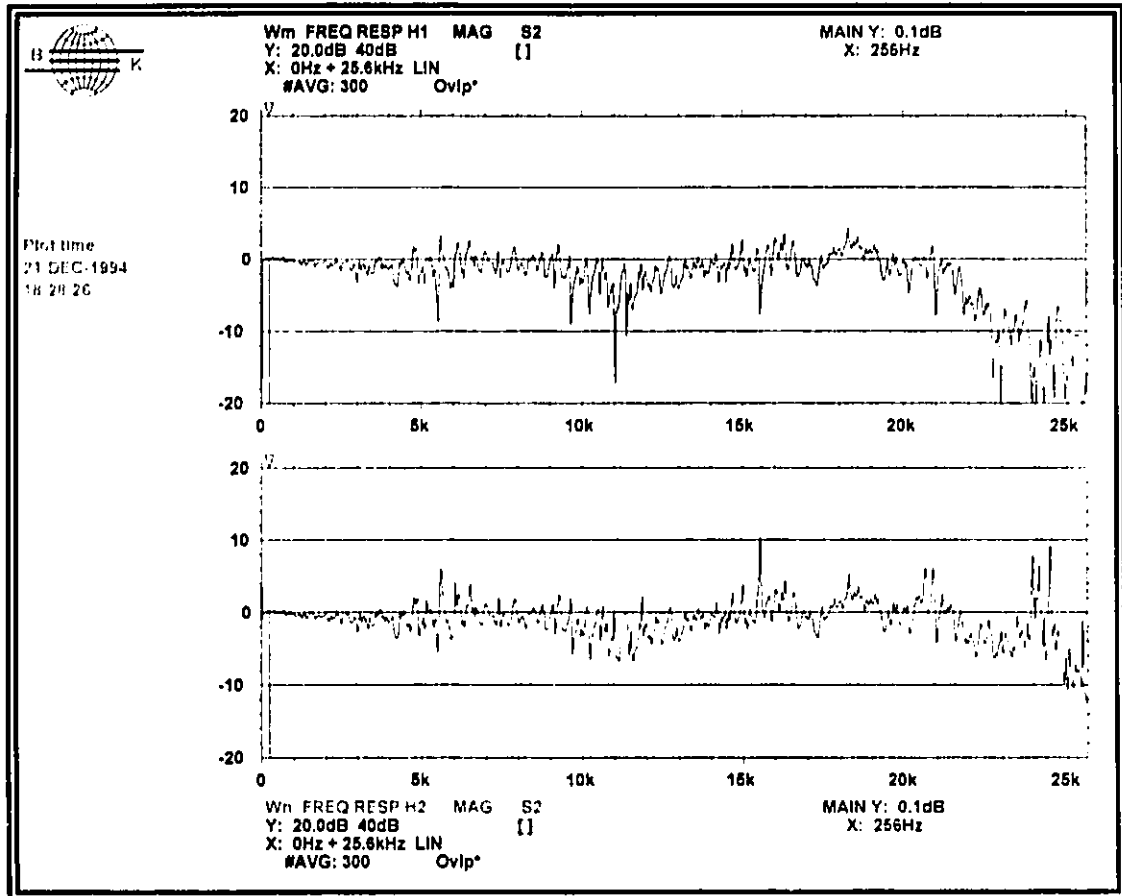

Figure 6.4 (b) Frequency response for the standard microphone.

Channel A - B&K 4138 microphone
Channel B - B&K 4155 microphone

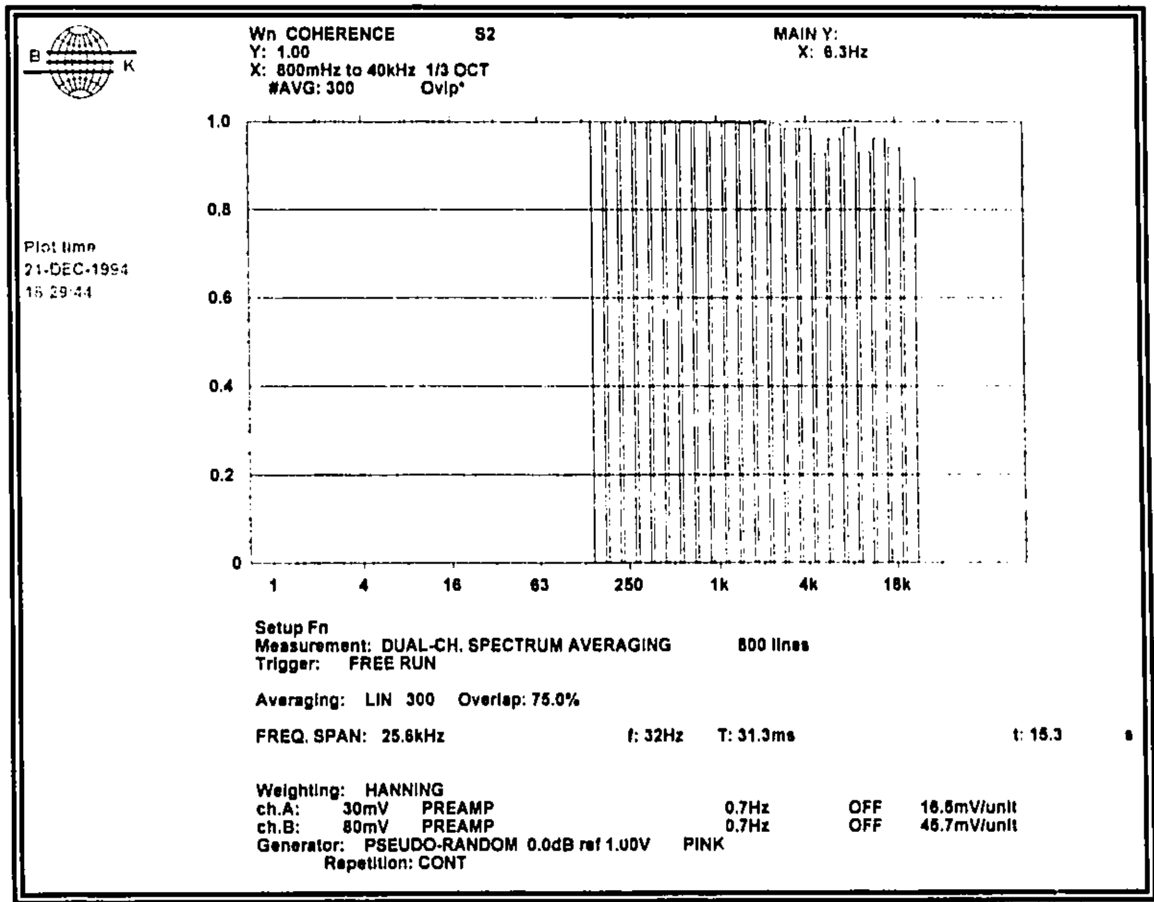

Figure 6.4 (c) Coherence between the standard microphones.

Channel A - B&K 4138 microphone
Channel B - B&K 4155 microphone

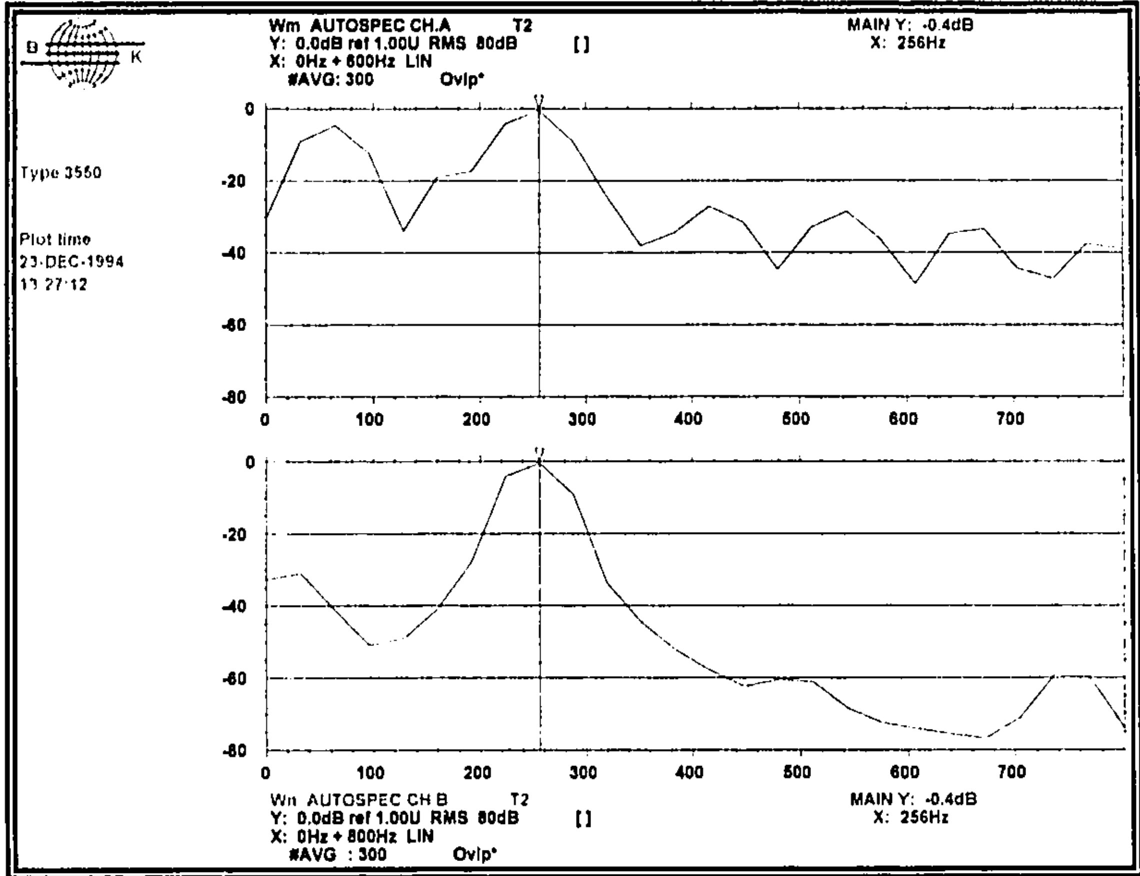

Figure 6.5 (a) Autospectra for the fabricated and reference microphones.

Channel A - Fabricated microphone
Channel B - B&K 4155 microphone (reference)

Fabricated Microphone:	shape:	Circular
	Membrane size:	Dia = 1.2 mm
	back electrode:	.636 mm^2(dia = 900μm)
	air gap:	12 μm

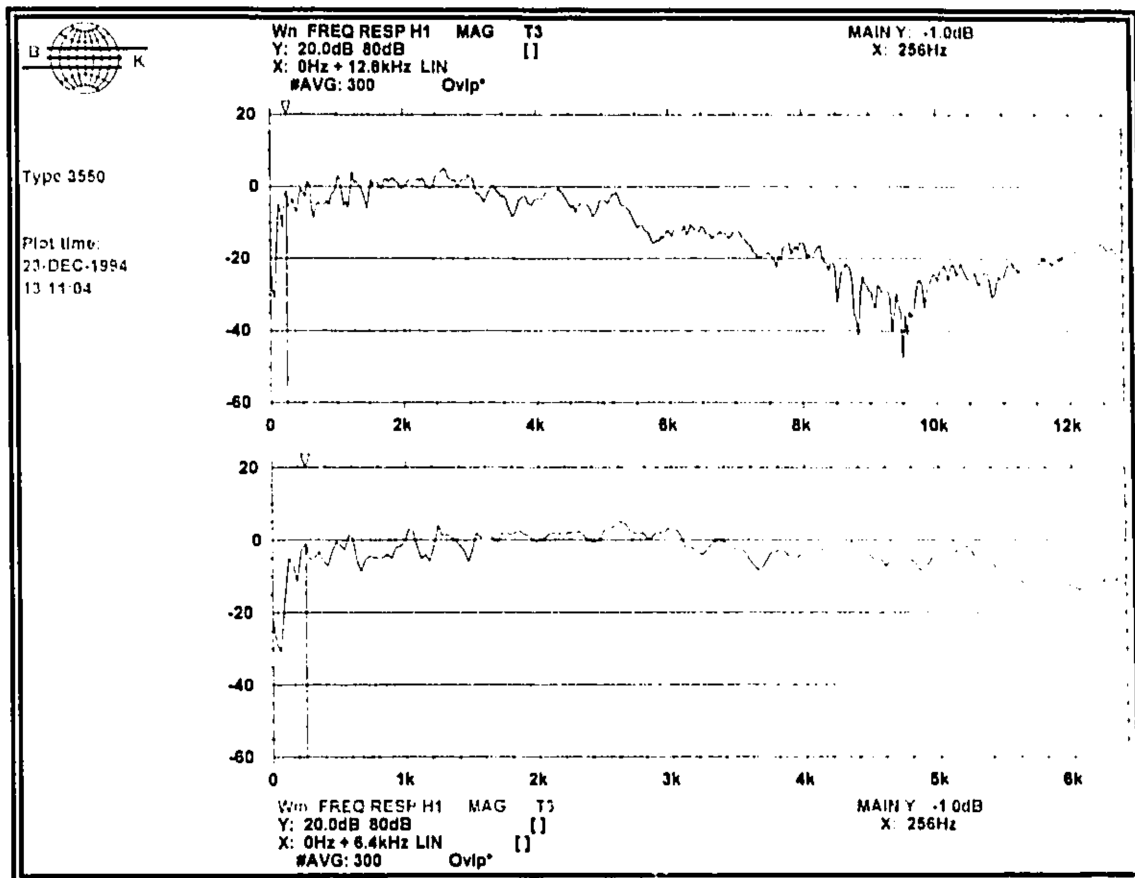

Figure 6.5 (b) Frequency response for the fabricated microphone.

Channel A - Fabricated microphone
Channel B - B&K 4155 microphone (reference)

Fabricated Microphone:	shape:	Circular
	Membrane size:	Dia = 1.2 mm
	back electrode:	.636 mm^2(dia = 900μm)
	air gap:	12 μm

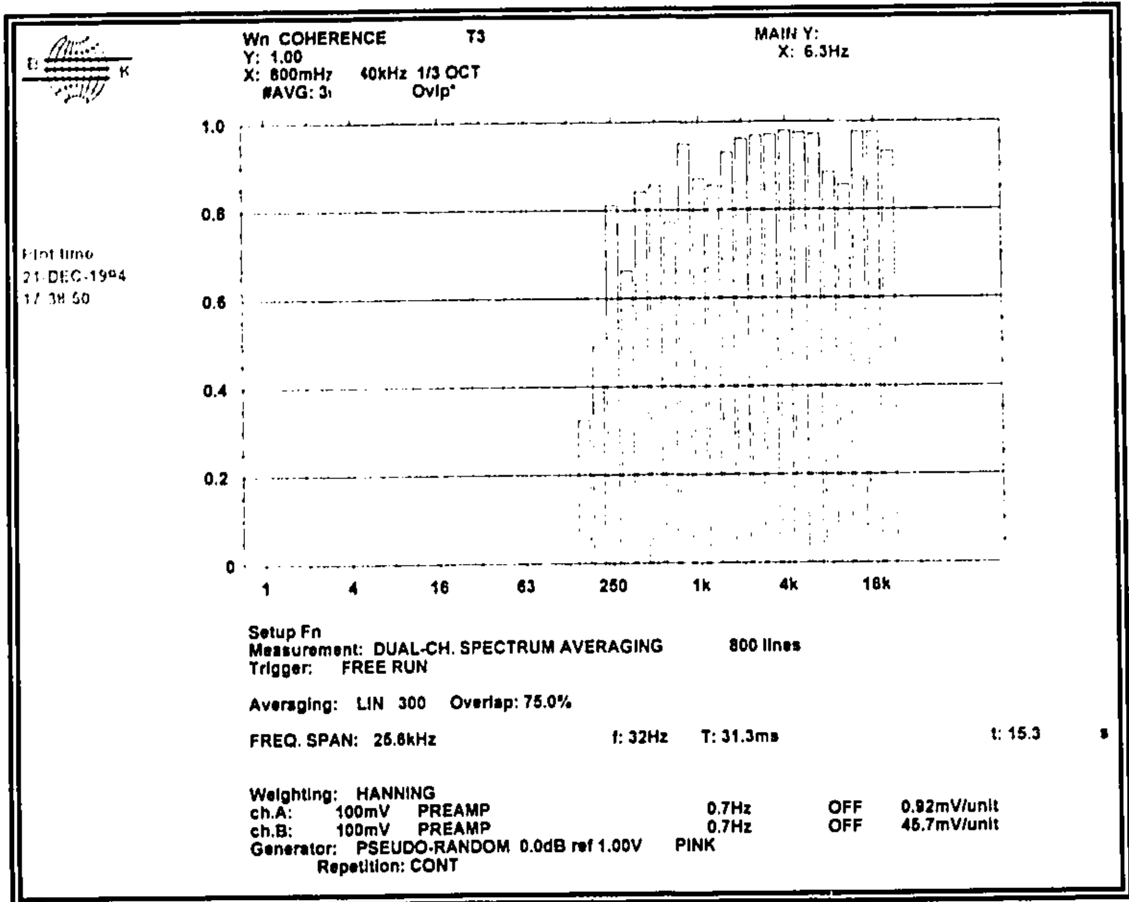

Figure 6.5 (c) Coherence between fabricated and reference microphone.

Channel A - Fabricated microphone
Channel B - B&K 4155 microphone (reference)

Fabricated Microphone:	shape:	Circular
	Membrane size:	Dia = 1.2 mm
	back electrode:	.636 mm²(dia = 900μm)
	air gap:	12 μm

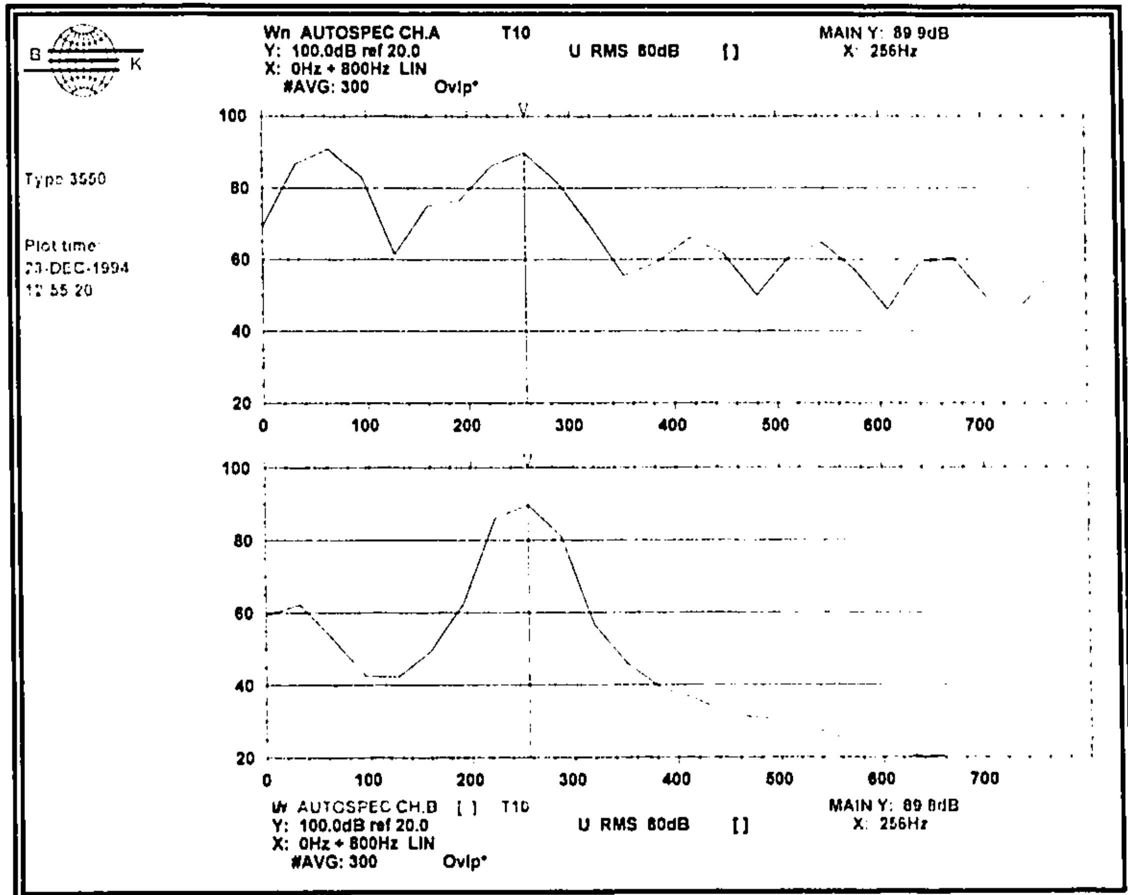

Figure 6.6 (a) Dual channel autospectra for the fabricated and reference microphones.

Channel A - Fabricated microphone
Channel B - B&K 4155 microphone (reference)

Fabricated Microphone:	shape:	Circle
	Membrane size:	dia= 1mm
	back electrode:	.502 mm^2 (dia = 750µm)
	air gap:	12 µm

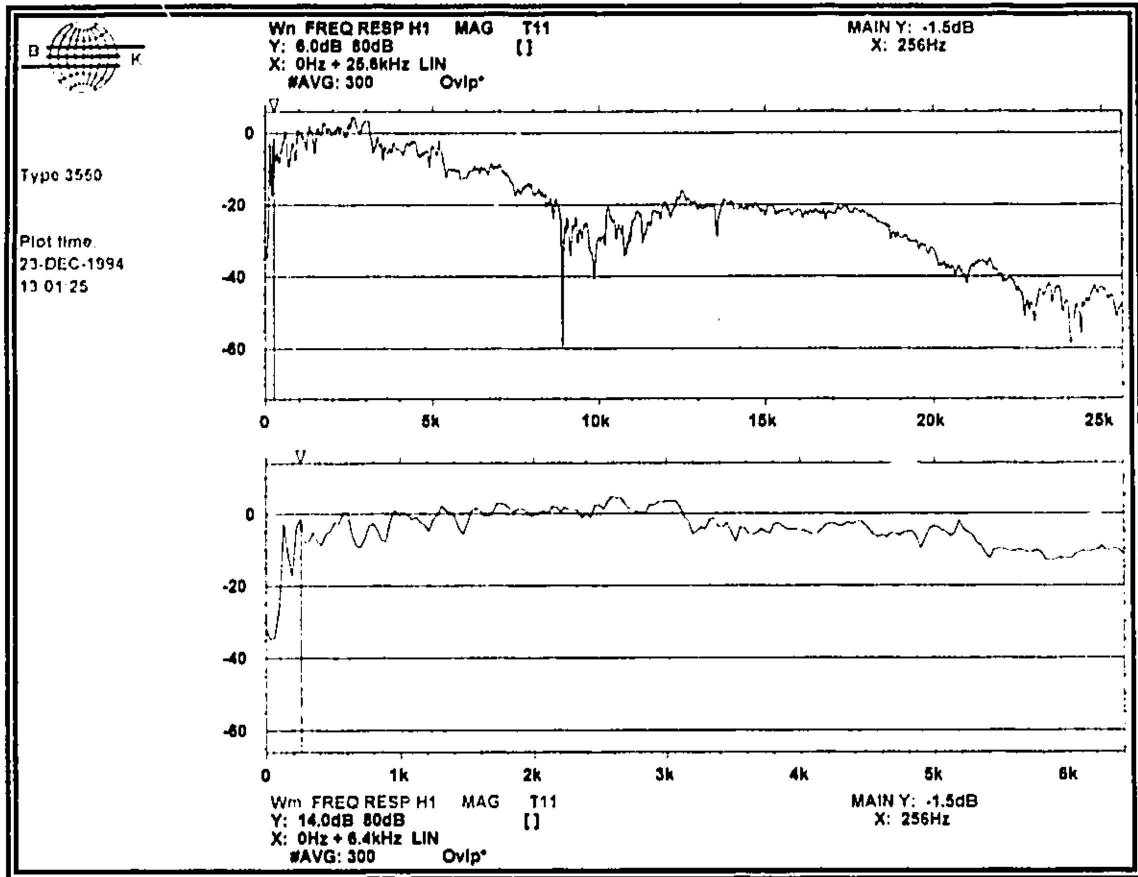

Figure 6.6 (b) Frequency response for the fabricated microphone.

Channel A - Fabricated microphone
Channel B - B&K 4155 microphone (reference)

Fabricated Microphone:	shape:	Circle
	Membrane size:	dia = 1mm
	back electrode:	.502 mm^2 (dia = 750µm)
	air gap:	12 µm

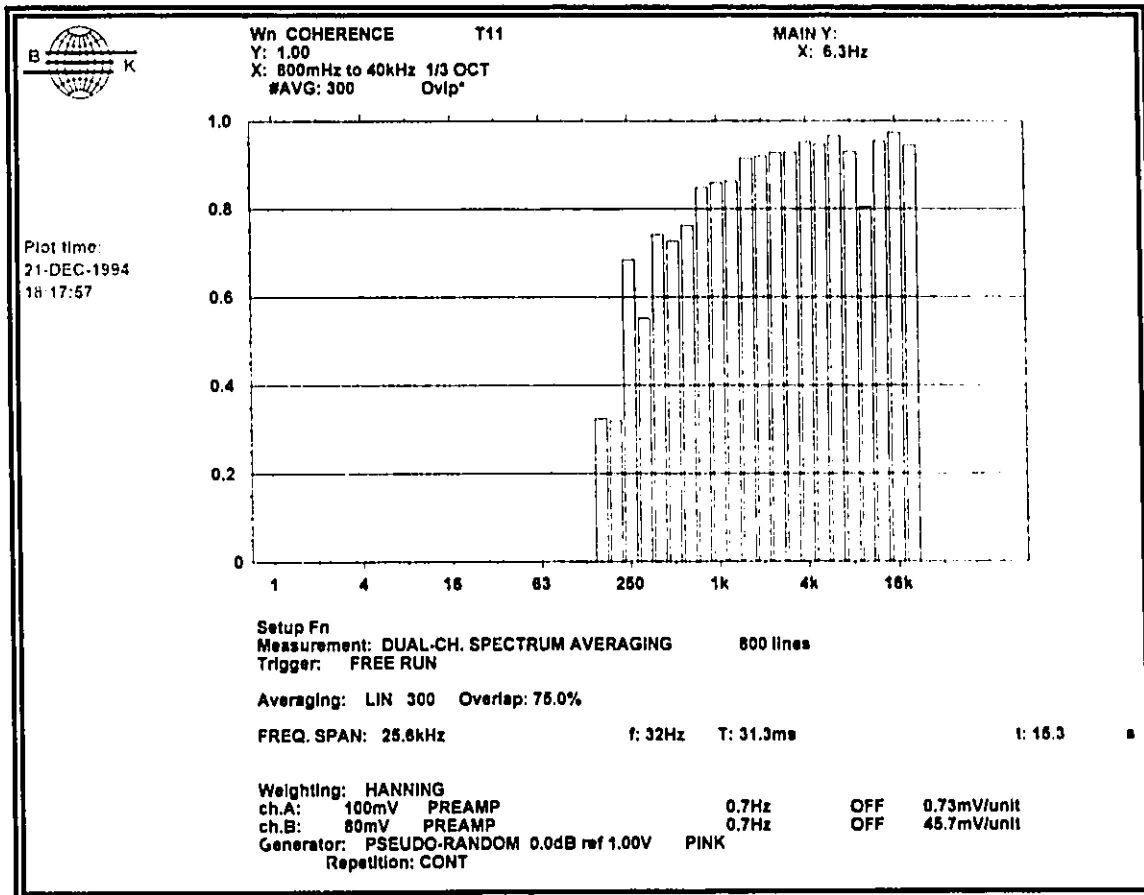

Figure 6.6 (c) Coherence between fabricated and reference microphone.

Channel A - Fabricated microphone
Channel B - B&K 4155 microphone (reference)

Fabricated Microphone:	shape:	Circle
	Membrane size:	dia= 1mm
	back electrode:	.502 mm^2 (dia = 750μm)
	air gap:	12 μm

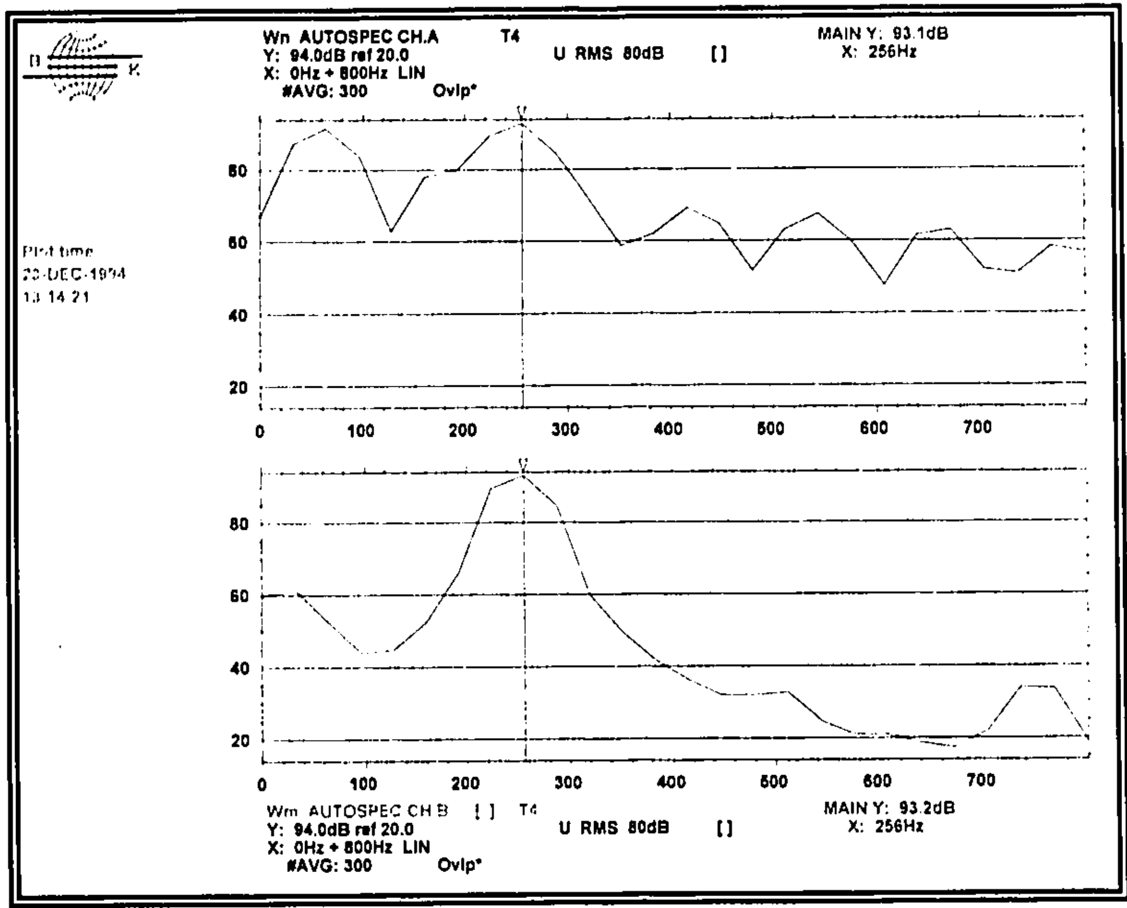

Figure 6.7 (a) Autospectra for the fabricated and reference microphones.

Channel A - Fabricated microphone
Channel B - B&K 4155 microphone (reference)

Fabricated Microphone:	shape:	Square
	Membrane size:	Side = 1 mm
	back electrode:	.640 mm^2 (side = 800μm)
	air gap:	12 μm

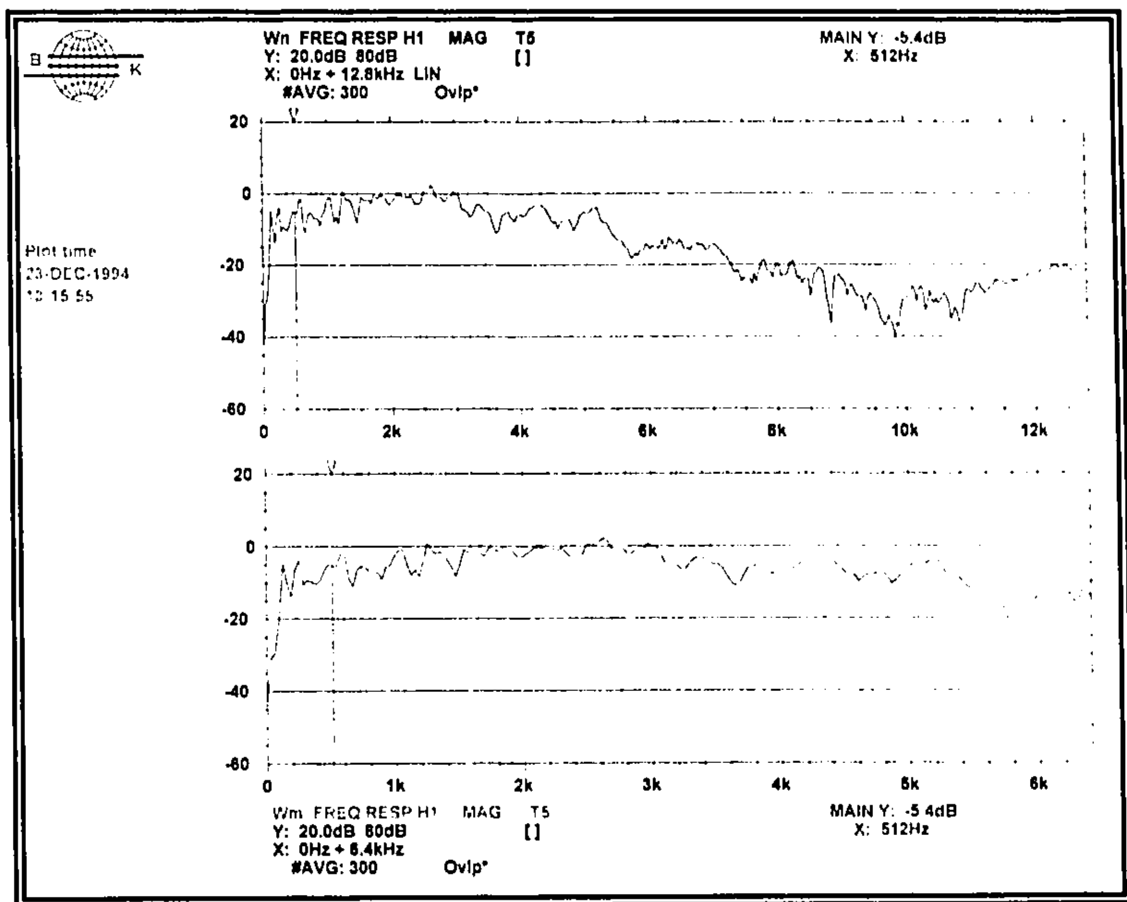

Figure 6.7 (b) Frequency response for the fabricated microphone.

Channel A - Fabricated microphone
Channel B - B&K 4155 microphone (reference)

Fabricated Microphone:	shape:	Square
	Membrane size:	Side = 1 mm
	back electrode:	.640 mm² (side = 800μm)
	air gap:	12 μm

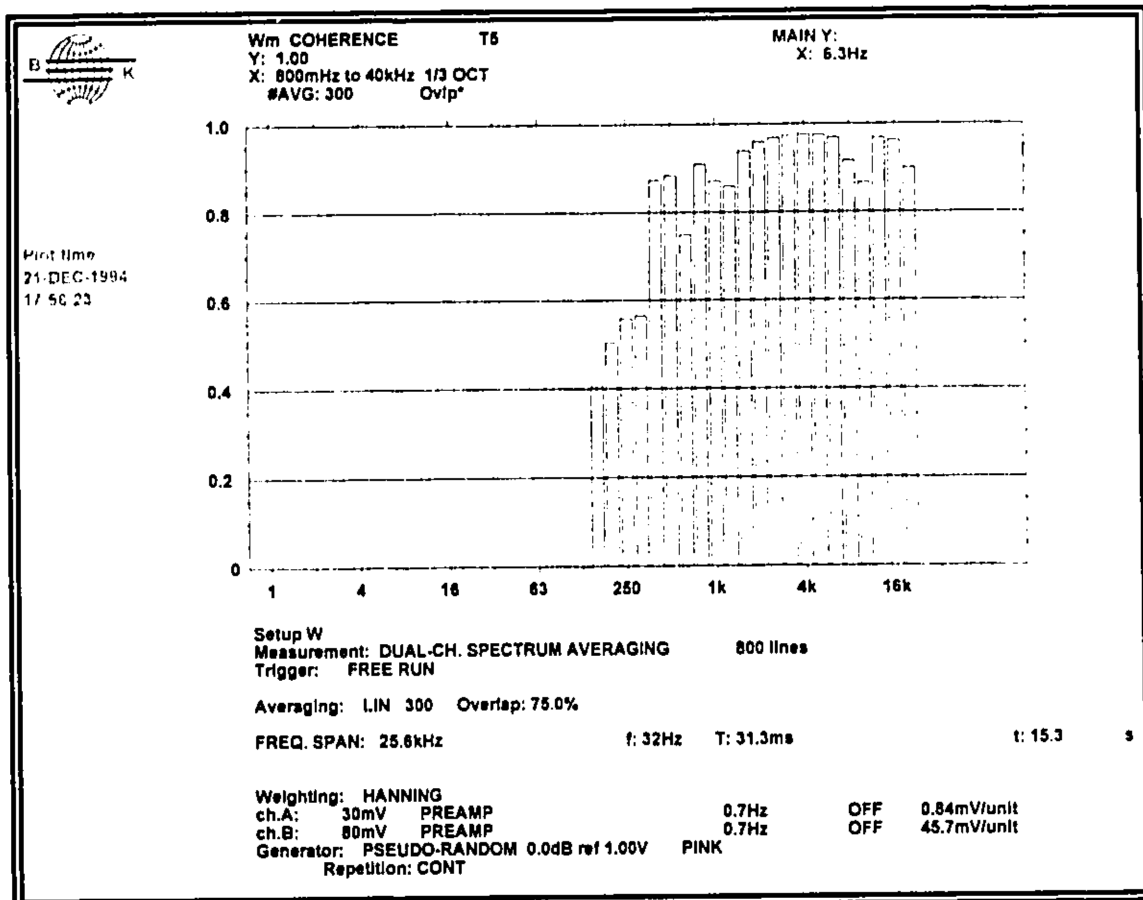

Figure 6.7 (c) Coherence between fabricated and reference microphone.

Channel A - Fabricated microphone
Channel B - B&K 4155 microphone (reference)

Fabricated Microphone:	shape:	Square
	Membrane size:	Side = 1 mm
	back electrode:	.640 mm^2 (side = 800μm)
	air gap:	12 μm

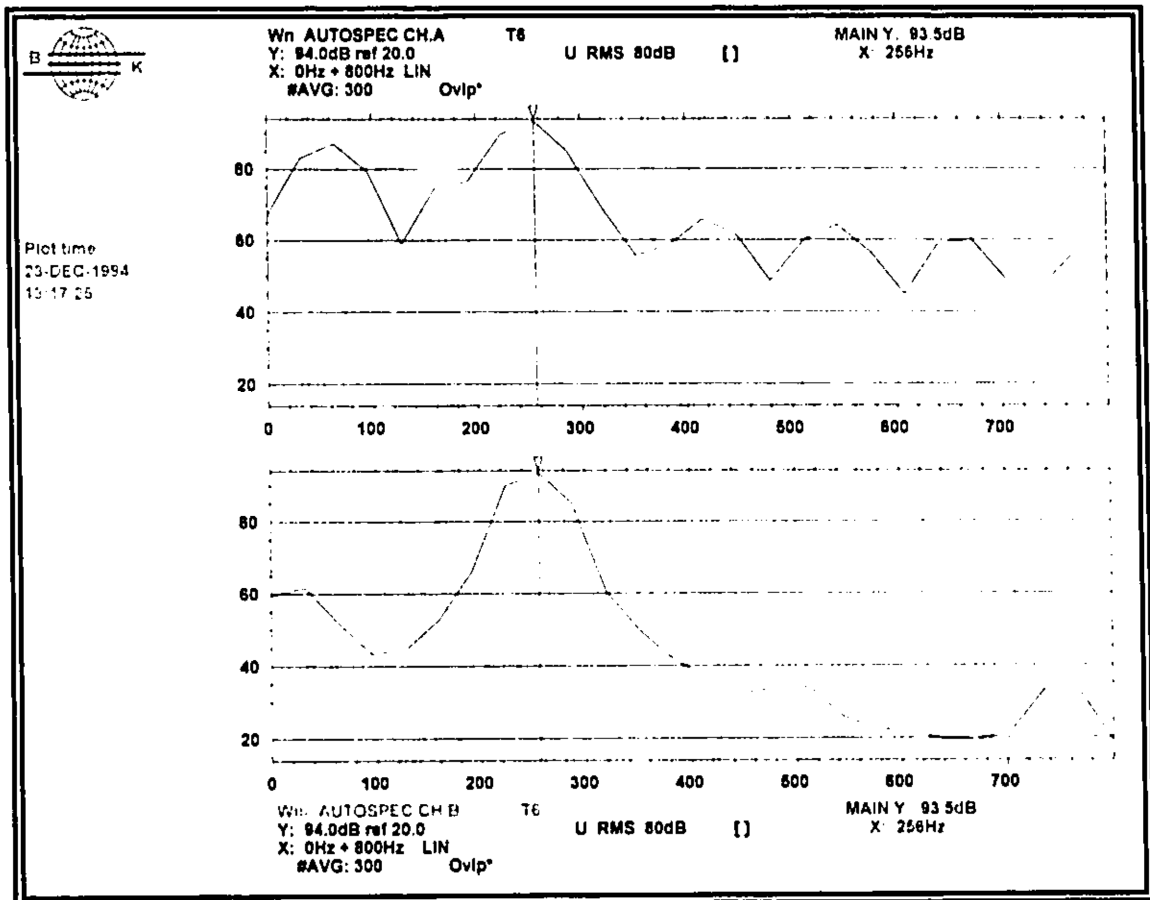

Figure 6.8 (a) Autospectra for the fabricated and reference microphones.

Channel A - Fabricated microphone
Channel B - B&K 4155 microphone (reference)

Fabricated Microphone:	shape:	Square
	Membrane size:	Side = 0.8 mm
	back electrode:	.360 mm^2 (side = 600μm)
	air gap:	12 μm

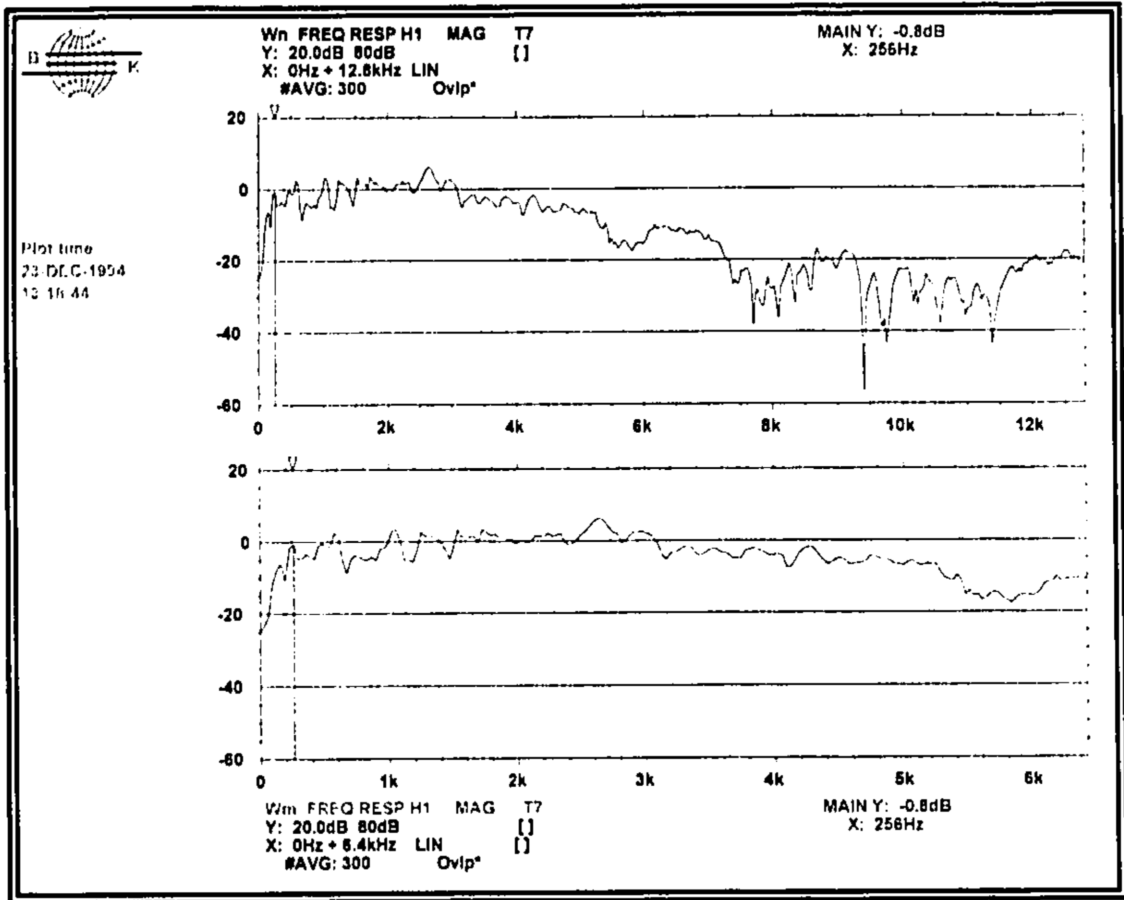

Figure 6.8 (b) Frequency response for the fabricated microphone.

Channel A - Fabricated microphone
Channel B - B&K 4155 microphone (reference)

Fabricated Microphone:	shape:	Square
	Membrane size:	Side = 0.8 mm
	back electrode:	.360 mm² (side = 600μm)
	air gap:	12 μm

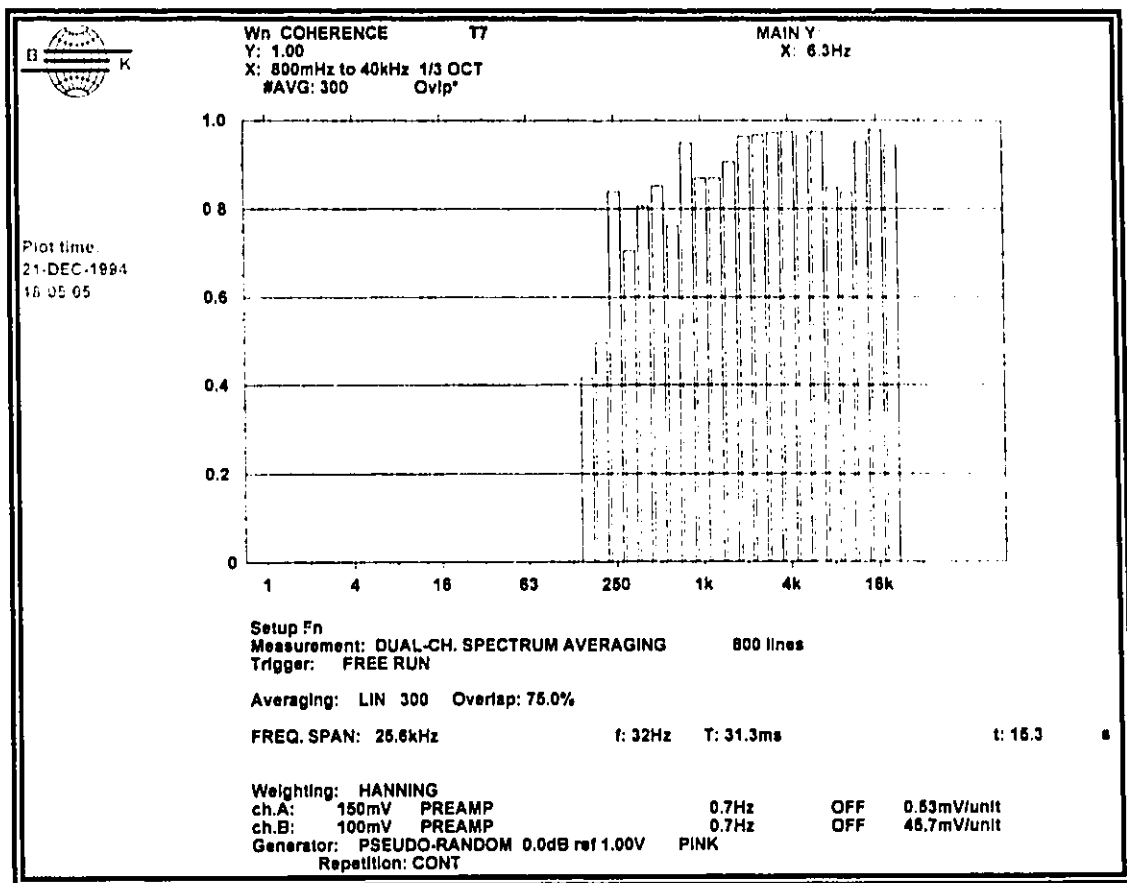

Figure 6.8 (c) Coherence between fabricated and reference microphone.

Channel A - Fabricated microphone
Channel B - B&K 4155 microphone (reference)

Fabricated Microphone:	shape:	Square
	Membrane size:	Side = 0.8 mm
	back electrode:	.360 mm² (side = 600μm)
	air gap:	12 μm

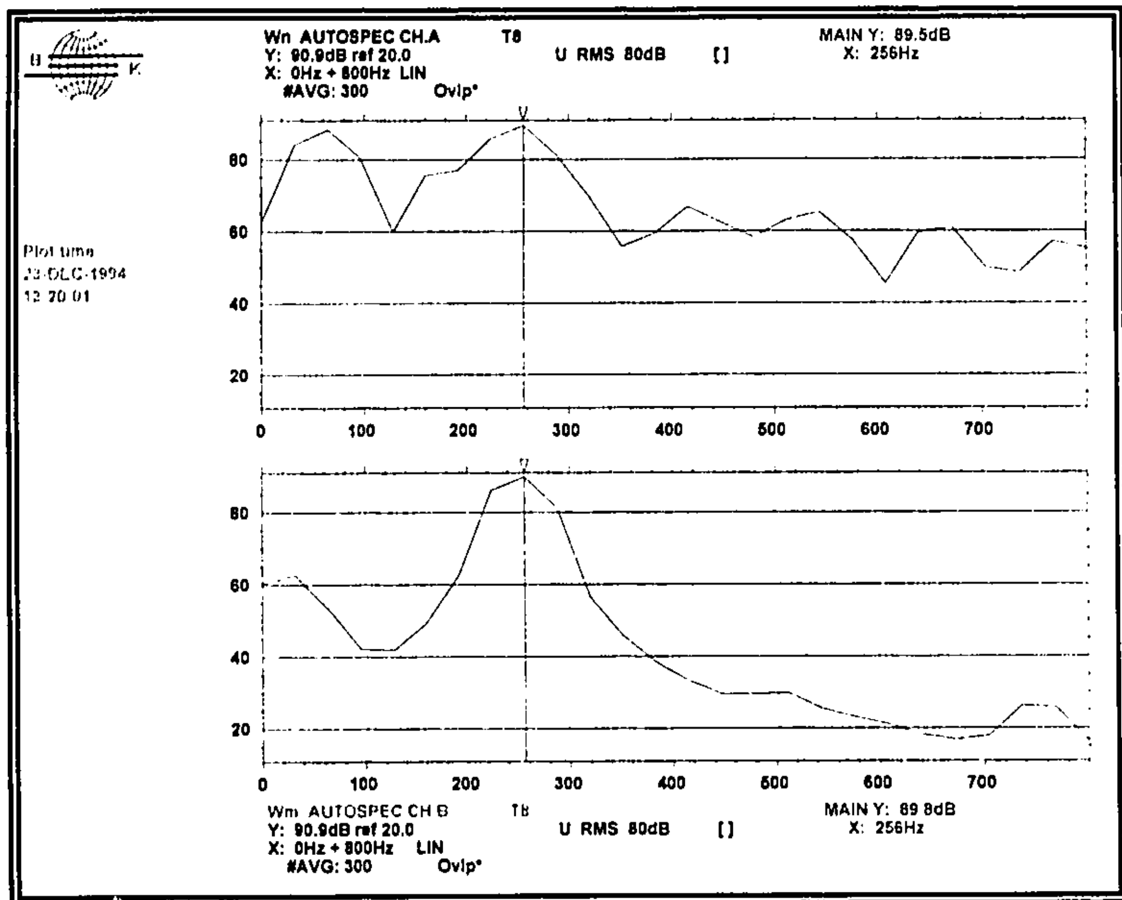

Figure 6.9 (a) Autospectra for the fabricated and reference microphones.

Channel A - Fabricated microphone
Channel B - B&K 4155 microphone (reference)

Fabricated Microphone:	shape:	Triangular (equilateral)
	Membrane size:	Side = 0.7 mm
	back electrode:	.433 mm^2 (side = 500μm)
	air gap:	12 μm

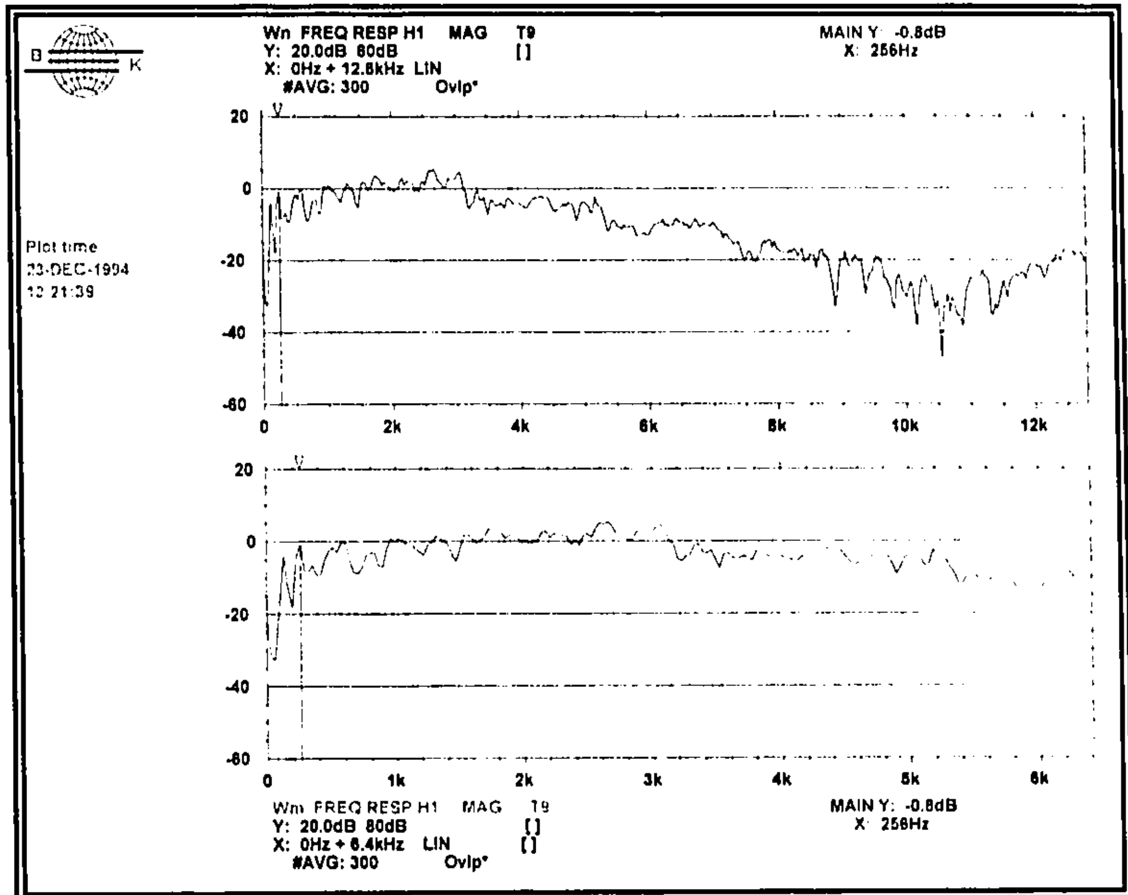

Figure 6.9 (b) Frequency response for the fabricated microphone.

Channel A - Fabricated microphone
Channel B - B&K 4155 microphone (reference)

Fabricated Microphone:	shape:	Triangular (equilateral)
	Membrane size:	Side = 0.7 mm
	back electrode:	.433 mm² (side = 500μm)
	air gap:	12 μm

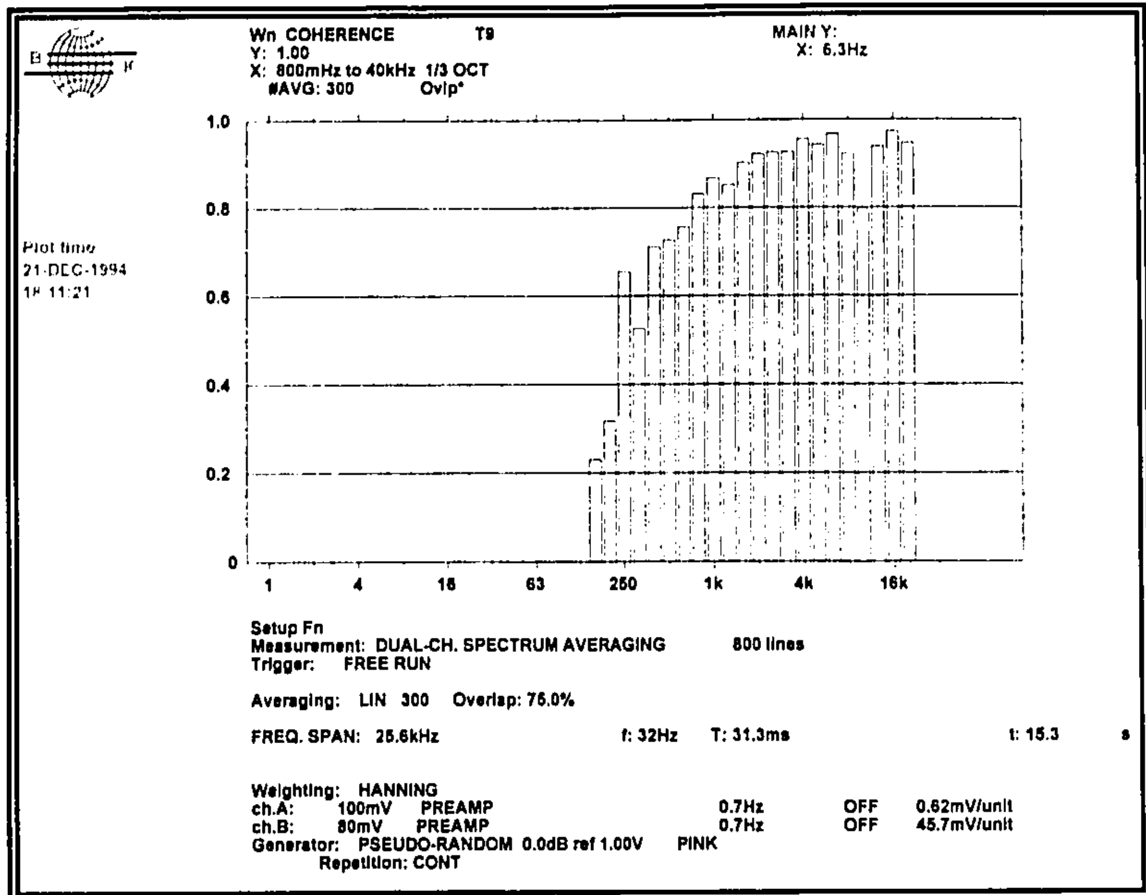

Figure 6.9 (c) Coherence between fabricated and reference microphone.

Channel A - Fabricated microphone
Channel B - B&K 4155 microphone (reference)

Fabricated Microphone:	shape:	Triangular (equilateral)
	Membrane size:	Side = 0.7 mm
	back electrode:	.433 mm^2 (side = 500μm)
	air gap:	12 μm

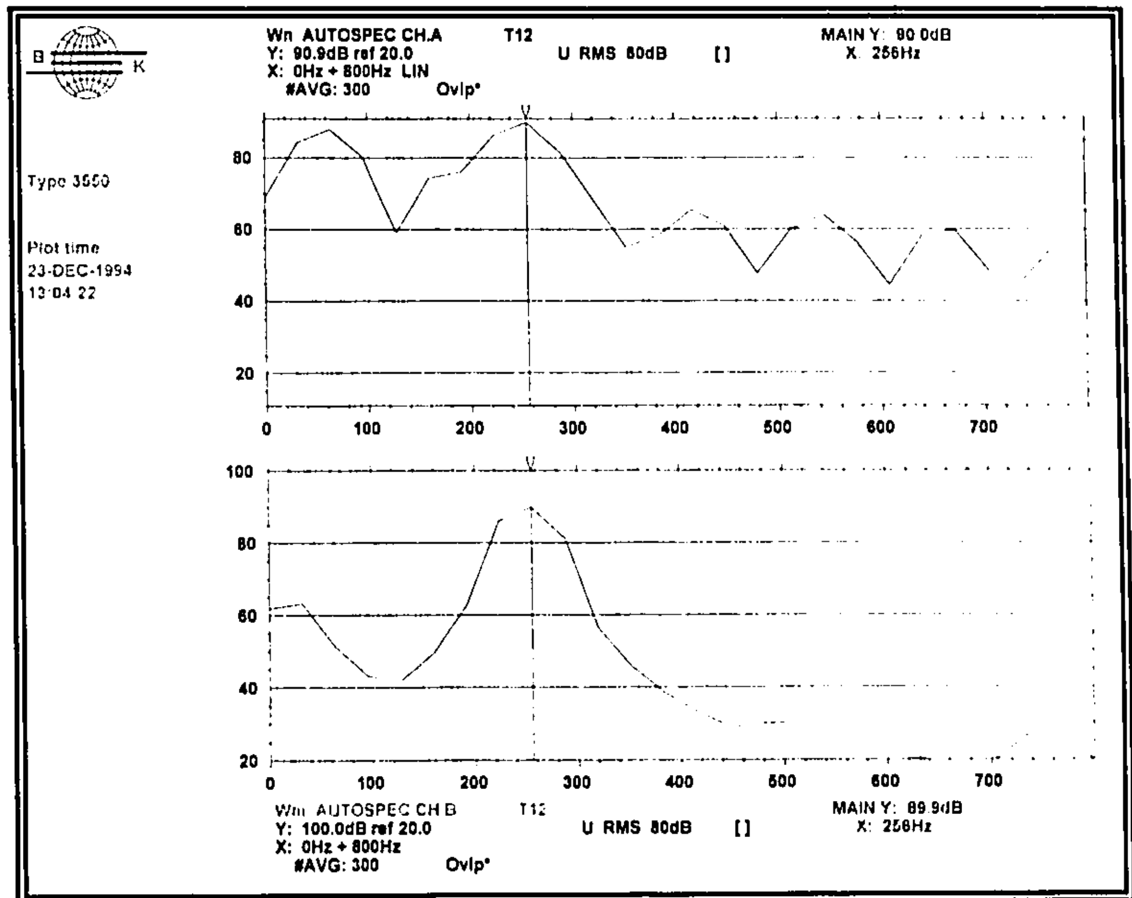

Figure 6.10 (a) Dual channel autospectra for the fabricated and reference microphones

Channel A - Fabricated microphone
Channel B - B&K 4155 microphone (reference)

Fabricated Microphone:	shape:	Hexagonal (regular)
	Membrane size:	Side = 0.5 mm
	back electrode:	.469 mm^2
	air gap:	12 μm

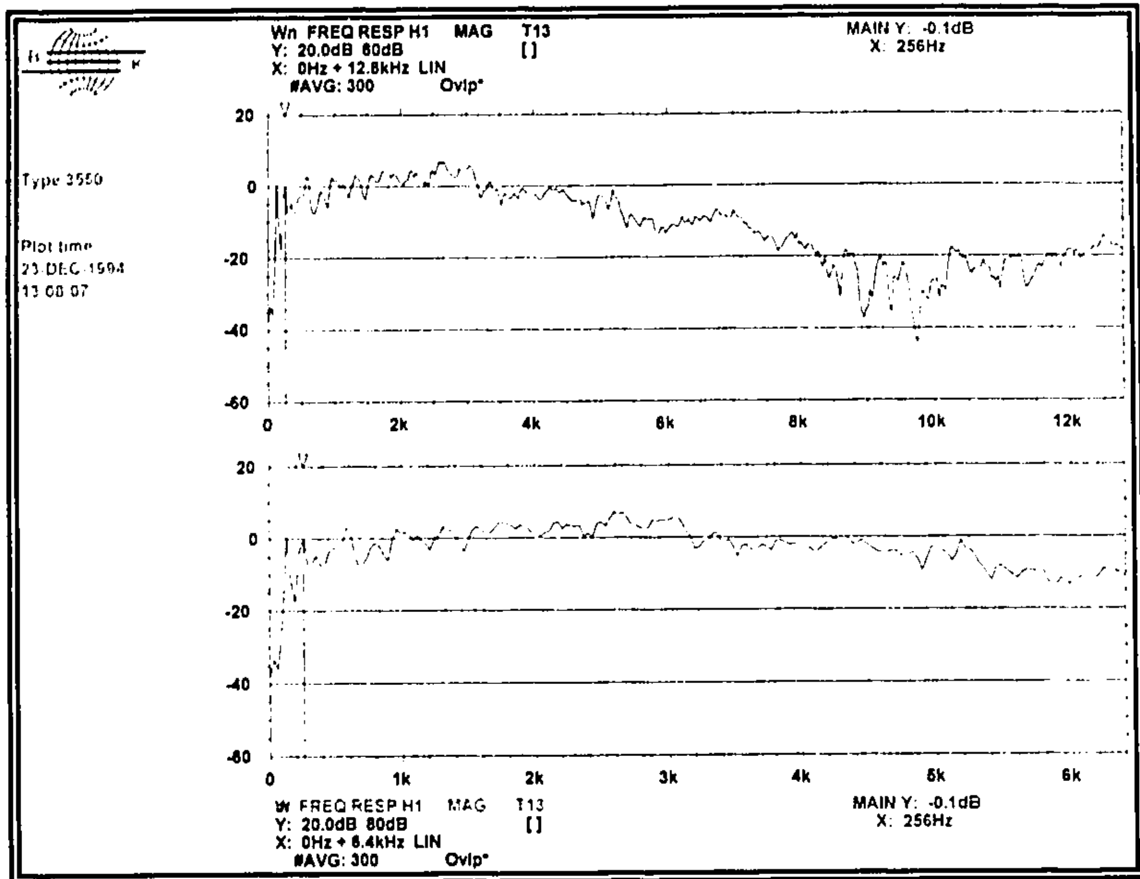

Figure 6.10 (b) Frequency response for the fabricated microphone.

Channel A - Fabricated microphone
Channel B - B&K 4155 microphone (reference)

Fabricated Microphone:	shape:	Hexagonal (regular)
	Membrane size:	Side = 0.5 mm
	back electrode:	.469 mm^2
	air gap:	12 μm

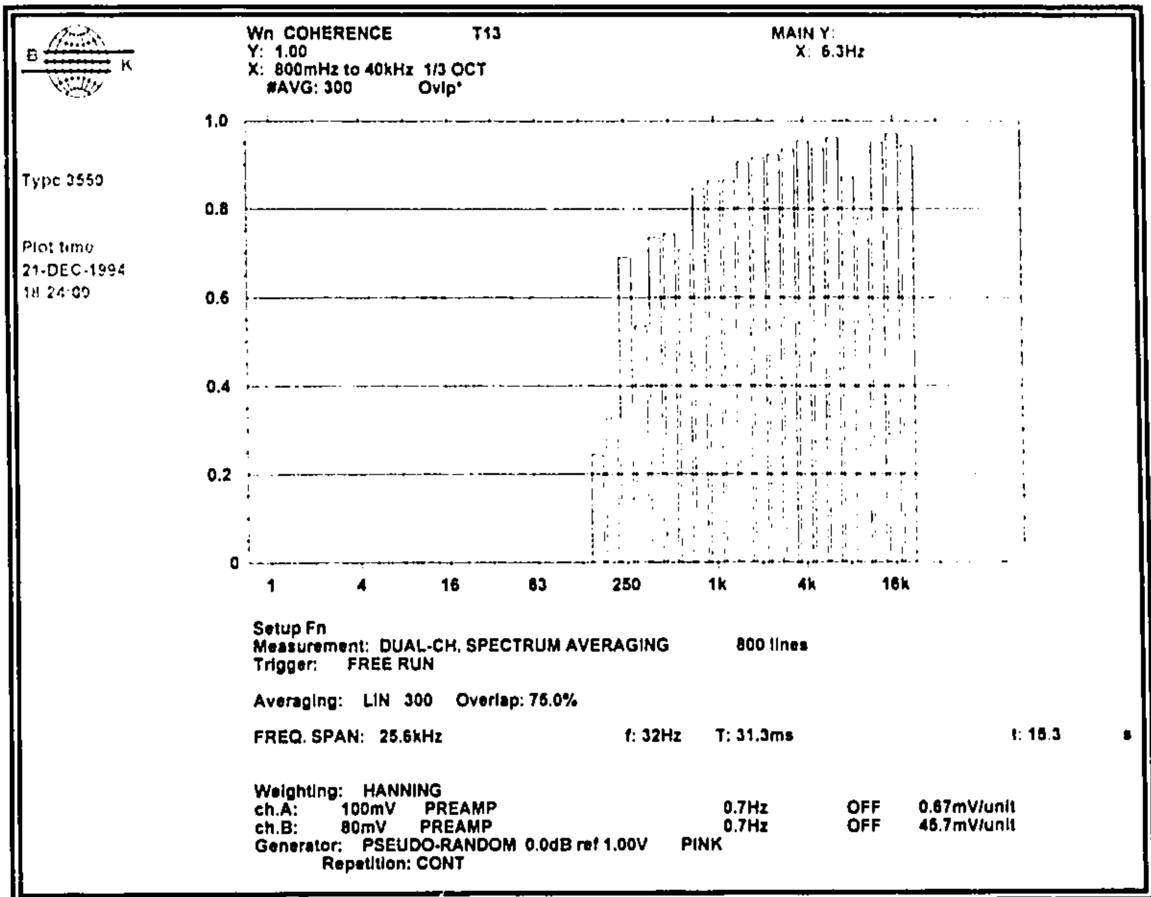

Figure 6.10 (c) Coherence between the fabricated and standard microphone.

Channel A - Fabricated microphone
Channel B - B&K 4155 microphone (reference)

Fabricated Microphone:	shape:	Hexagonal (regular)
	Membrane size:	Side = 0.5 mm
	back electrode:	.469 mm^2
	air gap:	12 µm

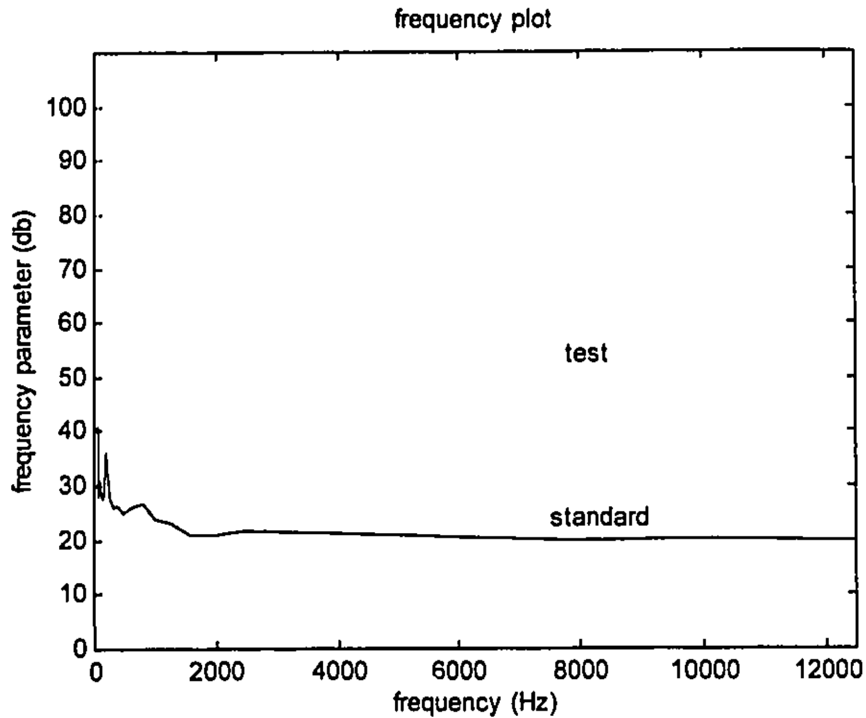

Figure 6.11 Noise level of fabricated (test) and standard microphone.

6.3 Summary

The use of silicon and glass as the two material in the micromachining process has resulted in the development of condenser microphones. The lithographic techniques have allowed the fabrication of miniature microphones with diaphragms of area less than 1 mm^2. Furthermore, silicon micromachining offers the opportunity to fabricate a specially shaped backplate to optimize the sensitivity and the frequency response. Silicon

condenser microphones, with narrow air gap have been developed that show reasonable sensitivity at low operating voltage. Consequently this type of silicon condenser microphone can operate without an electret.

An advantage of the application of silicon micromachining techniques for the fabrication of capacitive microphones is the possibility to increase the sensitivity by reducing the area of the backplate electrode. Since the deflection near the edge of the diaphragm is very small, the part of the electrode in this area mainly contributes to the parasitic capacitance loading the microphone. Consequently, if this part of the electrode is omitted, the capacitive signal attenuation is reduced, thus increasing the sensitivity.

For all the shapes designed, the natural frequency of the diaphragm was found to be ≥ 38.6 kHz, which is substantially above the audible frequency range. The measured cutoff frequencies of the fabricated microphones varies from 3.6 kHz to 5.4 kHz. Note that, even though the natural frequency of the diaphragm varies drastically for different shapes of the diaphragm, the measured cut-off frequency does not. The reason may be due to the airgap volume affecting the frequency response [59,60]. The sensitivity of the fabricated microphones was found to be in the range of 0.53 to 0.92 mV/Pa. The mechanical sensitivity of the microphone can be increased by decreasing the diaphragm thickness. Another possibility for increasing the mechanical sensitivity is the application of a corrugated microphone diaphragm. These diaphragms have been shown to have larger mechanical sensitivity than flat diaphragm of equal size and thickness [66,67]. These diaphragm can be easily made with micromachining techniques.

CHAPTER 7

Conclusions and Recommendations for Future Work

7.1 Overview

This investigation has examined two areas within the broader topic of silicon subminiaturized condenser microphone.

1. The development of suitable shapes of microphone diaphragms and obtain their natural frequencies and mode shapes in order to analyze their responses as acoustic devices.
2. The design, fabrication and testing of the subminiaturized silicon condenser microphone.

The main objective of the study was to design a subminiaturized silicon microphone working on the principle of capacitance, and design a process which requires minimum number of masking steps, taking into considerations the geometrical size of the microphone.

As a sensor of sound, a microphone must fulfill three basic requirements: to provide an electrical signal well above the microphone self noise level, to provide undistorted output over a wide dynamic range, and, when used with associated equipment, to respond equally well to all frequencies produced by

the sound source. The fundamental elements of a condenser microphone comprises a diaphragm, backplate, airgap and side volume cavity. Vibrational analysis was used to find the fundamental frequency of the diaphragm. The process design for the subminiaturized microphone was carefully planned to satisfy the primary objectives of the geometrical size. The fabrication of the condenser microphone requires three masking steps regardless of the geometrical parameters.

7.2 Conclusions for Plate Analysis

The Rayleigh Ritz method is widely used to obtain the approximate values for the natural frequencies and mode shapes. This was demonstrated by several authors cited in the reference for rectangular plates. The Rayleigh Ritz is one such method where, using assumed shape functions satisfying the boundary conditions, the system of equations is reduced to an eigenvalue problem. The solution of this problem provides the natural frequency coefficients and natural modes.

In the present study, orthogonal polynomials were used as shape functions in the Rayleigh Ritz method. The orthogonal polynomials were constructed using the Gram-Schmidt process, the first member of the set satisfying the geometrical and natural boundary conditions of the plate and all the rest satisfying the geometrical boundary conditions.

The ANSYS finite element program [54] is a large scale general purpose program which has the capabilities for a simple linear static analysis to a complex non-linear transient dynamic analysis. It utilizes the matrix displacement method for the analysis and the wavefront method for the matrix reduction and solution. The program contains many routines which are all inter-related. An extensive element library makes it feasible to analyze two or three dimensional structures.

The results of the Rayleigh Ritz method using orthogonal polynomials was compared in detail with those of the Ansys Finite Element Method. For plates with cutout, the natural frequencies increase for both methods as the cutout increases. The increase in the natural frequency with increase in cutout size suggests that the reduction in kinetic energy due to the cutout at the plate center is more significant as compared to the reduction in potential energy. In the Rayleigh Ritz method the deflection is expressed in terms of higher polynomials and hence, the strain energy in the region of the cutout is accounted for more accurately as compared to the finite element method. For plates with abrupt changes in thickness, the natural frequencies increase for both methods with the increase in inner and outer ratios.

The fundamental frequency parameters obtained using the two methods for fully clamped plates of different shapes are used to find the fundamental frequencies of the designed diaphragms.

The present analysis extends the use of orthogonal polynomials in Rayleigh Ritz method to rectangular plates with cutouts, rectangular plate with abrupt change in thickness, circular plates, annular plates, and circular plates with abrupt

changes in thickness. The agreement of the results with those available in the literature confirm the power and efficiency of the method. This is expected since the orthogonal plate function can be accurately used to describe the deflected shape of the rectangular and circular plates. This accurate numerical method for vibration of plates can be applied to any combination of clamped, simply supported and free boundaries.

7.3 Conclusions for the Subminiaturized Condenser Microphone

The use of silicon and glass as the two material in the micromachining process has resulted in the development of condenser microphones. The lithographic techniques have allowed the fabrication of miniature microphones with diaphragms of area less than 1 mm^2. Silicon condenser microphones, with narrow air gaps have been developed that show reasonable sensitivity at low operating voltage. Consequently this type of silicon condenser microphone can operate without an electret. A variety of semiconductor and other processes were used including chromium deposition, wet chemical etching, anodic bonding, etc., for the fabrication of the subminiaturized condenser microphone. The introduction of silicon technology allows accurate control of dimensions, a high degree of miniaturization, and batch fabrication of the microphone at low cost and with good reproducibility. Furthermore, silicon micromachining offers the opportunity to fabricate a specially shaped backplate to optimize the sensitivity and the frequency response.

The fabrication design was carefully planned to satisfy the primary objectives of the geometrical size. The fabrication of the condenser requires three masking steps regardless of the geometrical parameters. The mask design takes into consideration the size and tolerance required for each masking step.

An advantage of the application of silicon micromachining techniques for the fabrication of capacitive microphones is the possibility to increase the sensitivity by reducing the area of the backplate electrode. Since the deflection near the edge of the diaphragm is very small, the part of the electrode in this area mainly contributes to the parasitic capacitance loading the microphone. Consequently, if this part of the electrode is omitted, the capacitive signal attenuation is reduced, thus increasing the sensitivity.

Negative Photoresist was found effective because of the two different depth etched cavities on the glass wafer. The mask required for the fabrication of the microphone was made in the lab using the technique described in Appendix B.

The achieved dimensions were very close to the designed dimensions. Computation based on the measured capacitance value show that the achieved airgap depth was closer to 11 μm rather than designed depth of 12 μm. Achieved backplate dimensions match with ± 5 μm, which is between 0.5 to 1 % of the size dimensions. The airgap depth and the side volume depth was kept constant for all the designed microphone. The experiments were conducted on a single wafer, having all the designed microphones on it.

For all the shapes designed, the natural frequency of the diaphragm was found to be ≥ 38.6 kHz, which is substantially above the audible frequency range. The measured cutoff frequencies of the fabricated microphones varies from 3.6 kHz to 5.4 kHz. Note that, even though the natural frequency of the diaphragm varies drastically for different shapes of the diaphragm (Table 4.1), the measured cut-off frequency does not. The reason may be due to the airgap volume affecting the frequency response [59,60]. The sensitivity of the fabricated microphones was found to be in the range of 0.53 to 0.92 mV/Pa.

From a simple analysis of thermal expansion coefficient mismatch in the temperature range between the bonding temperature 350°C and operating temperature 20°C, the residual stress in the diaphragm is tensile and is estimated to be less than $1.64*10^7$ N/m^2. Tensile stress in the diaphragm increases the fundamental frequency. Therefore it should not adversely effect the cutoff frequency of the fabricated microphone.

Anodic bonding gives almost fully clamped boundary conditions [68]. The deviation from fully clamped conditions does not effect the cutoff frequency significantly, especially, since the anodic bonding temperature used here is lower than that used in the reference investigation [68]. This, if anything, should have the lowered the stress, improved the cutoff frequency, and made the boundary conditions even closer to fully clamped.

The shape of the microphone did not influence the cutoff frequency, as almost all the different microphone shapes had the same cutoff frequency in the range of 3.6 to 5.6 kHz. Manufacturing circular membranes is very difficult using etching

techniques rather than square membrane, if the membrane was manufactured from a silicon wafer because of the crystal orientation of the silicon wafer.

Silicon microphones will probably find applications in all fields where small dimensions rather than high signal-to-noise ratio are desired e.g. as probe microphones or as sensors as hearing aids.

7.4 Recommendations

The mechanical sensitivity of the microphone can be increased by decreasing the diaphragm thickness. Another possibility for increasing the mechanical sensitivity is the application of a corrugated microphone diaphragm. These diaphragm have been shown to have larger mechanical sensitivity than flat diaphragm of equal size and thickness [66,67]. These diaphragms can be easily made with micromachining techniques.

The cut-off frequency can be increased by having a large back volume. But one cannot have a very large back volume, if wet chemical etching technique is used to form the cavity. The cut-off frequency can also be increased by using a perforated backplate in between the diaphragm and the pyrex glass, which now has the back volume cavity only with no back electrode [50]. The back electrode would be part of the perforated backplate to complete the capacitor circuit.

The performance of the silicon condenser microphone can also be increased by integration of the microphone with a preamplifier. If there is a circuitry on the chip, the temperature of anodic bonding comes into question. Bonding temperature over 300°C effect the circuitry. Therefore bonding should be done below 300°C, or the circuitry would have to be hybridized to the sensor device in some way after anodic bonding operation. Bonding can be done below 300°C [70]. Bonding temperature and applied voltage depends on the thickness of the glass and silicon wafers.

Silicon microphones can be fabricated on a single wafer using the single wafer process proposed by Hijab and Muller [51]. The fabrication process is based on the sacrificial layer etching techniques.

More exhaustive experimental investigations need to be carried out to analyze the dynamic behavior of the microphone with the above recommendations. These developments are believed to be important for future silicon condenser microphones.

Appendix A

Metalization and Chromium Deposition

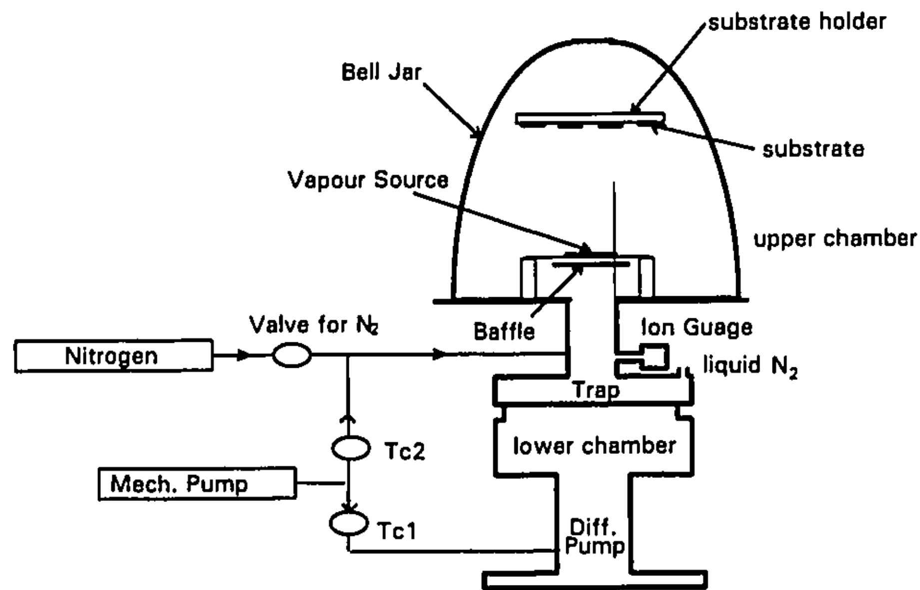

Fig. A1 Chromium deposition setup.

Metalization refers to formation of metal film used for interconnection and ohmic contacts. Metal film can be formed by vacuum evaporation, sputtering and Chemical Vapor Deposition. In the present study, Vacuum evaporation process was used, which is most widely used. The process is carried out in a high vacuum bell jar. The setup is shown in figure A1.

The substrate (pyrex glass) and source material (chromium) to be evaporated are mounted in the bell jar. Vacuum is created in the upper chamber (bell jar)

to the required pressure 50 mTorr (6.66×10^{-1} KPa). The lower chamber which is also at lower pressure because of the continuous operating of diffusion pump, is opened to the upper chamber. The mechanical pump is then shut off. the upper and lower chamber are allowed to stabilize at a pressure of 1×10^{-6} Torr. (1.33×10^{-7} KPa). Liquid nitrogen is filled inside the nitrogen tank which helps in maintaining the required pressure inside the lower chamber. The tungsten boat which contains the source material (chromium) pellets, is heated up by supplying an electric current of 50-55 Amperes. The heat produced by this current under the low pressure inside the chamber leads to the evaporation of chromium pellets. When the source material's vapor pressure exceeds that in the bell jar, the material vaporizes rapidly. Under a high vacuum, the mean free path of the vaporized atoms or molecules is greater than the distance between the source and the substrate. The vaporized atoms, radiated in all directions, condense on all lower temperature surfaces, the substrate and the bell jar, with which they collide forming a uniform thin film. The thickness of the chromium deposition is monitored by a sensor connected to the computer. Once the required thickness is achieved. The current supply is turned off. The evaporator is allowed to cool and nitrogen is passed inside the upper chamber before removing the chromium deposited substrate.

Appendix B

Lithography

Lithography is the technique of transferring patterns of geometric shapes of a design to a layer of radiation sensitive material (resist) which in turn transfers the patterns to the substrate through etching process. Photolithography, X-ray lithography, E-beam lithography and Ion-beam lithography are the radiation used. In our present study, Photolithography with UV light was used as radiation.

The major technique used in lithography are:

i) Fabrication of mask or Pattern generation

ii) Transfer of pattern from the mask to the wafer.

i) Mask Fabrication:

After a test design or computer simulation of a sensor is completed, the composite design of the layout is divided into mask levels, each corresponding to subsequent processing steps that requires a specific geometric pattern to be transferred to the wafer. After enlarged patterns (200 to 400 times the actual size) of each mask level is drawn with the specific geometrical layout on a plastic laminate. The pattern is reduced photographically (usually 10:1 to 20:1) on a first reduction photographic facility to form a glass reticle mask with high resolution, high contrast emulsion. The reticle mask is again reduced to its final size and duplicated

on the master mask by a step-and-repeat camera. Since a sensor size is generally in microns or millimeters, a wafer may have many units of the sensor made on it. Therefore, the mask may contain multiple images of the sensor. Mask was fabricated at the lab using the above process.

ii) Transfer of Pattern from the Mask to the Wafer

Photoresist can be classified as positive and negative. The pattern formed on the positive photoresist is the same as that on the mask, *i.e.*, the clear region of a mask is exposed and become soluble and is removed during the development process. The pattern on the negative resist is the reverse of the mask pattern, *i.e.*, the dark region of a mask is exposed and become soluble and is removed during the development process. Photoresist are processed in a clean room with yellow light. It is not sensitive to light with wavelength greater than 0.5 μm.

The procedure that was followed during fabrication of the condenser microphone is as follows:

1) The wafer is placed on the chuck of the spinner, negative photoresist is applied at the center of the wafer, and the wafer is accelerated to a constant rotational speed of 2000 rpm and maintained for a time of 18 seconds to give a uniform resist film of desired thickness.

2) Pre-bake the wafer with resist at 95 °C for 20 minutes in the oven.

3) The wafer is processed in the aligner for exposing of UV light. The time for exposure depends on the light intensity. For the experiments, the time of exposure is 60 seconds.

4) The exposed resist is developed using resist developer. The wafer was kept into the developer for 45 seconds and then rinsed into a rinsing solution for 30 seconds.

5) The wafer is post-backed at 145 °C for 15 minutes in an oven.

6) The wafer is etched using HF (49% Concentration) etchant to transfer the pattern on the resist to the underlying substrate (glass). The etch rate of HF on glass was found to be 9 μm/min. The etch rate decreases with time and increases with temperature.

7) The resist is stripped.

A lithographic cycle is then completed.

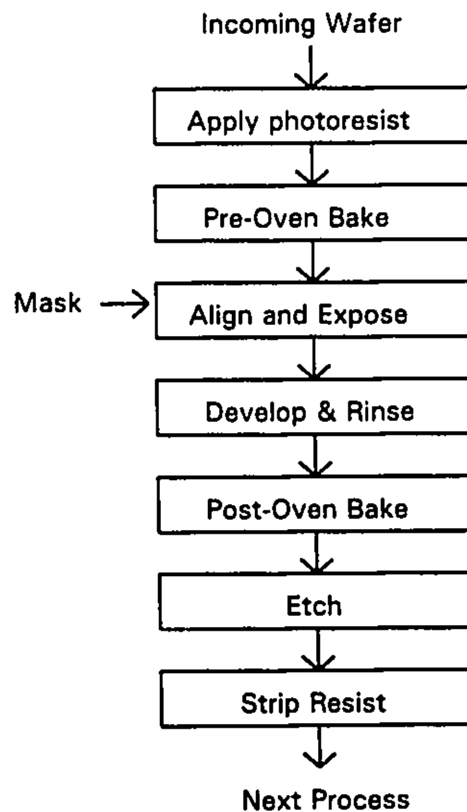

Fig. B1 A Lithographic Cycle

Appendix C

Anodic Bonding

The Anodic Bonding sealing process can be defined as a method of electrostatically bonding two dissimilar materials together to form a strong, hermetic which involves little alteration in the shape, size, and dimensions of the members making up the joint [70]. Anodic Bonding of silicon against Pyrex 7740 or equivalent glasses is a well known and industrial established method for mounting of micromechanical sensors.

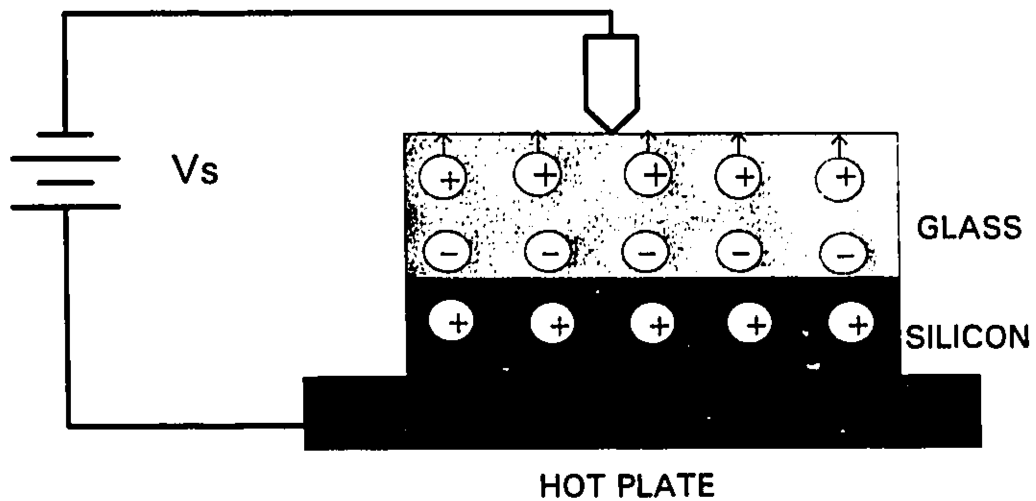

Vs = 200-1000V

Temp = 180 - 500° C

Fig C1. Anodic Bonding

The field-assisted thermal bonding process of glass to silicon can be accomplished in atmosphere or vacuum at temperature between 180° and 500°C *i.e.* near the annealing point but well below the melting point of glass. The bonding setup is shown schematically in figure C1. The optically polished glass substrate is placed against the polished surface of the silicon. A cathode electrode is held against the outer surface of the glass wafer and the whole assembly is heated up on a temperature controlled hot plate, which also serves as an anode. A 200-1000V potential (depending on the thickness of the glass) is then applied between the electrodes. The electrostatic forces created by the electric potential pulls the two substrates into contact . At elevated temperatures the two wafers are bonded instantly. Looking through the glass, the bonded region will become dark grey color; when this region expands the whole wafer, the bonding is completed. Anodic bonding was performed at 350°C with an applied voltage of 1000V for our experiments.

The main requirements for the material to be bonded are:

1. The glass must be slightly conductive at the process temperature.

2. the surface roughness of the glass and silicon wafers should be less than 1 μm rms and free from dust, organic residues and other contamination.

3. The thermal expansion coefficients of the two materials should be closely matched.

THEORY

i) At elevated temperature, the positive sodium ions in the glass become quite mobile and they are attracted to the negative electrode on the glass surface where they are neutralized. The more permanent bond negative ions in the glass are left, forming a space charge layer in the glass adjacent to the silicon surface to be sealed.

ii) After the Na^+ ions have drifted towards the cathode, most of the potential drop in the glass occurs at the surface next to the silicon to be sealed. The two chips then act as a parallel plate capacitor with most of the potential being dropped across the several microns wide air gap between them. The resulting electric field between them serves to pull them into contact. As long as the applied voltage is large enough to activate substantial Na^+ drift, the magnitude of the voltage needed to obtain bonding is independent of the glass film thickness.

iii) The electrostatic forces pulls the surfaces into close contact allowing formation of atomic bonds.

Appendix D

Wet Etching

Etching is used for 1) Removing surface damage, 2) Cleaning the surface to remove contamination prior to other process, 3) Delinating patterns and opening windows in insulating materials, 4) Fabricating 3-dimensional structures. At the completion of the post-oven baking of the wafer, where the mask pattern is defined in the photoresist layer, the wafer is ready for etch. The wafer are loaded into an etch resistant boat and immersed in a tank or beaker of the etchant. After a predetermined time in the beaker, they are processed through the rinsing and drying step. Etching uniformity and process control are enhanced by the addition of heaters and agitation devices.

The mechanism for wet etching involves three steps:

1) The reactants are transported to the reaction surface by diffusion.
2) Chemical reaction occurs at the surface, and
3) The products from the surface are transported away by diffusion.

Etching by wet chemical is usually isotropic. In our present study, HF was used as etchant to etch back volume and air gap cavity. The etch rate of HF on glass was found to be 9 µm/min. The etch rate decreases with time and increases with temperature.

Appendix E

Frequency Response Functions

Condensed form " B&K 2035 Operational manual" Vol 1-2. (1993). [71]

The main objective of system analysis is to measure input-output relationships. A dual channel FFT analysis of the input and output of a system, Fig. E1., permits the calculation of functions which describe its dynamic behavior, assuming the system is linear. These functions, which are the impulse response function h(t) and the frequency response function H(f), are related via Fourier transform and contain the same information about the system, but in different domains.

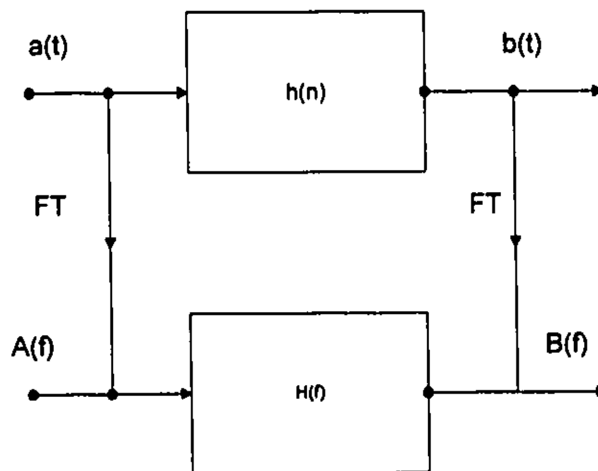

Fig. E1. System with input-output signals in time domain and frequency domain.

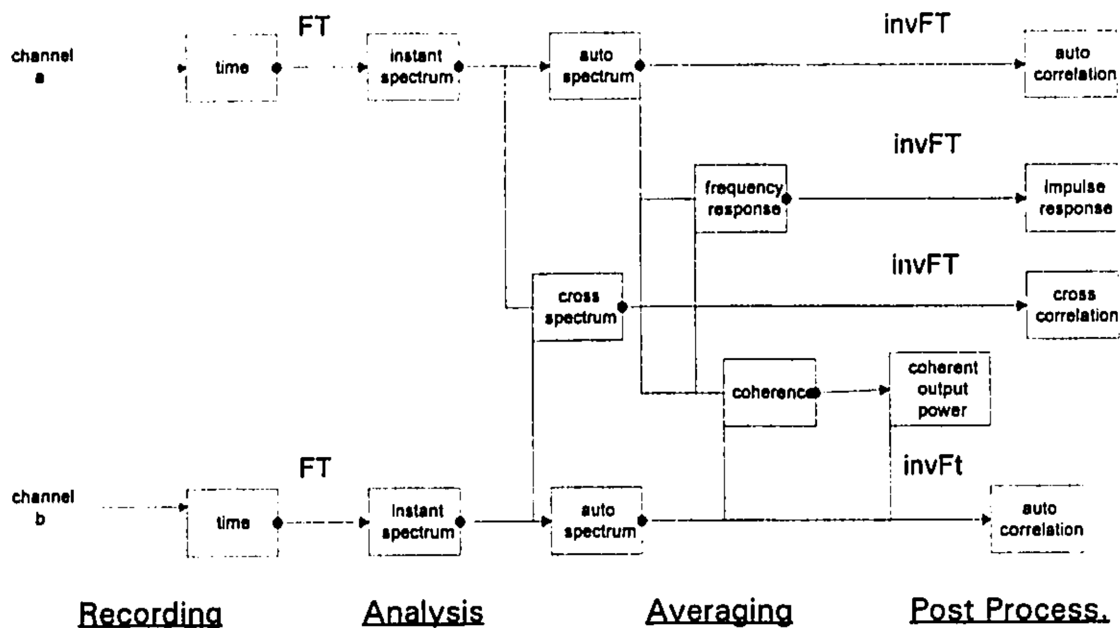

Fig. E2 Simplified block diagram of the analyzer in dual-channel spectrum averaging mode.

In the time domain the relation Between input and output is given by convolution theorem,

$$b(t) = a(t) * h(t).$$

In the frequency domain there is a simple relationship between input and output given by:

$$B(f) = H(f)A(f),$$

from which it is easy to derive the frequency response function, H(f). For our measurement purpose we used dual-channel measurements. A dual-channel measurement is a simultaneous of the cross-spectrum between the signals in the two channels, and of the autospectrum of each of the two channels, see Fig. E2.

All other functions, such as frequency response function, and coherence are derived from these three spectra.

Autospectra:

$$G_{AA} = \overline{A^{*}(f)} \cdot \overline{A(f)},$$

is the mean square of the Fourier spectrum, A(f). The autospectrum is real and positive being equal with a complex product of conjugate values. In other words we can say that the phase of autospectrum is equal to zero.

The **cross spectrum** is defined in a similar way:

$$G_{AB} = \overline{A^{*}(f)} \cdot \overline{B(f)}.$$

The cross-spectrum is a complex number and , thus contains a non-zero phase, which is the phase difference between the output and the input of the system under test. If the Fourier spectra in polar coordinates, for the input and output,

$$A(f) = |A(f)| \cdot e^{j \cdot \varphi_{A(f)}}$$
$$B(f) = |B(f)| \cdot e^{j \cdot \varphi_{B(f)}}$$

then, the cross-spectrum is:

$$G_{AB} = |A(f)| \cdot |B(f)| \cdot e^{j(\varphi_B(f) - \varphi_A(f))}$$

where the phase of the cross-spectrum is: $\varphi_B(f) - \varphi_A(f)$.

This is the phase difference between the input and the output. Another feature of the cross-spectrum is that it is insensitive to uncorrelated noise at both input and output, a feature that the autospectra do not have. Actually, in the cross spectrum, the effect of the noise is not eliminated, but reduced, through averaging. The number of averages needed in a noise measurement situation depends on the signal to-noise-ratio.

The **frequency response function** is defined as:

$$H(f) = \frac{B(f)}{A(f)}$$

Using random excitation, the estimator given by the above equation is very poor since random signals are not described by their Fourier transform. Since a dual-channel FFT analyzer produces three fundamental spectra, G_{AA}, G_{BB}, G_{AB}, these spectra are used for the calculations. The best estimator is to chose function of the noise problems of each measurement. For the output noise problem the best estimator is the one which is not using G_{BB}, for the input noise problem the best estimator is one which is not using G_{AA}.

The **coherence function** is defined as:

$$\gamma^2 = \frac{|G_{AB}|^2}{G_{AA} \cdot G_{BB}}, \quad 0 \le \gamma^2 \le 1$$

The coherence function expresses the degree of linear relationship between A(f) and B(f). Low coherence can be due to either difficult or bad measurements. If the coherence is low at a frequency, (say 0.1) this simply means that only 10% of the measured signal is linearly related to the input signal, the signal-to-noise ratio is 10/90=0.11. Thus the coherence is 0.1, independent of how many averages are taken, but the larger the number of averages, the better the cross-spectrum will be. In theory, after an infinite number of averages the measured cross-spectrum will be equal to the true cross-spectrum of the system under test. The coherence will still be 0.1 because the input noise is directly added the output spectrum, which will be 10 times higher than in the case where no noise is present. The effect of noise on the cross-spectrum is minimized through averaging. The more noise is present (and therefore the lower the coherence), the more averages required to yield a certain statistical accuracy. A large number of averages will also provide a better estimate of the coherence. In our measurements we consider 300 averages.

Difficult measurements could be caused by, for example:

- Extraneous noise at the output of the system
- Extraneous noise at the input of the system
- Other inputs not correlated with the measured input but passing through the system.

For any of these cases one should use the appropriate FFT estimator and take a sufficient number of averages.

Bad measurements could be caused by, for example:

- Leakage
- Time variation in a system
- Non-linearities in a system
- Degree of freedom jitter (Hammer excitation)

Excitation signals:

Different types of excitations are available, each having its own advantages and disadvantages. The types described here are continuos random, pseudo-random, periodic random, burst random, multisine and impulse:

- Random excitation has the main characteristic that each frequency of the system is excited by a different amplitude and phase in each analysis data block. This produces the best linear approximation of the system under test. The disadvantage is that this continuos signal does not fit the block length in the analysis, thus Hanning weighting must be applied, which causes leakage in the estimates.

- Pseudo-random excitation is made up of a segment of a random signal of length T, which is repeated after every period of time T, where T is the FFT record length. This signal is therefore periodic and consists of sine waves which coincide with the calculated FFT lines, so, if rectangular weighting is used, the measurements will be leakage free.

- Periodic random signal changing with time. Because it is pseudo random, the measurements are leakage free assuming rectangular weighting is applied. Because it is changing with time it produces the best linear approximation of a system. After each time the new pseudo-random sequence has been applied, one must wait a number of FFT records in order for the system to reach the steady state response before the measurement ca ı take place.

- Burst random signal has the same advantages as the periodic random, namely best linear approximation of the system and no leakage (if rectangular time weighting can be used in both channels). In most system analysis or testing applications, where the input-output relationships have to be measured, it is necessary to excite the system with a well-controlled and well-measured input.

- Multisine signal is a special pseudo-random signal where the crest factor is minimized. The signal is similar to a sine chirp where the length of the chirp matches the record length. Main advantages are no leakage (rectangular weighting) and its use for studying non-linearities. It gives no linear approximation of a non-linear system.

- Pulse excitation is a special case of the pseudo-random signal. It is especially useful for gated measurements, such as loud-speaker testing. The main disadvantages are a high crest factor and a poor signal-to-noise ratio. Generally, you have to use transient / exponential weightings in order to increase the signal-to noise ratio, but this may introduce leakage which will have the same effect as additional damping in the system. Correction can be

made subsequently. The most important advantages and disadvantages of the different excitation techniques are summarized in Table E1

Table E1. Advantages and Disadvantages of Different Measuring Techniques [B&K]

	Leakage in analysis	Best linear fit of a non linear system	Crest factor	Signal-to noise ratio	Control of Excitation Bandwidth	Speed
Random	Yes	Yes	Medium	Medium	Good	Fast
Pseudo random	No	No	Medium	Medium	Good	Very fast
Periodic Impulse	Depends on the weighting functions	NO	High	High	Limited (no zoom)	Very fast
Periodic Random	No	Yes	Medium	Medium	Good	Slower than random
Multisine	No	No	Low	Low	Good	Fast
Burst Random	No	Yes	Medium /High	Fair	Good	Slower than random

Measurement requirements and conclusions:

- When output noise is present, $H_1(f) = {G_{AB}}/{G_{AA}}$ is the best estimator since is not based on the output of the spectrum. The effect of noise in the cross-spectrum is minimized through averaging.
- When the input noise is present $H_2(f) = {G_{BB}}/{G_{BA}}$ is the best estimator since is not based on the input spectrum. The effect of noise in the cross-spectrum is minimized through averaging.
- When there is noise at both the input and the output all three estimators will be wrong:

  H_1 will be too small since noise is added to the input autospectrum.

  $H_2(f)$ will be too large since noise is added to the output of the autospectrum.

  $H_3(f)$ could be a reasonable compromise if the signal-to-noise ratio at the input is the same as the signal-to-noise ratio at the output, although this is the seldom case.
- If there are inputs to the system other than the measured one, then these input signals will show up a noise at the output. For this case the best choice is $H_1(f)$. In most cases it is possible to control the signal-to-noise ratio at the input to a certain degree. In these cases $H_1(f)$ is therefore the best choice. For very lightly damped mechanical structures there is often a drop in the force spectrum at resonance, because it is very difficult to apply a force to a very compliant structure. In such cases $H_2(f)$ might be a better choice in the vicinity of peaks.

At anti resonance all five cases show very clearly that H_1 is the best choice as estimator. The phase of all frequency response estimators is the same as the phase of the cross-spectrum.

Conclusions and Summary:

- in dual channel analysis, the basic measurement is the measurement of three spectra: two autospectra, G_{AA}, G_{BB} and the complex cross-spectrum, G_{AB}. The cross-spectrum measures the insensitive to noise at the input or the output.
- Frequency response function is a system descriptor, independent of the signals involved, and is defined as:

$$H(f) = \frac{B(f)}{A(f)}$$

Different estimators are: $H_1(f), H_2(f), H_3(f)$. The best choice is summarized in the table E2.

Table E2. Best Choice of FRF Estimator for Different Measurement Situations.

Accuracy of the system with:	H1	H2	H3
Input noise		Best	
Output noise	Best		
Input + Output Noise			Best
Peaks (leakage)		Best	
Valleys (leakage)	Best		

Bibliography

1. Young, D., "Vibration of Rectangular Plates by the Ritz method", Journal of Applied Mechanics, Vol. 17, 1950, pp. 448-453

2. Leissa, A.W., "The free Vibration of Rectangular Plates", Journal of Sound and Vibration, Vol. 31, 1973, pp. 257-293.

3. Dickinson, S.M., "The Buckling and F[illegible]ency of Flexural Vibration of Rectangular Orthotropic Plates using Rayleig[illegible] Method", Journal of Sound and Vibration, Vol. 61, 1978, pp. 1-8.

4. Trefftz, E., "Konvergenz und Fehterschatzung Biem Ritzchen Verfahren", Mathematische Annalen, Vol. 100, 1928, p. 503.

5. Courant, R., "Vibrational Methods for the solution of Problems of Equilibrium and Vibration", Bulletin of the American Mathematical Society, N.Y., Vol. 49, 1939, pp. 1-23.

6. Collatz, L., "Eigenwertprobleme", Chelsa Publishing Company, New York, N.Y., 1948.

7. Gorman, D.J., "An Analytical Solution for the Free Vibration Analysis of Rectangular Plates Resting on Symmetrically Distributed Point Supports", Journal of Sound and Vibration, Vol. 79 (4), 1981, pp. 561-574.

8. Bassily, S.F., Dickinson, S.M., "On the use of Beam Functions for plates Involving free edges", Transactions of the ASME, Vol. 42, 1975, pp. 858-864.

9. Dickinson, S.M., and Li, E.K.H., "On the use of Simply Supported Plate Functions in Rayleigh's Method Applied to the Flexural Vibration of Rectangular Plates", Journal of Sound and Vibration, Vol. 80, 1982, pp. 292-297.

10. Laura, P.A.A., "Comments on the use of Simply Supported Plate Functions in Rayleigh-Ritz's Method Applied to the Flexural Vibration of Rectangular Plates", Journal of Sound and Vibration, Vol. 84, 1982, pp. 595-597.

11. Goldfracht, E., and Rosenhouse, G., "Use of Lagrange Multipliers with Polynomials Series for Dynamic Analysis of Constrained Plates, Part 1: Polynomial Series", Journal of Sound and Vibration, Vol. 92, 1984, pp. 83-93.

12. Bhat, R.B., "Natural Frequencies of Rectangular Plates Using Characteristic Orthogonal Polynomials in Rayleigh-Ritz's Method", Journal of Sound and Vibration, Vol. 102, 1985, pp. 493-499.

13. Dickinson, S.M., and Blasio, A. Di "On the use of Orthogonal Polynomials in the Rayleigh-Ritz Method for the study of the Flexural Vibration and Buckling of Isotropic and Orthotropic Rectangular Plates", Journal of Sound and Vibration, Vol. 108, 1986, pp. 51-62

14. Monahan, J., Nemergut, P.J., and Maddux, G.E., "Natural frequencies and mode shapes of plates with interior cut-outs", The shock and Vibration Bulletin, Vol. 41,1970, pp. 37-49.

15. Paramasivan, P., "Free Vibration of Square Plates with square openings", Journal of Sound and Vibration, Vol. 30, 1973, pp. 173-178.

16. Aksu, G., and Ali, R., "Determination of Dynamic Characteristics of Rectangular Plates with cut-outs using Finite Difference Formulation", Journal of Sound and Vibration, Vol. 44, 1976, pp. 147-158.

17. Rajamani, A., and Prabhakaran, R., "Dynamic Response of Composite Plates with cut-outs, Part 1: Simply-Supported Plates" Part 2: Clamped Clamped Plates", Journal of Sound and Vibration, Vol. 54, 1977, pp. 549-576.

18. Lam, K. Y., and Hung, K. C., and Chow, S. T., "Vibration Analysis of Plates with cut-outs by the modified Rayleigh-Ritz Method", Applied Acoustics, Vol. 28, 1989, pp. 49-60.

19. Tham, L. C., Chan, A. H. C., and Cheung, Y. K., "Free Vibration and Buckling Analysis of Plates by the Negative Stiffness Method" Computers Structures, Vol. 22, 1986, pp. 687-692.

20. Rajalingham, C., Bhat, R.B., and Xistris, G. D., "Vibration of clamped elliptical plates using exact circular plate modes as shape functions in Rayleigh-Ritz method", International Journal of Mechanical Science, Vol. 36, 1994, pp. 231-246.

21 Itao, K., and Crandall, "Natural modes and natural frequencies of uniform, circular, free-edge plates", ASME Journal of Applied Mechanics Vol. 46, 1979, pp. 448-453.

22. Leissa, A.W., and Narita, Y., "Natural Frequencies of simply supported circular plates", Journal of Sound and Vibration, Vol. 70, 1980, pp. 221-229.

23. Sato, K., "Free flexural vibration of an elliptical plate with free edge", Journal of Acoustical Society of America, Vol. 54, 1973, pp. 547-550.

24. Narita, Y., "Natural Frequencies of free, orthotropic elliptical plates", Journal of Sound and Vibration, Vol. 100, 1985, pp. 83-89.

25. Kim, C.S., and Dickinson, S.M., "On the Lateral Vibration of Thin Annular and Circular Composite Plates subject to certain complicating effects", Journal of Sound and Vibration, Vol. 130, 1989, pp. 363-377.

26. Wah, T., "Vibration of circular plates", Journal of Acoustical Society of America, Vol. 34, 1962, pp. 275-281.

27. Jones, R., "An approximate expression for the fundamental frequency of vibration of elastic plates", Journal of Sound and Vibration, Vol. 38, 1975, pp. 503-504.

28. Johns, D. J., Comments on "An approximate expression for the fundamental frequency of vibration of elastic plates", Journal of Sound and Vibration, Vol. 41, 1975, pp. 385-387.

29. Rajalingham, C., Bhat, R.B., and Xistris, G. D., "Vibration of elliptical plates using characteristic orthogonal polynomials in the Rayleigh-Ritz method", International Journal of Mechanical Science, Vol. 33, 1991, pp. 705-716.

30. Vogel, S.M., and Skinner, D.W., "Natural frequencies of Transversely Vibrating Annular Plates", Journal Of Applied Mechanics, Vol. 32, 1965, pp. 926-931.

31. Vijaykumar, K., and Ramaiah, G.K., "On the use of coordinaye transformation for analysis of axisymmetric vibration of polar orthotropic annular plates", Journal of Sound and Vibration, Vol. 24, 1972, pp. 165-175.

32. Bhat, R.B., "Flexural Vibration of Polygon Plates Using Characteristic Orthogonal Polynomials in Two Variables", Journal of Sound and Vibration, Vol. 114, 1987, pp. 65-71.

33. Lam, K.Y., and Liew, K.M., "A set of orthogonal plate functions for flexural vibration of regular polygon plates", ASME Journal of Vibration and Acoustics, Vol. 113, 1991, pp. 182-186.

34. Peterson. K. E., "Silicon as Mechanical Material", IEEE proceedings Vol.70 (1982) pp. 420-457

35. Royer, M., Holmen, J.O., Wurm, M.A., Aadland,).S., and Glenn, M., "ZnO on Si integrated acoustic sensor", Sensors and Actuators, Vol. 4, 1983, pp. 357-362.

36. Franz, J., "Piezoelectric microphone", Proceedings of the 12th International Congress of Acoustics, Toronto, Canada, 1986.

37. Kim, E.S., and Muller, R.S., "IC-Processed piezoelectric microphone", IEEE Electron. Device Lett., EDL-8, 1987, pp. 467-468.

38. Schellin, R., and Hess, G., "A Silicon subminiature microphone based on piezoresistive polysilicon strain guages", Sensors and Actuators A, 32, 1992, pp. 555-559.

39. Homn, D., and Gerhard-Multhaupt, R., "Silicon-dioxide electret Transducer", Journal of Acoustical Society of America, Vol. 75, 1984, pp. 1297-1298.

40. Sprenkels, A.J., Groothengel, R., Verloop, A.J., and Bergveld, P., "Development of electret microphone in silicon", Sensors and Actuators, 17, 1989, pp. 509-512.

41. Murphy, P., Hubschi, K., Rooij N.de., and Racine, C., "Sub-Miniature Silicon Integrated electret capacitor microphone", IEEE Transactions Electrical Instrumentation, IE-24, 1989, pp. 495-498.

42. Homn, D., and Hess, G., "A Subminiature condenser microphone with silicon nitride membrane and silicon backplate", Journal of Acoustical Society of America, Vol. 85, 1989, pp. 476-480.

43. Bergqvist .J., Rudolf, F., "A new Condenser microphone in silicon", Sensors and Actuators, A21-A23, 1990, pp. 123-125.

44. Kuhnel, W., "Silicon Condenser microphone with Integrated field effect transistor", Sensors and Actuators, A25-A27, 1991, pp. 521-525.

45. Bourouina, T., Spirkovitch. S., Baillieu, F., and Vauge, C., " A new microphone with p+ Silicon membrane", Sensors and Actuators, A31, 1992, pp. 560-564.

46. Kuhnel, W., and Hess, G., "Micromachined Subminiature condenser microphone with silicon ", Sensors and Actuators, A32, 1992, pp. 149-152.

47. Kuhnel, W., and Hess, G., "A silicon condenser microphone with structed backplate and silicon nitride membrane", Sensors and Actuators, A30, 1992, pp. 251-258.

48. Lukosz, W., and Pliska, P., "Integrated Optical Interferometer as a light modulator and microphone", Sensors and Actuators, A25-A27, 1991, pp. 337-340.

49. Garthe, D., "A Fibre-Optic microphone", Sensors and Actuators, A25-A27, 1991, pp. 341-345.

50. Bergqvist .J., Rudolf, F., MaisanO, J., Parodi, F., and Rossi, M., "A Silicon Condenser microphone with highly perforated backplate", Tech. Digest. 6th Intl. Conf. of Solid-State Sensors and Actuators (Transducers '91), San Fransisco, CA, USA, June 24-28, 1991, pp. 408-411.

51. Scheeper, P.R., Van der Donk, A.G.H., Olthuis, W., and Bergveld, V., "Fabrication of silicon condenser microphone using single wafer technology", Journal of Microelectromechanical Systems, Vol. 1 # 3, 1992, pp. 147-154

52. Borwick, J., "Microphone: Technology and Technique", Focal Press, London, England, 1990, pp. 88-89.

53. Chihara, T.S., "Introduction to Orthogonal Polynomials" Gordon and Breach Science Publishers, London, England, 1978.

54. Ansys, Swanson Analysis. Houston, 1994

55. Irie, T., Yamada, G., and Narita, Y., "Free Vibration of Clamped Polygon Plates," Bulletin of the JSME, Vol. 21, 1978, pp. 1696-1702.

56. Timoshenko, S., and Woinowsky-Krieger, S., "Theory of plates and shells" Second edition, McGraw-Hill, New-York, 1959.

57. Love, A.E.H., "A treatise on the mathematical theory of elasticity" fourth edition, Dover publishers, New York, 1944.

58 Fraim. F., and Murphy P., "Miniature electret microphones" J. Audio Engineering Society, 18, 1970, pp. 511-517.

59. Skvor, Z., "On the acoustical resistance due to viscous losses in the air gap of electrostatic transducers" Acustica, Vol. 19, 1967, pp. 295-299.

60. Plantier G., and Bruneau, M., "Heat conduction effects on the acoustical response of a membrane separated by a very thin air film from a backing electrode", Journal d'Acoustique, Vol. 3, 1990, pp. 243-250.

61 Torrel J. R., Harrington M.I., and Miller R.A., "Laser-recrystallized silicon thin-film transistor on expansion-matched 800° C glass " IEEE Electron devices letters, EDL-8, 1987, pp. 576-578.

62. Product Data sheet "Ultrathin Silicon Membranes" Virginia Semiconductor Inc., Virginia, USA. 1994.

63. Friesser R.G., "The chromium glass Interface", Journal of Electrochem. Soc.: Solid-state science and technology, March 1972 pp. 360-363.

64. Product Data Sheet "Acneson Colloids Company" 1160 Washington Avenue, Port Huron, Michigan 48060. 1994

65. Product Data Sheet "Bruel and Kjaer" for B&K 4155 condenser microphone.

66. Zhang Y., and Wise K.D., "Performance of non-planar silicon diaphragms under large deflections" Tech. Digest, IEEE Micro

Electromechanical systems workshop, Fort Lauderdale, FL, USA, Feb 1993, pp. 284-288.

67. Scheeper, P.R., A.G.H., Olthuis, W., and Bergveld, V., "The Design, Fabrication and Testing of corrugated silicon nitride diaphragms", Journal of Microelectromechanical Systems, Vol. 3 # 1, 1994, pp. 36-42

68. George G., Stiharu I., Bhat R.B., Landsberger L., and Kahrizi M., "Characterization of the boundary conditions of silicon structures anodically bonded to pyrex glass" CSME Conference, June 27-29, 1994, Montreal, Canada. pp. 889-899.

69. Bergqvist .J., "Finite Element Modelling and Characterization of a Silicon Condenser microphone with highly perforated backplate", Sensors and Actuators A, Vol # 39, 1993, pp. 191-200.

70. Wallis G., and Pomerantz D.I., " Field-assisted Glass-Metal sealing", Journal of applied physics, Vol. 40, # 3, 1969 pp. 3946-3949.

71. Operational Manual " Brüel and Kjaer 2035 Frequency Analyzer" Volume 1-2.